Characterisation, Modelling, Finite element analysis, and optimisation of hyperelastic materials for Non-Pneumatic Wheels

Saahil Bhartu

(Student number: 843976)

School of Mechanical, Industrial and Aeronautical Engineering

University of the Witwatersrand

Johannesburg, South Africa.

Supervisors: Francesco Pietra

A dissertation submitted to the Faculty of Engineering and the Built Environment, University of the Witwatersrand, in fulfilment of the requirements for the degree of Masters in Mechanical Engineering.

Date: 01/02/2024

SCHOOL OF MECHANICAL, INDUSTRIAL & AERONAUTICAL ENGINEERING

UNIVERSITY OF THE WITWATERSRAND JOHANNESBURG

INDIVIDUAL DECLARATION WITH JOINT TASK SUBMITTED FOR ASSESSMENT

I, Saahil Bhartu 843976, am registered for MECN8006A MSc Dissertation: Mechanical and BMH in the year 2024.

I herewith submit the following task, “Characterisation, Modelling, Finite element analysis, and optimisation of hyperelastic materials for Non-Pneumatic Wheels” in partial fulfilment of the requirements of the above course.

I hereby declare the following:

- I am aware that plagiarism (the use of someone else’s work without their permission and / or without acknowledging the original source) is wrong;
- I confirm that the work submitted herewith for assessment in the above course is my own unaided work except where I have explicitly indicated otherwise;
- This task has not been submitted before, either individually or jointly, for any other course requirement, examination or degree at this or any other tertiary educational institution;
- I have followed the required conventions in referencing the thoughts and ideas of others;
- I understand that the University of the Witwatersrand may take disciplinary action against us if it can be shown that this task is not our own unaided work or that we have failed to acknowledge the sources of the ideas or words in our writing in this task.

Signature: **Date: 1 February 2024**

Private Bag 3, Wits, 2050, South Africa
Tel: +27 11 717 7321
Fax: +27 11 717 7049
http://www.wits.ac.za/academic/ebe/5122/mecheng.html

Abstract

This abstract concludes the exploration of hyperelasticity within the context of mechanical engineering. Through this section, we have delved into the substantial elastic deformations characteristic of hyperelastic materials, their capacity for energy conservation during deformation, and their inherently non-linear behaviour. The calibration of non-linear material models has been informed by a rigorously designed experimental regimen, where preferred methodologies and necessary precautions were identified to ensure the integrity of the data obtained.

Theoretical foundations for the development of constitutive models have been established, with a discussion of prevalent models frequently employed in engineering applications. Practical modelling applications introduced have provided a tangible context for the utilization of hyperelastic material models. While our focus was predominantly on nearly or fully incompressible materials, foundational concepts for compressible behaviour were also addressed, setting the stage for further investigative pursuits.

Polyurethane (PU) materials exemplify hyperelastic behaviour. Through computational simulation, we assessed the deformation in a structured wheel to be 4.6mm, utilizing a 9;5 and 2 parameter Mooney-Rivlin model for the PU material. Experimental testing was conducted measuring deformation to be 4.1mm

From the results, the deformation patterns, stress distributions, and contact pressures were analysed, indicating the wheel’s ability to endure a contact pressure of 7.36MPa, deformation of 4.6mm, Von-Mises stress of 3.9MPa.

This investigation not only corroborates the distinctive properties of hyperelastic materials but also illustrates how analysis results can inform and optimize design iterations. It demonstrates the practical applications of hyperelastic material models in design engineering, providing a comprehensive understanding that is indispensable for the modelling and analysis of hyperelastic components.

Table of Contents

List of Figures

List of Tables

1. Introduction

1.1 Purpose of the Study Research

Polyurethanes (PU) are derived in many different forms and types which makes it difficult to characterise and model a specific PU. For this reason, it is essential to develop a methodology for the characterisation, modelling for simulation purposes, verification and validation of the PU's produced at Urethane Moulded Products (UMP). UMP is involved in the design and development of non-pneumatic wheels to target the international market specifically the USA and Europe. To do design and development surrounding PU it is essential that PU be characterised, and accurate modelling can be done on finite element analysis (FEA). Without FEA simulation it will be cost inefficient to design moulds to manufacture wheels and test them in stages to develop a working product. The purpose of this research is to characterise and accurately model the mechanical characteristics of PU and develop a working simulation to optimise the non-pneumatic wheel behaviour.

1.2 Basic chemistry of Polyurethanes

Polyurethane refers to a material with a specific chemical structure. This structure can be bonded with a variety of other molecule chains to create different variations with versatile properties. The structure that is common to creating a polyurethane is the NCO (Nitrogen, Carbon and Oxygen) group as seen in Figure 1. The NCO group is the reactive component which plays a critical role in the bonding process. The molecule which contains the NCO group is known as the Isocyanate Prepolymer. The second component is a curative. The curative contains hydrogen atoms that are necessary for the reaction with the NCO group.

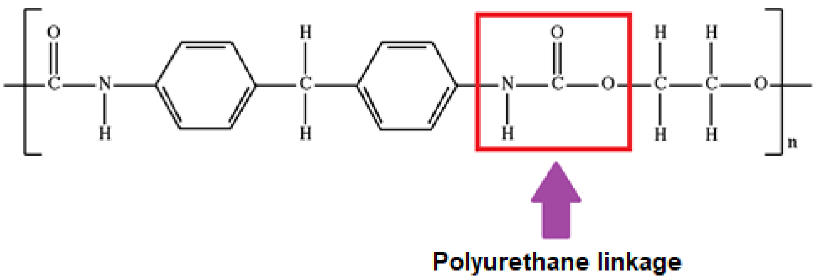

Figure 1: Polyurethane chemical structure [1]

When the NCO group from the prepolymer reacts with the hydrogen in the curative it leads to the formation of the chemical structure characterised as a polyurethane. Polyurethanes (PU) used to refer to the chemical structure however in more recent times it refers to the synthetic material produced from this bonding process famed for its durability. PU represents a versatile and widely used material in modern engineering and manufacturing, stemming from a specific chemical reaction.

PU is used in a variety of industrial applications, especially in high abrasion environments such as pump impellers, wheels and hydrocyclones. The following range of molecules make up the building blocks of PU:

Isocyanates: TDI, MDI, pPDI, HDI, IPDI, H12MDI

Low monomer isocyanates: LF TDI, LF MDI, LF HDI, LF pPDI, LF IPDI

Polyols: polyester, PTMEG, PPG, PCL, PC

Curatives: diamines, diols, triols, and specialty formulated curatives

Additives: catalysts, antioxidants, plasticizers, flame retardants, pigments, and fillers. [2]

A variety of these raw materials allows an endless range of tailor-made products with different physical properties. This variety has made it difficult to characterise and model PU in an engineering environment as the individual polymer material can display a range of characteristics and behaviour from elastic solid to a viscous liquid depending on the combination of constituents. PU will always have a non-linear elastic deformation response.

To design and prevent failures of these components in any application it is vital to understand the mechanical characteristics of the various materials. To design complex components like non-pneumatic wheels cannot be done without calculating and predicting the mechanical capabilities of the polyurethanes used. This makes the ability to model polyurethane vital to the business.

2 Background/Context

Material characteristics and properties are easily available for metals detailing stress-strain data is commonly found in material libraries like Ansys Granta [3] and Matlab[4]. Metals are known for its rigidity and typically high tensile strength. Ductile materials such as metals typically display similar material characteristics and therefore have a general stress-strain graph like the one displayed in Figure 2. The behaviour is a well-defined linear elastic region followed by plastic deformation, where the material undergoes permanent deformation. This behaviour is generally characterised by a stress-strain curve that demonstrates a clear yield point and a subsequent region of strain hardening, before necking and failure occurs.

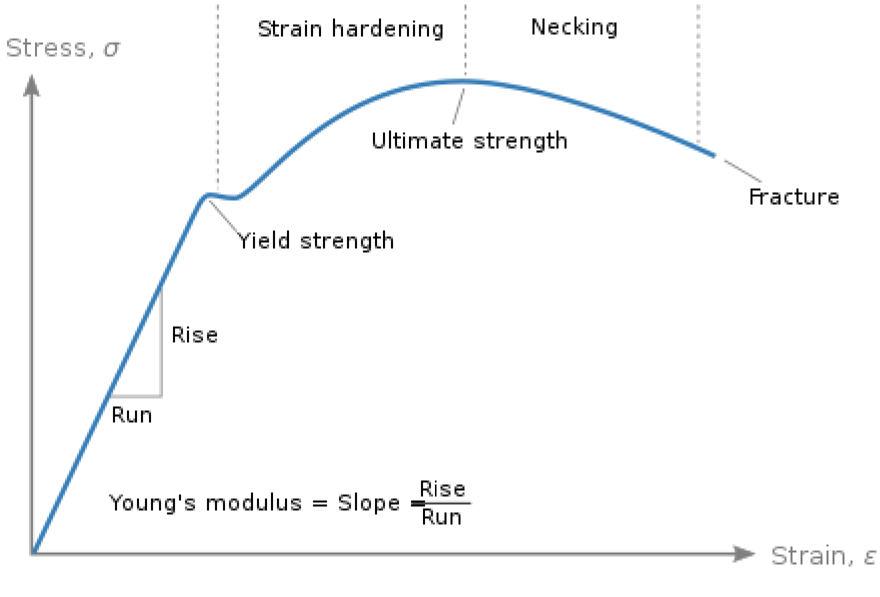

Figure 2: Typical Stress-Strain graph for ductile materials [5]

Elastomers, a class of polymers, however, involve a much more deeper understanding of material science. Elastomers exhibit unique characteristics that are substantially different from those of traditional linear elastic materials like metals. The primary reasons for the complexity in modelling hyperelastic materials can include:

- Non-linear Stress-Strain Relationship

Unlike linear elastic materials, where stress is proportional to strain, hyperelastic materials display a non-linear stress-strain relationship. This non-linearity means that the deformation behaviour under various load conditions is not straightforward, requiring complex mathematical models to accurately describe the material response.

- Large Deformations

Hyperelastic materials can undergo very large strains without permanent deformation. This large, reversible deformability introduces additional complexity in the modelling process, as conventional assumptions of small strains (often used in linear elasticity) are no longer valid, necessitating the use of more sophisticated finite deformation theories.

- Rate Dependence

Some hyperelastic materials exhibit rate-dependent behaviour, meaning their response is time-dependent.

- Material Instabilities

Hyperelastic materials can experience instabilities like buckling or wrinkling under certain loading conditions. Predicting these instabilities is crucial for accurate modelling and requires a deep understanding of the material behaviour beyond the initial linear region.

- Complex Constitutive Models

To accurately represent the behaviour of hyperelastic materials, constitutive models (mathematical descriptions of how a material responds to stress and strain) need to be complicated. These models often involve complex mathematical functions with multiple parameters that need to be determined experimentally.

- Computational Challenges

The non-linear nature of hyperelastic materials often requires iterative and numerically intensive computational methods to solve the governing equations, especially for complex geometries and loading conditions.

Elastomers have unique elastic properties which make it ideal for various applications. This behaviour exhibits a vastly different stress-strain characteristic unlike metals. Elastomers typically undergo huge strains in the order of several hundred percent without any permanent deformation region this is why they are commonly referred to as hyperelastic materials. There is typically no yield limit, and the stress-strain behaviour is seen to be highly nonlinear and monotonically increasing [6]. This results in the modulus of elasticity changing as a function of the strain. This characteristic allows elastomers to absorb significant amounts of energy and makes them ideal for applications requiring energy absorption or vibration damping.

To design components that leverage these inherent material advantages of elastomers requires a critical understanding of the nature of the material properties. This facilitates material selection per application and allows accurate prediction of how these elastomers will behave under various loading conditions ensuring desired reliability and performance.[7]

Polyurethanes are deemed as a hyperelastic material which unlike elastic materials have a non-linear stress-strain function. Hyperelastic materials are characterised using the strain energy density function which defines the energy stored due to deformation on the material. The strain energy density is the strain energy per unit volume which is the area under the stress-strain curve. The strain energy density function allows us to develop a relationship between the stress and strain and perform calculations at high strain values up to 800%.

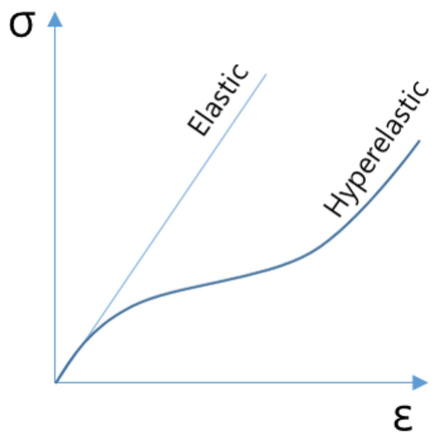

Figure 3: Stress-Strain graph of a hyperelastic material vs an elastic material [8]

2.1 Research Motivation

Urethane Moulded Products (UMP) is a polyurethane specialist design and manufacturing company which produces specialised polyurethane formulations. These formulations need to be characterised, modelled into a FEA simulation to effectively design and develop products to meet specific requirements for its clients. The reasoning for this research is to be able to calculate and analyse designs without manufacturing the product as it is done currently. This proves to be extremely cost and time intensive method which is why the need for this research has presented itself. The research is centred on evaluating the practicality and efficacy of instituting a design cycle that is exclusively reliant on simulation-based methodologies. With this investigative the aim is to distinguish the viability and potential benefits of integrating comprehensive simulation tools throughout the entire design process, thereby streamlining development, enhancing precision, and potentially mitigating the necessity for expensive and time-consuming physical prototypes. The objective is to establish a robust framework that leverages advanced simulation technologies to predict real-world performance, optimize design parameters, and expedite the innovation cycle in a cost-effective and efficient manner.

2.2 Problem Statement

Characterising and modelling hyperelastic polyurethanes produced by Urethane Moulded Products for the preparation of finite element analysis for the development and optimisation of non-pneumatic wheels. This will allow the design and development of wheels for various applications. The simulations have to be able to predict a working concept. The simulation will be validated with experimental testing by manufacturing one prototype and conducting incremental load testing to verify that the design cycle from material testing to simulation is accurate.

3 Literature Review

3.1 Non-pneumatic tyres

Non-pneumatic tyres (NPTs) are wheels which do not use pneumatics (pressure from a gas) to support the vehicle it is attached to, rather it uses a structured design to support the load. Figure 4 shows an NPT that was manufactured at UMP for the USA military by trial and error in the early 2000's.

Figure 4: NPT manufactured at UMP.

Run-flat inserts (RFIs) are a structured wheel inserted into a pneumatic wheel such that when the tyre fails the RFI takes over and allows the vehicle to continue operating.

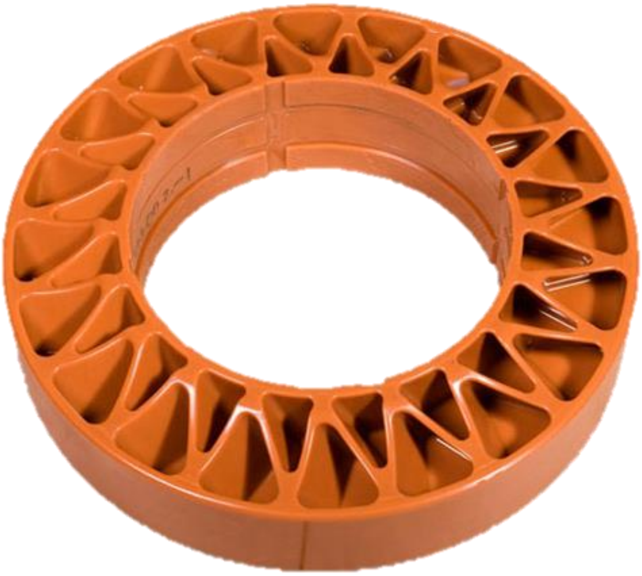

Figure 5: Polyurethane RFI manufactured at UMP.

Both NPT's and RFI's are gaining market traction at an exponential pace due to its significant advantages in many applications. Despite their long-standing dominance in the automotive industry, pneumatic tyres have several inherent drawbacks, such as higher rolling resistance, reduced durability, susceptibility to deflation from punctures, and the need for periodic air pressure checks to ensure optimal performance. Applications such as military vehicles, unmanned vehicles, vehicles without a dedicated suspension and agricultural vehicles can all benefit from the use of NPT's.

A fundamental driving force for the development of NPT's is the need to overcome the inherent characterises of pneumatic tyres. These can include weight (unsprang mass), stiffness, durability, contact pressure and rolling resistance. NPT's can aid to reduce contact pressure with a better distribution area. NPT's can also be designed to have a larger load bearing index for industrial vehicles. RFI's assist when a tyre has a blow out to keep the vehicle operational.

An NPT can be made up of flexible spokes surrounded by a thread. A solid design can also be used however this presents its own set of disadvantages the biggest been a lack of damping.

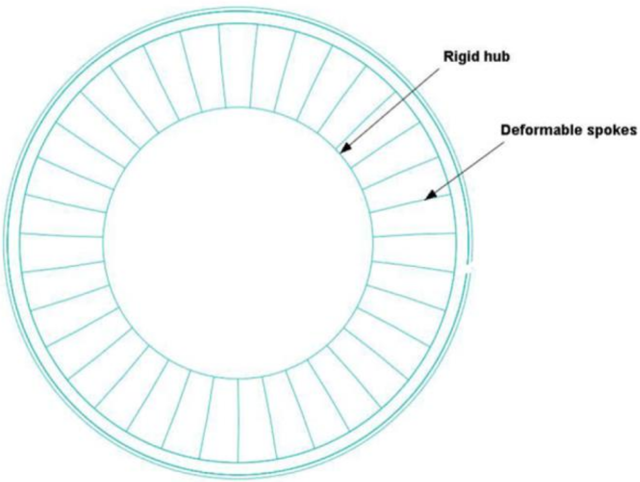

Figure 6: Non-Pneumatic Tyre (NPT) [9]

3.2 Polyurethane as a hyperelastic material

Polyurethane characteristics are very different to that of metals thus resulting in different behaviours and responses when stressed. When a stress is applied large elastic deformation can occur, this deformation is fully recoverable when the load is unloaded. Polyurethane is characterised as an incompressible material as when a load is applied there is negligible volume change. The resulting stress-strain curve is a non-linear curve.[10] This non-linearity makes it difficult to model the behaviour of polyurethane with conventional isotropic material models. Polyurethane exhibits viscoelastic behaviour which is a combination of solid like and viscous liquid behaviour. Viscoelastic materials display time-dependent behaviour an applied load does not immediately create a deformation however, there is a delay between the application of the load and the resulting deformation. The speed of the applied load affects the subsequent deformation in polymeric materials.

When the applied load is removed, the elastic response is linear and all work input into the system is lost. On the other hand, the viscous response is nonlinear, with the force and deformation depending on the rate of loading and the passage of time. By combining the two phases, we now get the Kelvin-Voigt model, which is a viscoelastic material that is graphically represented by a Hookean spring running parallel with a Newtonian dashpot as seen in Figure 7.

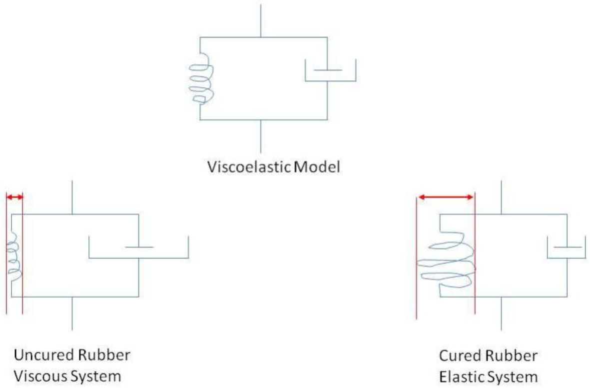

Figure 7: Kelvin-Voigt Viscoelastic System [11]

According to Hooke's law, stress and strain have a linear relationship in elastic solids.

$$\sigma(t) = E\varepsilon(t) \tag{1}$$

Or

$$\frac{d\sigma}{dt} = E\frac{d\varepsilon(t)}{dt} \tag{2}$$

Where:

σ – Stress (MPa)

ε – Strain (mm/mm)

E – elastic modulus (MPa)

T – time (s)

Newtons law for a viscous liquid:

$$\sigma(t) = \eta\frac{d\varepsilon(t)}{dt} \tag{3}$$

The Kelvin-Voigt model for a linear viscoelastic material by combining equations (1) and (3) is obtained:

$$\sigma(t) = E\varepsilon(t) + \eta\frac{d\varepsilon(t)}{dt} \tag{4}$$

Polyurethane is still modelled as a hyperelastic material using the certain hyperelastic material models to aid in its characterisation. These models are used to account for behavioural effects like hysteresis, stress relaxation, Mullin's effect, creep, which makes it difficult to predict the nature [4].

Commonly, elastomers are defined by the strain energy density function. *"W"* which is based on three strain invariants: I_1, I_2 and I_3 [6].

$$W = f(I_1, I_2, I_3) \tag{5}$$

The three invariants represent the principle stretch ratios λ_1, λ_2 and λ_3 which is:

$$I_1 = \lambda_1^2 + \lambda_2^2 + \lambda_3^2 \tag{6}$$

$$I_2 = \lambda_1^2 \lambda_2^2 + \lambda_2^2 \lambda_3^2 + \lambda_3^2 \lambda_1^2 \tag{7}$$

$$I_3 = \lambda_1^2 \lambda_2^2 \lambda_3^2 \tag{8}$$

Where:

λ – ratio of final length to initial length in each direction.

This use of the strain energy density function is currently the acceptable way to characterise elastomers from a first principle state as this is used to determine the specific material constants.

The work required per unit volume to deform a material from a stress-free reference or initial state to a final state is known as the strain energy density of a solid. Utilizing statistical mechanics and continuum mechanics with invariant and stretch-based methods, the strain energy density functions were created.

3.2.1 Statistical Mechanics Approach using Gaussian and Non-Gaussian Models

According to the statistical mechanics method, elastomeric material is composed of randomly arranged molecule chains. The total end-to-end length of a chain (r) in the Gaussian model is specified by:

$$P(r) = 4\pi \left(\frac{3}{2\pi n l^2}\right)^{\frac{3}{2}} r^2 \exp\left(-\frac{3r^2}{2nl^2}\right) \tag{9}$$

where l is the length of each link and n is the number of chains in the connection. The root mean square value of r determines the chain's initial length.

$$L_0 = \left(\overline{r^2}\right) = (nl^2)^2 = \sqrt{nl} \tag{10}$$

The chain structure deforms when a force is applied, especially if N chains are deformed by a primary stretch state $(\lambda_1, \lambda_2, \lambda_3)$ and the deformation causes the chain length r to be smaller than the chain's complete length *nl*. The difference in entropy between the loaded and unloaded (free) states is used to calculate the strain energy function W.

$$W = -\frac{1}{2} N k \theta (\lambda_1^2 + \lambda_2^2 + \lambda_3^2 - 3) \tag{11}$$

where T is the absolute temperature and *k* is the Boltzmann's constant. Only when *r* is much less than the total length *nl* (*r*<<*nl*) does equation (11) hold true. The actual force deflection behaviour diverges significantly from that predicted by the Gaussian model for larger deformations of *r/nl* >.40. The non-Gaussian nature of the chain stretch must therefore be considered for higher deformations. Given by is the chain's consequent non-Gaussian force-extension connection.

$$f = -\frac{k\theta}{l} L^{-1} r' = -\frac{k\theta}{l} L^{-1}\left(\frac{\lambda}{\sqrt{n}}\right) \tag{12}$$

where the inverse Langevin function $L^{-1}\, r/nl$ is defined as

$$\frac{r'}{nl} = \coth\beta - \frac{1}{\beta} = L\beta; \quad \beta = L^{-1}\left(\frac{r'}{nl}\right) \tag{13}$$

A network structure is built to get a model that correlates the extension of the individual chains to the applied force-deformation. The network models are displayed in Figure (1.6). The relationship between chain deformation and unit cell deformation differs in each of the three models. The chains of the "3-chain" concept are positioned along the cube's axes. The stretch on each chain then corresponds to the principal stretch value as the chains deform uniformly with the cell. Next, we obtain the strain energy density function from:

$$W = \frac{Nk\theta}{3}\sqrt{n}\left[\lambda_1\beta_1 + \sqrt{n}ln\left(\frac{\beta_1}{\sinh\beta_1}\right) + \lambda_2\beta_2 + \sqrt{n}ln\left(\frac{\beta_2}{\sinh\beta_2}\right) + \lambda_3\beta_3 + \sqrt{n}ln\left(\frac{\beta_3}{\sinh\beta_3}\right)\right] \tag{14}$$

Where:

$$\beta_i = \mathcal{L}^{-1}\left(\frac{\lambda_i}{\sqrt{n}}\right)$$

For *i* = 1; 2; 3

The chains of the "8-chain" model, also called the Arruda-Boyce model, are positioned along the unit cell's diagonals, and change shape along with the cell. The stretch in each individual chain is equal to the root mean-square of the applied stretches, and the strain energy function is given by. This is possible because of the symmetry of the chain construction, which keeps the interior point at the same location throughout the applied deformation.

$$W = Nk\theta\sqrt{n}\left[\beta_{\text{chain}}\lambda_{\text{chain}} + \sqrt{n}ln\left(\frac{\beta_{\text{chain}}}{\sinh\beta_{\text{chain}}}\right)\right] \tag{15}$$

3.2.2 Invariant Based Continuum Mechanics Approach

The three different strain invariants can be defined using equations 6, 7 and 8 for a material that is isotropic and hyperelastic, according to the assumption that the strain energy density function must depend on the stretch ratio. The stretch ratio is defined as:

$$\lambda_i = 1 + \varepsilon \tag{16}$$

stretch ratios are used as a deformation metric in elastomer theory because of the large magnitudes of deformations occurring. The strain energy density function can be expressed in general as

$$W(I_1, I_2, I_3) = \sum_{i,j,k=0}^{N} C_{ijk}(I_1 - 3)^i (I_2 - 3)^j (I_3 - 3)^k + \sum_{i=1}^{N} \frac{1}{D_i}(J_{\mathrm{el}} - 1)^{2i} \tag{17}$$

Since the elastomeric material is assumed to be incompressible, the third strain invariant (I_3) equals 1, and the strain energy function only depends on I_1 and I_2. C_{ijk} and D_i are material parameters in Equation 17, and D_i specifies the material's compressibility. The value of D_i is zero for an incompressible substance. Consequently, the equation becomes equation 18:

$$W(I_1, I_2) = \sum_{i,j=0}^{N} (I_1 - 3)^i (I_2 - 3)^j \tag{18}$$

When C_{ij} with $j \neq 0$ are zero, the simplest material model can be attained which is called the Neo-Hookean material model and is shown in equation 19:

$$W = C_{10}(I_1 - 3) \tag{19}$$

When *N = 1*, equation 20 is obtained which is known as the Mooney-Rivlin material model:

$$W = C_{10}(I_1 - 3) + C_{01}(I_2 - 3) \tag{20}$$

As it depends on the second strain invariant, the Mooney-Rivlin form can be regarded as an improvement over the Neo-Hookean form (l_2). It is essential to notice that the linear function of the invariants is utilized by both the Neo-Hookean and Mooney-Rivlin forms. The function takes on a reduced polynomial form when the second strain invariant (l_2) from Equation 17 is removed. The strain energy function's Yeoh form is determined as follows by the reduced polynomial function with N = 3.

$$W = \sum_{i=1}^{3} C_{i0}(I_1 - 3)^i + \sum_{i=1}^{3} \frac{1}{D_i}(J_{\mathrm{el}} - 1)^{2i} \tag{21}$$

3.2.3 Stretch Based Continuum Mechanics Approach

The stretch-based continuum mechanics approach is based on the notion that the major stretches rather than the invariants can be used to express the strain energy potential. The strain energy function's Stretch based Ogden form is defined as equation 22:

$$W = \sum_{i=1}^{N} \frac{2\mu_i}{\alpha_i^2} \left(\lambda_1^{-\alpha_i} + \lambda_2^{-\alpha_i} + \lambda_3^{-\alpha_i} - 3 \right) + \sum_{i=1}^{N} \frac{1}{D_i} (J_{\mathrm{el}} - 1)^{2i} \tag{22}$$

where *Di = 0* for an incompressible material and μi and αi are material constants. The material and the stretch ratios (strains) it will experience over its service life have a significant role in the material model selection. As a rule, simple models like Mooney-Rivlin are adequate for small strains of approximately 100% or $\lambda \leq 2$, but for higher strains, a higher order material model like the Ogden model may be necessary to accurately simulate the "upturn" or strengthening that can occur in some materials at higher strains. Biomaterials, including as human tissues and polymeric materials used in medical implants (such as cardiac pacemaker seals, artificial spinal discs, and artificial knee joints), can also be tested using the theory of elastomeric materials.

3.3 Hyperelastic materials in Simulations

To handle the large strains in hyperelastic materials in simulations there are techniques that can be applied to achieve results. Material testing data must be performed to plot stress-stain responses per material. There are three main strategies to help process experimental data to deduced elastic properties of materials built up of idealized representations to the highly non-linear hyperelastic data:

3.3.1 Statistical Models

Using statistical mechanics, models such as Arruda-Boyce model and the Gent model have been developed. Both models are, fundamentally based on the first strain invariant, and the Statistical Mechanics Approach using Gaussian and Non-Gaussian Models by which the state of their near or complete incompressibility is defined.

3.3.2 Phenomenological Models

This category of models approaches the problem from the perspective of molecular structure pertaining to continuum material behaviour. The Neo-Hookean model, the Polynomial model, the Mooney-Rivlin model, the Yeoh model, are the notable models in this category. The underlying principle of these models bases on strain invariants to give a macroscopic outlook in materials' deformation.

3.3.3 Response Function Models

These models are derived from the derivatives of elastic potential functions and offer a mathematical description of the material's response to deformation. A prominent example within this category is the Ogden model, distinguished by its formulation based on the principal stretch ratio.

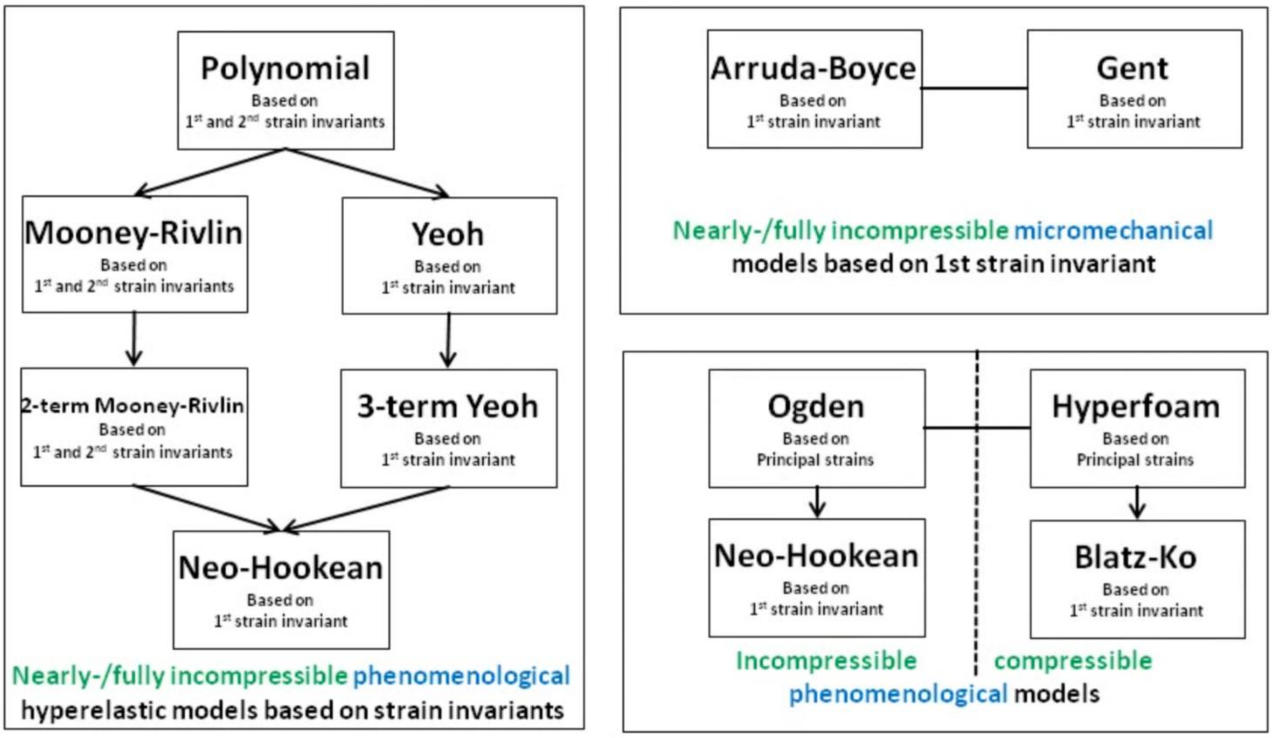

Figure 8: Summery of hyperelastic models [12]

Many Finite Element Analysis (FEA) software packages like ANSYS have offered a variety of hyperelastic models to serve various simulation needs. Some of the most common models supported by these applications are the following:

1) Neo-Hookean Model
2) Mooney-Rivlin Model
3) Ogden Model
4) Polynomial Model
5) Yeoh Model
6) Arruda-Boyce Model

3.4 Mould making and designing of moulds for casting PU.

Moulds can be made of many different types of materials. The mould design must consider:

- Number of castings
- Finish of product
- Cost
- Time
- Demoulding

Metal moulds can be cleaned in solvent. Solvents or release agents containing solvents should not be used on polymer moulds. (PU absorbs solvent. It swells and deteriorates). The solvent NMP (900S) will completely dissolve urethane elastomers.

The surface of metal moulds can be highly polished, giving an excellent appearance to the product and easier demould. It is important that whatever mould material is used, the surface is clean and free from pinholes, contaminants, and other imperfections.

3.4.1 Moulding methods

3.4.1.1 Open casting:

A simple and often used method. The components are mixed together and poured into the mould. If a large article is being cast, it can be cast in stages, provided that the time delay between castings is short. It is important to pour carefully to avoid air entrapment.

The open surface is flat but has a meniscus which may not be acceptable where dimensions must be accurate. It may be possible to grind it flat in some cases. This is dependent on both the particular grade of material and the finish required. In cases where the mould has an intricate design, it may be preferable to fill from the bottom using a filling tube. This may help to eliminate air entrapment.

3.4.1.2 Compression moulding:

This method may be used where close tolerances are required. The resin is poured into a compression mould and held together under pressure until gelled. Mould venting is usually not required but depends on mould design.

3.4.1.3 Rotational moulding:

This method is used for casting hollow objects, such as a ball. The resin is deposited into one half of the mould which is then closed and rotated until the resin has gelled. The potlife should be long and ideally the viscosity increase should be uniform for the best results possible to cast with wall thickness of 1.3 cm. The speed of rotation will have to be determined and is likely to be between 2-15 rpm along two axes.

3.4.2 Mould temperature.

For hot casting, the mould is usually preheated in the oven to 80°C - 100°C. Other systems may require a different mould temperature. Please note that in some systems higher mould / oven temperature can lead to lower hardness.

The mould temperature will affect:

- Shrinkage
- Potlife
- Demould

3.4.3 Shrinkage:

To minimize shrinkage for hot cures it is recommended that the mould temperature is ± 10°C higher than the material temperatures. The average linear shrinkage of urethanes is ± 1.5% - 2.0%. Where close tolerances are required (e.g. seals) you will have to account for the amount of shrinkage. The shrinkage will vary according to the system used and the mass of the casting.

3.4.4 Cold mould

Some systems are more prone to give cold mould effect, this is seen as a tree effect on the PU after casting. This is where the exotherm of the system causes the material to shrink and pull away from the colder mould surface. The material in contact with the cold mould takes longer to gel and it flows into the gaps formed by the shrinkage. The mould is usually heated to a higher temperature to prevent this from happening.

3.4.5 Mould design

The mould for the casting of the testing materials were chosen to be CNC machined from aluminium. Aluminium was chosen to produce a cast PU product of high surface quality. Due to the good thermal conductivity of Al, it also is beneficial to negate any air entrapments into the PU during casting. To aid in the release of air Locating pins are used for the two parts of a mould need to be put together accurately.

3.5 Testing of polyurethane

The polyurethane developed for this analysis will need to be characterised by physical testing to plot the stress-strain curves. One subject of the research is to fully characterise polyurethane using one or ideally all of the physical test available such as:

1. Uniaxial tension
2. Uniaxial compression
3. Planar shear
4. Volumetric compression

3.5.1 Uniaxial Tension Test

Test for Uniaxial Tension: The dumbbell specimen is used for this test. The ASTM D412 standard and the ISO 37 standard are the two standards that are applicable to this test.[13] According to the specification, this test must be carried out at room temperature with a 500mm/min strain rate. Stress-strain data is logged throughout the test and the test is continued until the specimen fails.

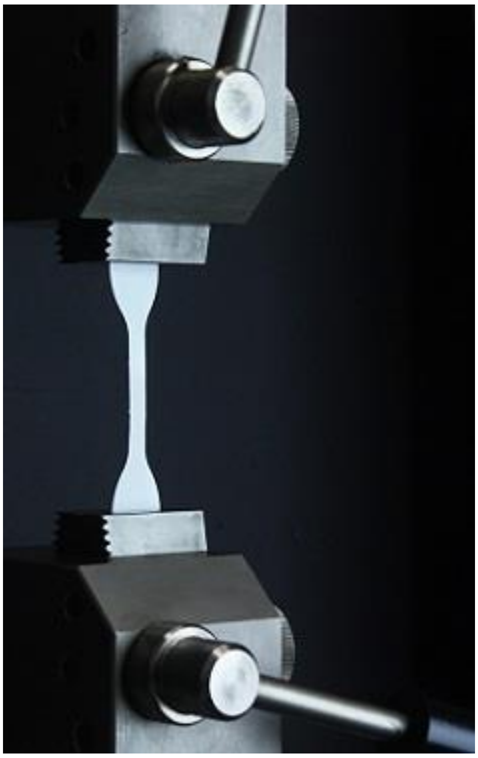

Figure 9: Uniaxial Tension Testing [14]

3.5.2 Uniaxial Compression Set

A button specimen is used for this test. The ASTM D595 standard and the ISO 7743 standard are the two standards that are currently available for this test. This test is run at room temperature. This test yielded information on stress-strain and force deflection. Uniaxial compression test specimens, in contrast to uniaxial tension test specimens, are button-shaped with a diameter of 29mm and a thickness of 12.5mm. [15]

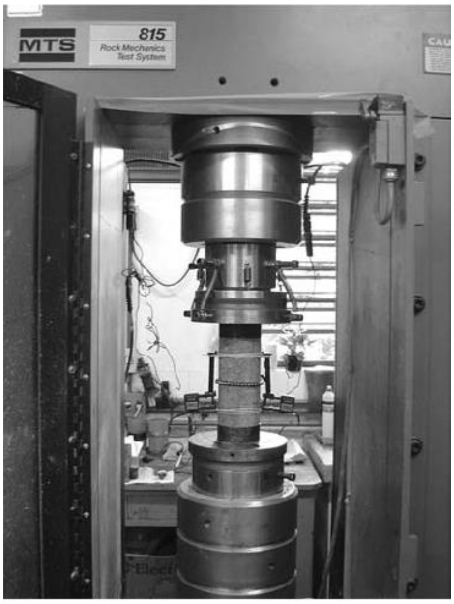

Figure 10: Uniaxial compression test equipment [16]

3.5.3 Pure Shear Test

This test is often referred to as a planar tension test due to it being a wide tension test. Since hyperelastic material is almost incompressible, the specimen experiences pure shear stress during testing. To prevent the specimen from thinning laterally, the breadth of the specimen is kept greater than the length of the specimen. The breadth to length ratio is maintained at greater than 10:1. The strains that occur during testing can be calculated directly from the grasp travel of the machine [17] or evaluated using non-contacting extensometers.

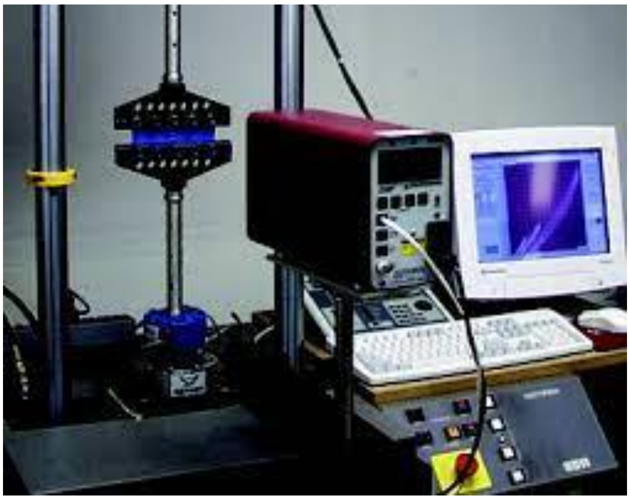

Figure 11: Shear testing [18]

3.5.4 Volumetric Compression Test

Bulk modulus test is another name for the volumetric compression test. This is because the bulk modulus may be determined from the curve's starting slope, which was obtained during this test. This test looks at the material's capacity for compression. A button-like specimen is used in this test. By putting more pressure on it, it is compressed. Consequently, a graph of pressure to volume ratio is produced. [19]

Figure 12: Volumetric compression test [18]

3.6 FEA Implementation

Engineering strain and stress data should be derived from the mechanical tests. For the curve fitting, only engineering stress and strain data are employed. In the volumetric testing real stress measurements are necessary. The stress-strain data needs to be processed to a more efficient, useable format that can be provided to ANSYS as an input as a stress-strain curve that accurately depicts a material curve without an exorbitant amount of data. Large amounts of data require high amounts of processing power making the process inefficient. The right hyperelastic model is selected based on the percentage strain and curve fit is used with the least amount of error to determine the material constants of the hyperelastic models. To determine whether a material is defined correctly in ANSYS is to analyse a simulation that has already been run and compare the findings with experimental data. [20]

3.6.1 Material Assumption as a hyperelastic elastomer

1. No hysteresis losses – work done on the PU is stored as internal energy and all energy is recovered upon unloading.
2. PU is nearly or fully incompressible.
3. PU is isotropic.

3.6.2 Curve fitting.

Curve-fitting is utilized to generate the material constants from the stress-strain data from the FEA support tests. By comparing the stress-strain findings from the material model to the stress-strain data from experimental tests, the constants are determined. The constants are obtained through an iterative process utilizing the least squares fit method, which lowers the relative error between the anticipated and experimental values. When fitting material models with coefficients that are linear, such as Neo-Hookean, Mooney-Rivlin, Yeoh, etc., one uses the linear least squares fit method. A nonlinear least squares method is utilized for material models, such as Ogden and others, that have nonlinear co-efficient relationships. The relationships for the biaxial test take the form of equation 23:

$$\lambda_1 = \lambda_2 = \lambda_B, \quad \lambda_3 = \frac{1}{\lambda^2}$$
$$S_B = \frac{\partial U}{\partial \lambda_B} \tag{23}$$
$$S_B = 2\left(\lambda^2 - \frac{1}{\lambda^4}\right)(C_{10} + \lambda^2 C_{01})$$

where λ_B and S_B are the stretch and nominal stress.

Finding the material constants is crucial for modelling hyperelastic materials. To reduce the inaccuracy in fitting the experimental data points, a function is assumed, and its coefficients are calculated. The coefficients C_{10} and C_{01} would be the unknowns in this situation, and the function would be the relation for stress (S_B) stated in Equation 23.

3.6.3 Regression Analysis

A regression analysis objective is to create a model that fits the stress-strain data as closely as possible. The outcomes of the regression analysis for Mooney-Rivlin constants using the least squares method are displayed in Figure 13.

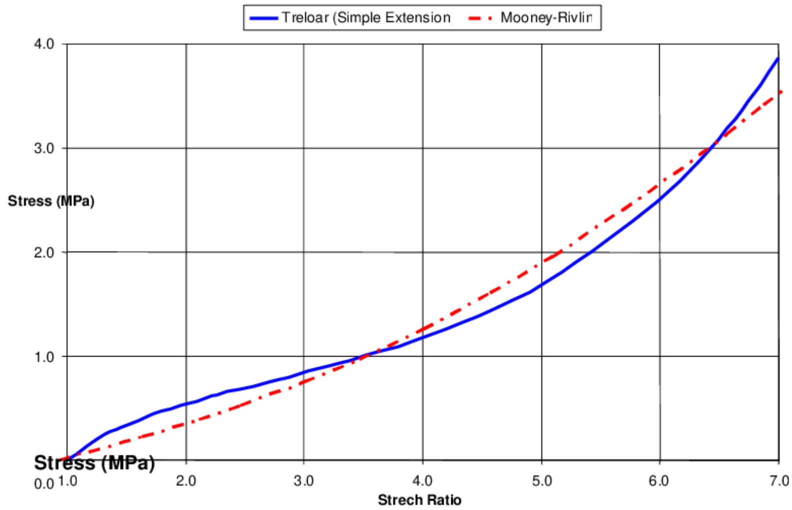

Figure 13:Regression Analysis using Mooney-Rivlin [20]

Equation 23 illustrates the function that can be applied to a biaxial test to forecast the nominal stress value in a biaxial state (S_B). Equation 23 can then be reduced to equation 24:

$$\sigma = 2\left(\lambda^2 - \frac{1}{\lambda^4}\right)C_{10} + 2\left(\lambda^4 - \frac{1}{\lambda^2}\right)C_{01} \tag{24}$$

A function can be created after estimating the material properties C_{10} and C_{01} using the linear least-squares method and is expressed in equation 25:

$$f = \sum_{i=1}^{n}(C_{10}\psi_1(\lambda_i) + C_{01}\psi_2(\lambda_i) - \sigma)^2 \tag{25}$$

Where:

$$\psi_1(\lambda_i) = 2\left(\lambda^2 - \frac{1}{\lambda^4}\right)$$
$$\psi_2(\lambda_i) = 2\left(\lambda^4 - \frac{1}{\lambda^2}\right) \tag{26}$$

The following condition must also be met by the data points that follow equation 24:

$$\frac{\partial F(C_{10}, C_{01})}{\partial C_{10}} = 0 \tag{27}$$

$$\frac{\partial F(C_{10}, C_{01})}{\partial C_{01}} = 0 \tag{28}$$

Which is the same as equation 27 and 28:

$$2\sum_{i=1}^{n}(C_{10}\psi_1(\lambda_i)+C_{01}\psi_2(\lambda_i)-\sigma)\psi_1(\lambda_i)=0 \quad (29)$$

$$2\sum_{i=1}^{n}(C_{10}\psi_1(\lambda_i)+C_{01}\psi_2(\lambda_i)-\sigma)\psi_2(\lambda_i)=0 \quad (30)$$

Which can then be rearranged to equation 29 and 30:

$$\left(\sum_{i=1}^{n}\psi_1^2(\lambda_i)\right)C_{10}+\left(\sum_{i=1}^{n}\psi_1(\lambda_i)\psi_2(\lambda_i)\right)C_{01}=\sum_{i=1}^{n}\psi_1(\lambda_i)\sigma_i \quad (30)$$

$$\left(\sum_{i=1}^{n}\psi_1(\lambda_i)\psi_2(\lambda_i)\right)C_{10}+\left(\sum_{i=1}^{n}\psi_2^2(\lambda_i)\right)C_{01}=\sum_{i=1}^{n}\psi_2(\lambda_i)\sigma_i \quad (31)$$

Calculating ψ1 and ψ2 using equation 26. The values of each term can be found using equations 32 to 37:

$$\sum_{i=1}^{n}\psi_1^2(\lambda_i)=a \quad (32)$$

$$\sum_{i=1}^{n}\psi_1(\lambda_i)\psi_2(\lambda_i)=b \quad (33)$$

$$\sum_{i=1}^{n}\psi_1(\lambda_i)\sigma_i=c \quad (34)$$

$$\sum_{i=1}^{n}\psi_1(\lambda_i)\psi_2(\lambda_i)=d=b \quad (35)$$

$$\sum_{i=1}^{n}\psi_2^2(\lambda_i)=e \quad (36)$$

$$\sum_{i=1}^{n}\psi_2(\lambda_i)\sigma_i=f \quad (37)$$

It is now possible to determine the constants for the Mooney-Rivlin material model by resolving the linear system of equations:

$$\begin{bmatrix} a & b \\ b & e \end{bmatrix}\begin{Bmatrix} C_{10} \\ C_{01} \end{Bmatrix}=\begin{Bmatrix} c \\ f \end{Bmatrix} \quad (38)$$

The method shown above demonstrates an easy way to determine the material constants analytically.

3.7 Non-linear FEA

Non-linear FEA requires methodologies capable of accurately characterizing the behavioural responses of hyperelastic materials. Consequently, the strain energy function emerges as a quintessential candidate for modelling hyperelastic materials in FEA software. This function is generally articulated as contingent on the strain tensor within the material, and the stress engendered within the entity at any given strain is derivable from this strain energy function. Typically, the strain energy function is decomposed into deviatoric and volumetric strain energies, underscoring the fact that the stress response of the material is intrinsically linked to the nature of strain it experiences.

It is imperative to recognize the modalities of deformation that these materials may undergo. Within a FEA solver hyperelastic materials require three principal modes of deformation: uniaxial tension, uniaxial compression, and shear deformation to be defined such that models can calculate the stress tensor in a simulation.

In the realm of hyperelastic material modelling, several models are prevalent, each with its unique formulation and application spectrum. The Neo-Hookean model, characterized by a linear relationship between strain energy potential and the first strain invariant, stands out for its simplicity. Despite the linear equation, the inherent non-linearity of the strain invariant ensures that the model retains a non-linear character. The general form of neo-Hookean strain energy potential as explained in equation 40:

$$U = C_{10}(I_1 - 3) + \frac{1}{D_1}(J_{el} - 1)^2 \tag{40}$$

Where:

U is the strain energy per unit volume.

C_{10} and D_1 are temperature dependent material parameters.

The initial shear modulus (μ_0) and bulk modulus (K_0) are related to C_{10} and D_1 as shown in equation 41:

$$\mu_0 = 2C_{10}, \quad K_0 = \frac{2}{D_1} \tag{41}$$

The Mooney-Rivlin model, on the other hand, incorporates additional invariants and material constants, rendering it adept at capturing more non-linear material behaviours. The Mooney-Rivlin form of strain energy potential in equation 42:

$$U = C_{10}(I_1 - 3) + C_{01}(I_2 - 3) + \frac{1}{D_1}(J_{el} - 1)^2 \tag{42}$$

Where:

U is the strain energy per unit volume.

C_{10}, C_{01} and D_1 are coefficients of the Mooney-Rivlin material function.

The initial shear modulus (μ_0) and bulk modulus (K_0) are related to the parameters by the following relation:

$$\mu_0 = 2(C_{10} + C_{01}), \quad K_0 = \frac{2}{D_1} \tag{43}$$

Likewise, the Ogden model, formulated using principal stretches, allows for an increased number of terms to accommodate heightened non-linearity, with each term contributing material constants to the overall model.

Addressing the particularities of compressible materials, models such as the Ogden 4 are tailored to account for the significant volumetric deformation characteristic of such materials. This model, and others similar to it, exhibit a tight coupling between deviatoric and volumetric terms, essential for accurately capturing the material's deformation behaviour in an FEA approach. The determination of the number of terms to be included in a model is guided by the material's response characteristics, with each term typically representing a distinct aspect of the material's microstructure, such as polymer chain configurations bearing load.

The incompressibility term in hyperelastic material models in FEA, particularly in modelling nearly incompressible materials. This term, intimately associated with the material's initial bulk modulus, dictates the degree of incompressibility, with a diminutive value signalling heightened incompressibility. For materials exhibiting marginal compressibility, the initial bulk modulus is recommended to be several magnitudes higher than the initial shear modulus to derive a suitably small value for the incompressibility parameter.

3.8 Choice of materials

The use of hyperelastic materials, such as PU, is critically important due to their inherent shearing characteristics. These characteristics significantly influence a multitude of factors, including flexibility, energy dissipation, damping, and the distribution of pressure between the Non-Pneumatic Tyre (NPT) and the road surface. This interplay of material properties and mechanical behaviour is pivotal in enhancing the performance and operational efficiency of tyre-road interactions. The choice of materials for testing and ultimately for the casting of the wheel was based on the following factors:

- outstanding dynamic performance
- excellent retention of properties
- high load bearing capabilities

A PU system which expands performance and provides extending part life in demanding mechanical applications and in harsh chemical and thermal environments is needed.

4. Research Questions

4.1 Critical Research Question

How can polyurethane be characterised, modelled and be validated in FEA for the design of non-pneumatic wheels?

1. What is an appropriate method to characterise material behaviour of polyurethanes (hyperelastic materials)?
2. How can test data be formatted into FEA to define a material for analysis either using varies hyperelastic material models or creating a response function?
3. How accurately can FEA modelling predict behaviour?
4. How can the design of non-pneumatic wheels be optimised with FEA?

4.2 Research Objectives

- Characterise polyurethane material behaviour.
- Determine an accurate hyperelastic model for polyurethane manufactured at UMP.
- Develop a method to simulate non-pneumatic wheels in ANSYS.
- Verify and validate simulated results with experimental results.
- Optimise wheel design geometry for the most cost-effective use of polyurethane for a wheel.

5. Research Method

5.1 Material Testing

To characterise PU as a hyperelastic material it must be defined and satisfy a mathematical material model for nonlinear finite element analysis. The testing is often misconducted as there are no appropriate experimental tests defined as an international standard for the characterising of elastomers. The complex mathematical models used to define the nonlinear and incompressible properties of elastomers require specific stress-strain data. The stress-strain data is produced by stretching the PU samples in various modes of deformation to define how the material will react in various loading conditions. At least 3 different modes of stress-strain curves are required to accurately map out a materials behaviour to characterise the behaviour in 3 different state planes. Uniaxial compression, planar shear and uniaxial tension tests were conducted to capture the elastomeric behaviour. The test rate is quasi-static and run at a very slow speed, approximately $0.02s^{-1}$ strain rate.

The testing of materials for the stress-strain data at varying temperatures is pivotal for characterising hyperelastic materials due to several factors:

5.1.1 Temperature-dependent material behaviour

Hyperelastic materials display mechanical properties that are influenced by temperature. Properties like hardness and modulus are significantly affected by temperature changes. Hence, conducting tests at various temperatures is vital to discern how these properties transform with temperature fluctuations.

5.1.2 Validation of material models

Models like Mooney-Rivlin or Ogden, which describe hyperelastic materials, often include temperature-dependent parameters. To simulate material behaviour accurately under different conditions, it is imperative to have experimental data from tests conducted at various temperatures. This aids in the validation and calibration of these models, leading to more realistic predictions of how the material behaves in actual applications.

5.1.3 Heat Generation

Hyperelastic materials can also generate heat when an alternating stress is applied. Understanding the behaviour of these materials under diverse thermal conditions is essential for developing products that maintain reliable performance over a broad temperature range. Temperature testing is crucial, offering invaluable insights for product development and design enhancement.

The testing temperatures decided based on melting temperature of the PU. PU general operating conditions is between -45℃ and 80℃. If the PU exceeds 80℃ it will fail. For this reason, 60℃ should be the maximum operating range for the PU. Therefore, the PU stress-strain data will be tested at:

- Ambient temperature - 23℃
- 40℃
- 60℃

Such data are fundamental for accurately characterising hyperelastic materials, validating material models, ensuring product reliability, and supporting ongoing research and development within the domain of mechanical engineering.

Figure 14: PU sample been tensile tested.

5.1.4 Tensile testing

For pure tensile strain state during experimental testing, it is imperative that the specimen be considerably elongated in the direction of tensile loading, exceeding its dimensions in width and thickness in its overall height. This experimental condition is designed to eliminate lateral constraints, thereby preventing the specimen from experiencing thickness reduction. It is a fundamental requirement that the specimen's length be a minimum of ten times its width or thickness to ensure the integrity of the tensile strain distribution.

While the conventional "dogbone" specimen geometry is commonly used, it is not an absolute necessity for this experimental setup, as the primary objective is to prevent premature failure of the specimen, testing can be seen in Figure 15. The experimental design does not stipulate a definitive size for the specimen; however, length in this context specifically denotes the span between the clamps of the testing apparatus.

The act of securing the specimen within the clamps introduces a complex and undefined state of stress and strain within the constraints of the clamping area. Consequently, it is crucial to measure the strain on the specimen at a region sufficiently distanced from the clamps, where a state of pure tensile strain is assuredly present. This careful approach is paramount in ensuring the accuracy and reliability of the strain measurements, thereby upholding the integrity of the experimental results.

Figure 15: PU been tested in a heating chamber.

5.1.5 Compression Testing

The analysis of elastomers commonly employs compression experiments. These tests aim for pure states of strain, yet achieving this experimentally in compression proves very challenging. Friction between the test specimen and the instrument's platens hinders the specimen from fully expanding laterally during compression. Even minimal friction coefficient levels, for instance, $\mu = 0.1$, between the specimen and the platen can induce significant shearing strains, altering the stress response to straining. Notably, the maximum shear strain often surpasses the maximum compression strain. Correction of the data is impossible due to the actual friction been an unknown.

5.1.6 Volumetric Compression

This method investigates material compressibility. It involves compressing a cylindrical specimen, confined within a fixture. The actual displacement during this process is minimal, necessitating precise measurement of only the specimen's compliance, disregarding the instrument's stiffness. The bulk modulus is defined by the initial slope of the stress-strain function's outcome. Typically, this value is 2-3 orders of magnitude higher than elastomers' shear modulus.

Figure 16: Compression testing of PU sample.

5.1.7 Pure Shear Testing

The Pure Shear specimen test is extensively utilized to characterize the stress-strain properties in terms of a shearing stress applied. It involves a thin rectangular sheet that is secured or adhered at its sides to inhibit expansion in direction 1 while the material is stretched in the direction of its length (2 plane). The sheet is allowed to contract in the thickness dimension (3 plane). To ensure proper constraint and uniformity, the width of the specimen must be at least eight times greater than its height. Additionally, this test piece is also recognized by the terms Constrained Tension and Planar Tension. The schematic representation of the test piece is depicted in Figure 17:

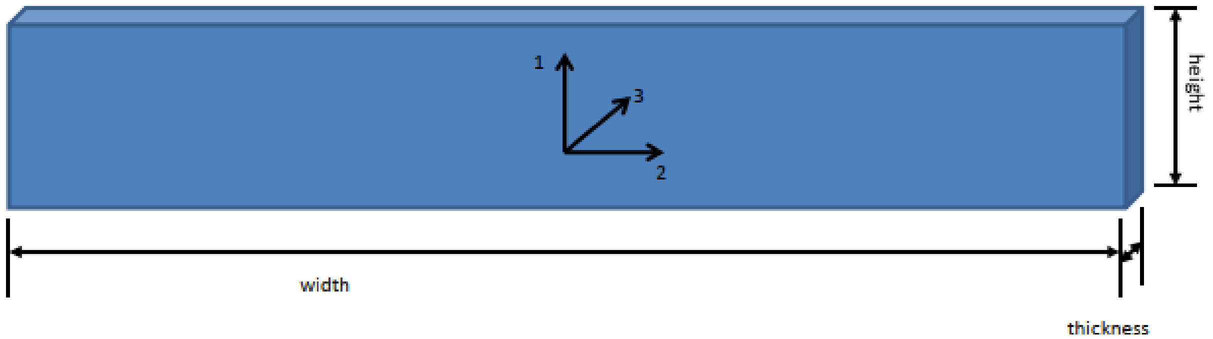

Figure 17: While constraining the strain in the 2, the clamping jaws only permits strain in 1.

The term "shear" is used to describe a deformation in which the parallel planes keep on being parallel but develop lateral displacement relative to one another, hence skewing the lines being originally perpendicular to the displacing direction. For instance, look at the piece under a Simple Shear test shown in Figure 2. It is gripped or bonded along its long edges. The deformation is imposed by displacing the top grip parallel to the bottom grip.

Figure 18: To achieve a shear stress in the perpendicular lateral direction, strain is applied on the lateral displacement of the clamping jaws therefore creating displacement perpendicular to the lateral.

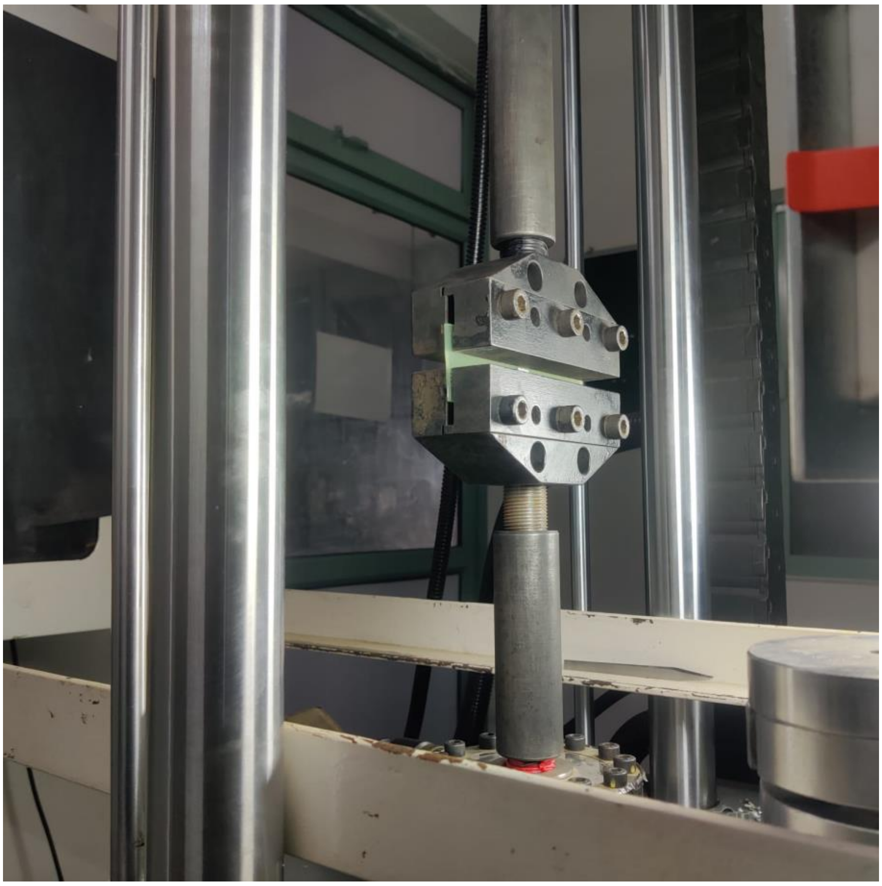

Figure 19: Planar Shear testing on PU.

Describing the state of deformation in a homogenously strained Pure Shear test piece. The deformation gradient F is written in terms of the axial stretch λ. Incompressibility is assumed.

$$F = \begin{bmatrix} \lambda & 0 & 0 \\ 0 & 1 & 0 \\ 0 & 0 & \lambda^{-1} \end{bmatrix} \tag{44}$$

Calculating the velocity gradient tensor L in equation 40:

$$L = FF^{-1} = D + W = \frac{i}{2}\begin{bmatrix} 1 & 0 & 0 \\ 0 & 0 & 0 \\ 0 & 0 & -1 \end{bmatrix} \tag{45}$$

D is the symmetric rate of deformation tensor, identical with L, because of L's symmetry. This also implies that the anti-symmetric spin tensor W is zero. Mohr's circle can be constructed for the rate of deformation tensor.

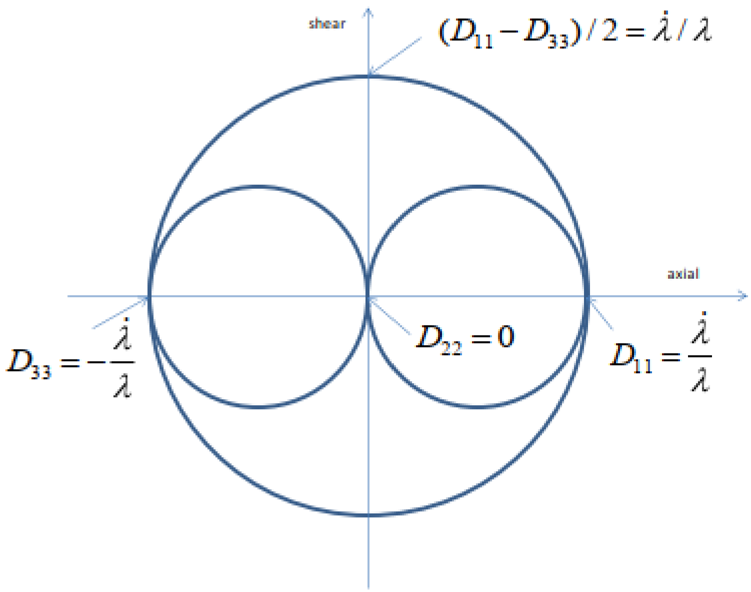

Figure 20: Mohr’s circle on the rate of deformation tensor for the Pure Shear test piece.

Mohr’s circle connecting the major and minor principal deformation rates is centred at zero. Hence the value of the maximum shearing deformation rate equals the major principal deformation rate. Using the plane of the maximum shearing rate, the associated axial deformation rate is zero. This is the first sense in which the subject test piece is producing a “Pure Shear”.

5.2 Moulds for material testing

To perform the material tests the specific formulation of PU will have to be cast into test buttons and plaques to fit into the clamping jaws of the material testing machines. The samples required are: 7-8 ASTM Plaques of 150mm x 150 mm x 1-3 mm thickness and 6 compression set buttons (29 mm diameter and 12.5mm height).

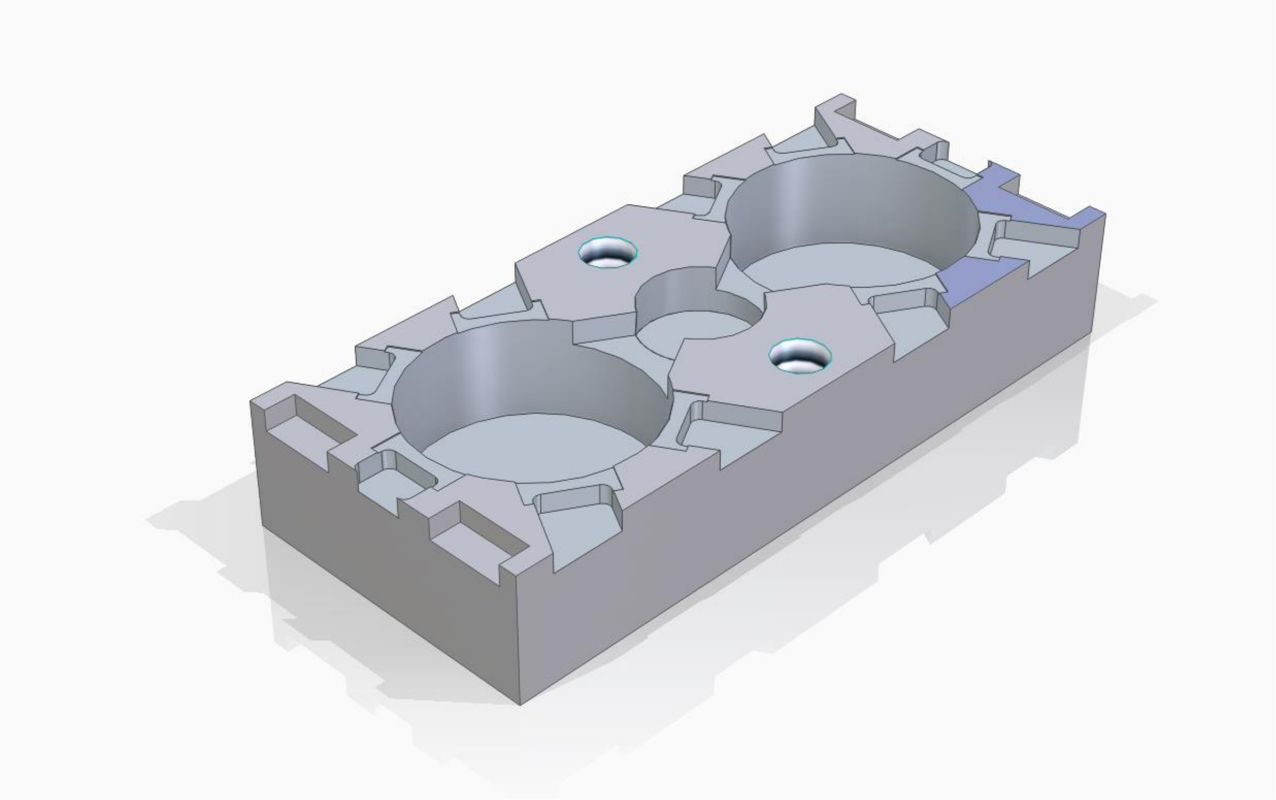

Figure 21: Mould to cast round buttons.

Figure 22: CNC Al mould.

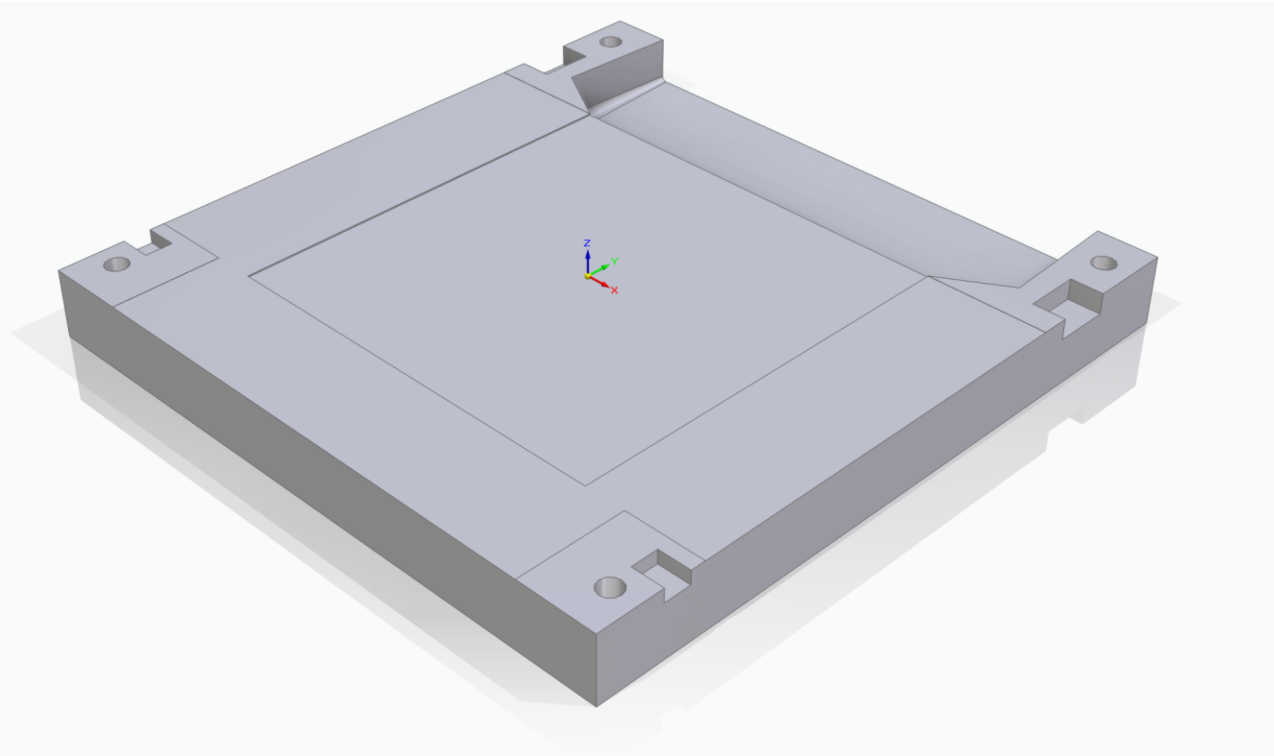

Figure 23: Square Mould

5.3 Wheel structure

When thinking about the forces applied on the wheel as it is under load, the spokes or centre carcass undergoes deformation as it will begin buckling under load. The outer diameter where the carcass ends is characterised as a “shear band” as this region will be “stretched” and the other extreme will be the thread region.

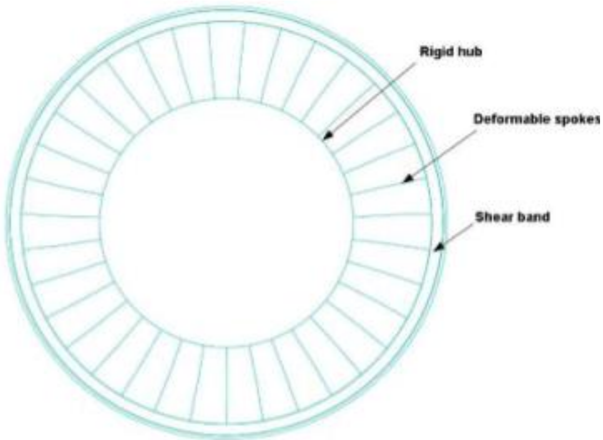

Figure 24: Structured wheel basic layout

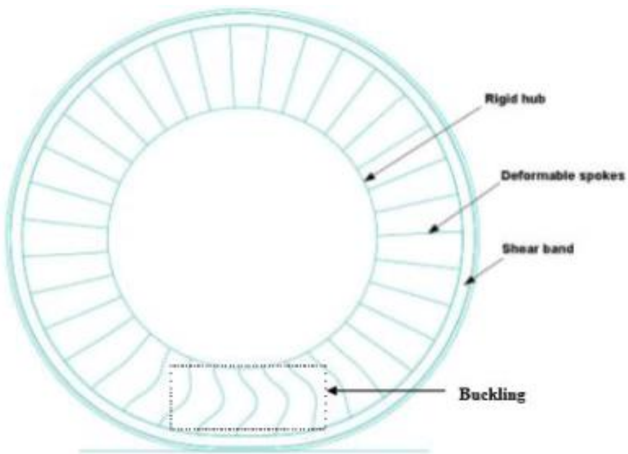

Figure 25:Structured wheel under load.

5.4 Material Selection

For this research, an aluminium alloy central hub will be used as a rim for the purpose of securing the wheel assembly to the vehicle framework. The Al alloy is 7075-T6, and its material properties can be found in Table 1.

Table 1: Material properties for rim [21]

Base material	**Density (kg/m3)**	**Young's modulus, *E* (GPa)**	**Poisson's ratio, ν**
Aluminium-Alloy (7075-T6)	2800	72	0.33
Steel, high strength (ANSI 4340)	7800	210	0.29

Aluminium alloy 7075-T6 as it is an excellent mould material due to its combination of high strength, light weight, and good machinability. This alloy is known for having one of the highest strength-to-weight ratios among aluminium alloys, which makes it particularly valuable in high-stress applications like aerospace and automotive industries. It has an impressive tensile strength of up to 503 MPa [22][23], which ensures that the material can handle the demanding wear of cyclic mould operations. The high strength of the material means that it is less likely to deform under stress when demoulding, maintaining the precision of the mould design.

The alloy's composition includes zinc as the primary alloying element, which significantly enhances its corrosion resistance, contributing to the durability and longevity of moulds made from this material. Despite its strength, it has a relatively low density, around 2.81 g/cm^3, which is advantageous for applications where weight is a concern such as moulds for spinning and for demoulding by hand. Moreover, the material has excellent machinability, allowing for intricate designs and precision in mould-making. It's also capable of being welded with appropriate techniques, which can be beneficial for complex mould constructions.

In the context of mould-making, 7075-T6 aluminium's superior thermal conductivity is particularly important. It is up to five times more efficient in this regard compared to mild steel, which can result in a reduction in cycle time for the moulding process by up to 30%. This not only leads to increased productivity but also contributes to cost savings in the long run. Due to its machinability, moulds made from this aluminium alloy can be produced faster and more easily than those made from harder materials like steel. Additionally, the ability to avoid additional heat treating or stress relief during the production process is a significant advantage, saving time and resources.

In summary, the combination of high strength, good thermal properties, light weight, and excellent machinability makes 7075-T6 a preferred choice for durable and efficient moulds in various industrial applications, especially where cost efficiency and quick production cycles are critical.

This Al alloy rim is designated as structurally rigid, thereby ensuring that it does not exert any influence on the configuration of the PU structure. The PU is bonded to the rim via a specific bonding agent, Cilbond 49SF [24], which functions as an elastomer-to-metal bonding agent. Cilbond 49SF is characterised by its strength and durability against both static and dynamic fatigue, maintaining its bond integrity in the presence of a wide array of substances, including, but not limited to, fuels, oils of various classifications, lubricants, glycols, inks, lacquers, paints, and a spectrum of cleaning solvents. However, it is noteworthy that the resistance it offers is most pronounced when contending with particularly aggressive solvents. The formulation of Cilbond 49SF incorporates Cilcure B, a variant of diphenylmethane diisocyanate, distinguished by it is select functional properties, which serves to augment the environmental resilience of the bonded assemblies.

Empirical evidence [25], derived from experimental procedures where polyether/MOCA or polyester/Ethacure cured compounds were affixed to mild steel substrates, substantiates Cilbond 49SF's superior performance in hot and cold environments. This was particularly evident in trials involving complete submersion of the bonded structures for a period of 28 days in water maintained at 80°C, subsequent to which the samples exhibited a complete retention of their rubber integrity when subjected to peel testing. Additionally, the bonds facilitated by Cilbond 49SF display a robust resistance to impact forces and maintain their non-brittleness down to temperatures as low as -40°C. When utilized in conjunction with Cilcure B as a bipartite adhesive system, Cilbond 49SF demonstrates an expanded utility spectrum, particularly excelling in applications demanding lower temperature bonding and an exemplary resistance to water-dominant conditions, such as boiling water or protracted exposure to moist environments. This system is also notably efficient in applications necessitating resistance to elevated temperatures, up to 180°C. In such instances, the dual application of Cilbond 49SF and Cilcure B, especially when employed as a priming layer beneath Cilbond 49SF, markedly enhances the versatility of the adhesive system.

The core structural element of the PU wheel, termed the carcass, is the immediate section bonded to the metal rim. This section of the wheel also accommodates the spoke architecture, which is subjected to varying stress distributions, experiencing tension in the upper segment of the wheel and compression at the lower segment, these forces collectively contribute to the observable buckling phenomena inherent to the wheel's operational dynamics when under load seen in Figure 24 and Figure 25.

Projected radially outward from the carcass lies the shear region. Upon the application of load onto the wheel, this shear region undergoes deformation, specifically flattening at the point of contact with the surface, thereby establishing a contact patch. The integration of a stiff shear band serves to counterbalance the shear forces and confer stability to the wheel assembly. This shear band creates a distribution of surface contact pressure against the road surface when under load. Concurrently, the presence of the shear band allows the use of a softer tread material, which, while ensuring adequate traction, also contributes to the wheel's overall damping characteristics.

The selection of PU as a material of choice is primarily attributed to its hyperelastic properties, which significantly contribute to the wheel's flexibility, energy dissipation capabilities, and overall damping efficacy, thereby enhancing the operational performance of the wheel assembly.

For this reason, three PU materials were selected for testing. These three different materials were selected based on material hardness since a wheel can be manufactured from three materials to make up the inner carcass, a stiff band and a soft thread.

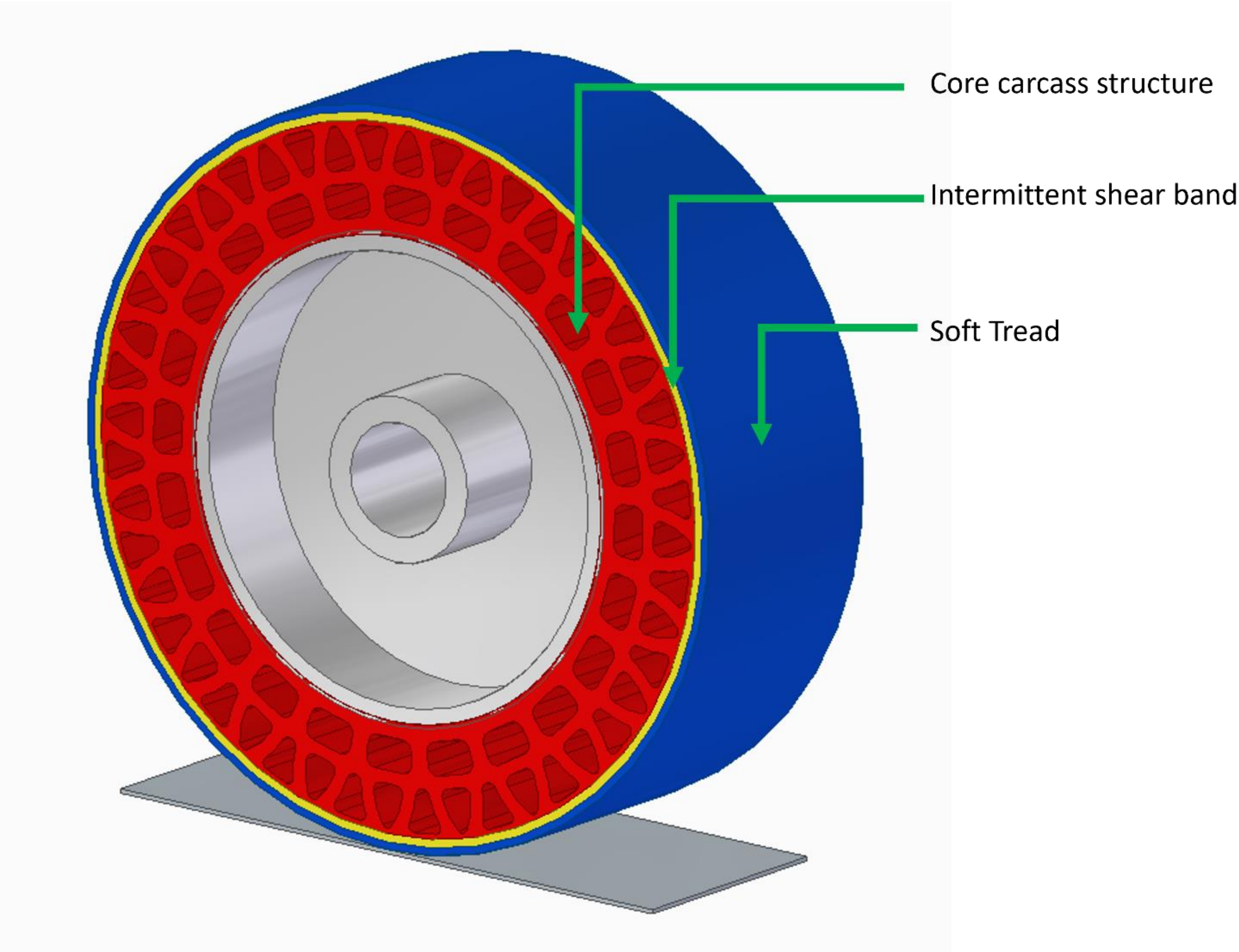

Figure 26: Wheel with various sections labelled.

5.4.1 Carcass Material – LF950A

In the design of structural section of the Non-Pneumatic Tyre (NPT), the selection of an appropriate material for the tyre carcass is paramount, particularly due to the substantial load-bearing requirements, often reaching upwards of 1 ton. Such demand is typical in applications predominantly involving heavy-duty vehicles, notably in military operations and unmanned vehicle systems. Consequently, a material possessing the requisite hardness to withstand these demanding conditions is essential. The identified hardness spectrum for optimal performance was defined within the range of 90 Shore A to 60 Shore D.

Following a comprehensive evaluation, the material chosen was Adiprene LF 950A, a product of Lanxess. This material is characterized as a TDI-terminated polyether prepolymer, distinguished by its markedly low content of free TDI (toluene diisocyanate). Upon curing with 4,4’-methylene-bis-(o-chloroaniline) (MBCA), the resulting product is a high-grade polyurethane elastomer, boasting a hardness of 95 Shore A. This elastomer is recognized for its compatibility with a multitude of high-performance applications, rendering it an ideal candidate for the intended use.

Adiprene LF 950A possesses several advantageous properties, which include a low free TDI content, reduced viscosity, extended pot life, and superior high-temperature dynamic characteristics. These attributes collectively offer significant processing benefits, particularly when juxtaposed with conventional TDI-based prepolymers of comparable hardness. Notably, the extended pot life and reduced viscosity of Adiprene LF 950A facilitate a more efficient casting process, which inherently minimizes scrap production while concurrently broadening the spectrum of products that can be manufactured via this method.

A notable merit of employing Adiprene LF 950A lies in its exceptional performance under dynamic conditions. The material exhibits minimal heat accumulation, attributed to reduced hysteresis, even in scenarios involving high-speed and high-load applications, such as in the manufacturing of rolls, tyres, and wheels. This characteristic significantly extends the applicability of polyurethane, potentially incorporating its use in more dynamically demanding scenarios that necessitate a 95 Shore A hardness elastomer.

Table 2: Properties of carcass LF950[26]

Property	**Values**
Hardness, Shore A	95 - 97
Hardness, Shore D	48 - 52
Tensile (MPa)	37.9
Elongation, %	350
100% Modulus, (MPa)	15.2
300% Modulus, (MPa)	28.3
D-470 Split Tear, (kN/m)	21.9
Die C Tear, (kN/m)	87.6
Bashore Rebound, %	42
Compression Set, Method B (22 Hrs. @ 70°C)	32
Compressive Modulus, (MPa) @ 5%	3.4

Compressive Modulus, (MPa) @ 10%	5.8
Compressive Modulus, (MPa) @ 15%	8.3
Compressive Modulus, (MPa) @ 20%	11.4
Compressive Modulus, (MPa) @ 25%	14.5
Specific Gravity	1.13
Viscosity @ 30°C (Centipoise, Pa·s)	6000
Viscosity @ 60°C (Centipoise, Pa·s)	1000
Viscosity @ 70°C (Centipoise, Pa·s)	500
Viscosity @ 100°C (Centipoise, Pa·s)	150
Specific Gravity @ 30°C	1.07
Specific Gravity @ 70°C	1.03
Specific Gravity @ 100°C	1.01
Adiprene LF 950A temperature (°C)	66
MBCA (°C)	116
pph MBCA, 95% theory	18.3
Mould Temperature (°C)	100
Pot Life (time to 200 poise) (min)	7.3
Demould Time (min)	25
Recommended Cure Cycle	16/100-110 Hrs/°C

5.4.2 Stiff shear band material – LF750D

In the search of selecting an optimal material for the construction of stiff shear band for the wheel, a material with a substantial degree of hardness is required. Consequently, the hardness parameter was stringently defined to exceed 70 Shore D. The material that was eventually selected for this application was Adiprene LF 750D, a distinguished product offered by Lanxess. LF750D is a TDI-terminated polyether prepolymer, notable for its remarkably minimal content of free TDI. When cured in conjunction with 4,4’-methylene-bis-(o-chloroaniline) (MBCA), the result is a high-calibre polyurethane elastomer, whose performance is robust, achieving a hardness in the range of 74-75 Shore D, thus rendering it exceptionally suitable for a myriad of high-performance applications.

The properties of Adiprene LF 750D are multifaceted and include a low presence of free TDI, reduced viscosity, extended pot life, and superior dynamic properties at elevated temperatures. When considering Adiprene LF prepolymers, of which Adiprene LF 750D is a variant, these materials present a plethora of benefits to cast polyurethane processors. Specifically, Adiprene LF 750D is advantageous relative to traditional TDI-based prepolymers of comparable hardness, primarily due to its extended pot life and reduced viscosity. These attributes are instrumental in enhancing the efficiency and versatility of casting operations, as they contribute to a reduction in wastage and facilitate the production of a wider array of products through the casting process.

Additionally, a significant merit of utilizing Adiprene LF 750D lies in its exceptional dynamic performance in wheel applications. This material exhibits minimal heat generation due to hysteresis, particularly in scenarios involving high-speed and high-load bearings, such as in the case of rolls, tyres, and wheels. This characteristic significantly broadens the scope of polyurethane applications, extending its utility to dynamically demanding scenarios that necessitate an elastomer with a hardness of 74-75 Shore D.

Table 3: Liquid Prepolymer Specifications (Adiprene LF 750D) [26]

Property	**Value**
% NCO	8.75 – 9.05
AE	464 – 480
Brookfield Viscosity, poise @30°C	155.0
Brookfield Viscosity, poise @100°C	2.4
Colour, Gardner	0-3
Appearance @25°C	Clear viscous liquid, free from contamination

Table 4: Typical Properties (Adiprene LF 750D) [26]

Viscosity at a specific Temperature	**Centipoise Value (Pa·s)**
30°C	10500
60°C	1250
100°C	140

Table 5: Specific Gravity (Adiprene LF 750D) [26]

Specific gravity at specified temperature	
30°C	1.12
60°C	1.10
80°C	1.08
100°C	1.06

Table 6: Processing Conditions (Adiprene LF 750D) [26]

Property	**Value**
Adiprene LF 750D temp, °C	64
MBCA, °C	116
pph MBCA, 95% theory, AE= 472	26.9
Mould Temperature, °C	100
Pot Life (time to 200 poise), Mins	2.8
Demould Time, Mins	15
Recommended Cure Cycle: Hrs/°C	16/100

Room temperature moulds may also be used. However longer demould times will be required.

Table 7: Physical Properties (Adiprene LF 750D Cured with MOCA) [26]

Property	**Value**
Hardness, Shore D	73 – 75
Tensile, psi (MPa)	48.9
Elongation, %	230
100% Modulus, psi (MPa)	36.5
200% Modulus, psi (MPa)	40.7
D-470 Split Tear, pli (kN/m)	24.5
Die C Tear, pli (kN/m)	158
Compressive Modulus, psi	@ 5%: 2150 (14.8), @ 10%: 3700 (25.5), @ 15%: 4700 (32.4), @ 20%: 6000 (41.4), @ 25%: 7250 (50.0)
Specific Gravity	1.20

Table 8: Processing Conditions (Adiprene LF 750D with Ethacure 300) [26]

Property	**Value**
Adiprene LF 750D temp, °C	64
Ethacure®300 temp., °C	38
pph Ethacure 300, 95% theory, AE= 472	21.5
Mould Temperature, °C	100

5.4.3 Soft thread material – V6060

In the selection of materials for the thread section, an ideal material will have a softer hardness, specifically within the 50-65 Shore A hardness spectrum. The chosen material must exhibit not only this flexibility but also ensure substantial traction. Generally, the Coefficient of Friction (CoF) of polyurethane is slightly lower than rubber with rubber having a CoF = 0.7. [27] A notable characteristic within the domain of polyurethane materials is the inverse relationship between hardness and CoF, harder polyurethanes generally demonstrate a reduced CoF, while their softer counterparts exhibit an elevated CoF. For applications utilizing typical polyurethane, the kinetic CoF spans a broad range, from 0.2 to 2.5. [28]

Given these considerations, Vibrathane 6060 emerges as an optimal choice. This material not only aligns with the required hardness parameter, presenting a hardness of 60 Shore A, but also maintains a CoF within the range of 0.3 to 0.4. Vibrathane 6060, a polycaprolactone-based TDI terminated liquid urethane prepolymer, is renowned for its processability through both conventional hand and machine mixing methodologies. When cured with 4,4'-methylene-bis(2-chloroaniline), Vibrathane 6060 cures in high-calibre vulcanizates, predominantly within the 60 Shore A hardness range. These vulcanizates are distinguished by their low hardness, remarkable abrasion resistance, and minimal compression set.

This unique prepolymer formulation engenders a high-performance 60A elastomer upon curing with MBCA. This process precludes the necessity for mixed curatives or plasticizers, which are customarily requisite to attain such a hardness level. Vibrathane 6060 is an exemplary product, specifically engineered for high-wear mining applications. It is distinguished by its extended pot life and reduced viscosity, which collectively facilitate the casting of both large-scale and intricate fabricated components.

Table 9: Liquid Prepolymer Specifications [26]

Property	**Specification**
Available isocyanate, %	3.20-3.50
Appearance	Solid free from contamination
Color, Gardner	0-3 (Light Amber)
Odor	Slight isocyanate
Specific Gravity @ 75°C (167°F)	1.118
Specific Gravity @ 100ºC (212ºF)	1.113
Brookfield Viscosity, poise @100ºC (212ºF)	5.0-10.50
Storage Stability	Excellent if protected from moisture, heat or freezing. For information on proper storage of polyurethanes, see bulletin AP-110.10 (R1)

	“Toxicity and Safe Handling of “Adiprene/Vibrathane.”
Solubility	Soluble in aromatic or chlorinated hydrocarbons, ketones, and esters.

An optimized procedure for the thermal preparation of VIBRATHANE 6060. This process is critical to ensure the material's optimal performance and processability.

To facilitate the pre-heating of VIBRATHANE 6060, a variety of apparatuses, including melting ovens, thermostatically controlled warming blankets, or drum heaters, are recommended. These devices must be calibrated to provide a uniform and controlled heating environment. The pre-heating process should be conducted at an approximate temperature of 70°C. The duration of this pre-heating phase is contingent on the volume of the material being processed. For instance:

- A 19-litre pail of VIBRATHANE 6060 typically necessitates a pre-heating duration ranging from 16 to 24 hours.
- Conversely, a 205-litre drum requires a more extended pre-heating period, approximately between 36 to 48 hours.

It is crucial to acknowledge that PU subjected to sub-optimal temperatures, notably lower than 24°C during transit or storage phases, may mandate an elongated pre-heating timeframe to achieve the desired viscosity and homogeneity.

In alignment with best practices, it is advocated that containers of VIBRATHANE 6060 undergo a thorough agitation, preferably through rolling, prior to utilization. This procedural step is instrumental in ensuring the material's uniformity and consistency, thereby optimizing its performance in subsequent applications.

Table 10: Typical Vulcanizate Properties of VIBRATHANE 6060 Cured with MBCA [26]

Material	**Quantity or Condition**
VIBRATHANE 6060	100 pts
MBCA	10.3 pts
% of Theory	95
VIBRATHANE 6060, °C	100
MBCA, °C	115
Mould, °C	115
Cure, hours: °C	1.0 @ 240
Post-Cure, hours: °C	16 @ 115
Working Life at Mix temp, minutes	9.0

*All samples were conditioned 7 days @ 24°C (75°F) and 50% RH before testing.

Table 11: Properties of VIBRATHANE 6060 Cured with MBCA [26]

Property	**Value**
Hardness, Shore A	60-62
100% Modulus, (MPa)	2.1
300% Modulus, (MPa)	3.4
Tensile Strength, (MPa)	30.1
Elongation at Break, %	480
Bashore Rebound, %	30
Tear Strength, ASTM D-470, (kN/m)	3.8
Tear Strength, Die C, (kN/m)	33.2
Bell Brittle Point, (°C)	-57
Compression Set, Method B, % after 22 hrs. @ 70°C	6
Compression Modulus, @ 5%	0.28
Compression Modulus, @ 10%	0.55
Compression Modulus, @ 15%	0.90
Compression Modulus, @ 20%	1.24
Compression Modulus, @ 25%	1.7
Tabor Abrasion, H-18 100gm Load Average Loss/1000 Cycles	0.0239 gms

Table 12: Effect of MBCA level on the Physical Properties of VIBRATHANE 6060 [26]

Vibrathane 6060 %NCO = 3.36	**MBCA[1] pts**	**% Theory**	**Shore A Hardness**	**100% Modulus (MPa)**	**300% Modulus (MPa)**	**Tensile, (MPa)**	**Elongation, %**	**Tear, Die C (kN/m)**	**Tear D-470 (kN/m)**	**Compression Set, % Type B, 22 hrs @70°C**	**Bashore Rebound**
100	9.1	85	62	(2.1)	(3.6)	(26.1)	460	(33.2)	(4.4)	12	29
100	9.6	90	63	(2.2)	(3.7)	(30.8)	470	(33.2)	(4.5)	8	31
100	10.1	95	62	(2.1)	(3.4)	(30.1)	480	(33.2)	(3.8)	6	30
100	10.7	100	61	(2.0)	(2.8)	(25.5)	520	(31.5)	(6.1)	11	30
100	11.2	105	58	(1.6)	(2.2)	(17.1)	580	(31.5)	(5.2)	28	31

5.4.4 Curative for the prepolymer

The curative that will be used on the prepolymers for the carcass, stiff shear band and thread will all be the same, MOCA (MBCA). MOCA has the chemical name 4,4' methylene-bis-(ortho-choroaniline) with the chemical formula $C_{13}H_{12}Cl_2N_2$. It is a common curative for TDI polyether or polyester polyols. From experience in working with other curatives such as Ethacure 300 and MCDEA, MOCA produces a good balance of physical properties as well as a useable pot life in order to cast larger volumes without curing too quickly.

Table 13: Physical Properties of MOCA [26]

Bulk Density at 24℃	0.8-0.9 (g/cm^3)
Liquid Density at 107℃	1.26 |(g/mL)
Amine Value	7.4-7.6 (mmol/g)
Free Aniline	1%
Colour	<4 Gardner
Acetone Insoluble Matter	<0.04 %
Storage stability	Stable, decomposes above 200℃

5.5 Analysing material data and Development of a Consistent Data Set

The raw data produced from the material testing will have to be processed into a useable format for the curve fitting process as the raw data contains duplicates, outliers etc. This is known as dirty data. Despite separate executions, all individual experiment data needs to be compiled into a useable set. Consistency in material use across experiments is imperative. While material variations from test to test might arise due to differences in instrument clamps or moulding processes, such variability within the data set is unacceptable and needs to be excluded. The data portrays a "snapshot" in time; even minor inconsistencies between experiments can lead to the formation of an impractical material model in the analysis software.

Each material test is run three times and any outliers in the data is excluded. The mean stress-strain data points in produced by using large data handling techniques in MATLAB. A code script was developed in Annexture A which would calculate the mean between testing runs. It will also reduce the number of data points while maintaining the shape of the data function such that the curve fitter can handle the data set.

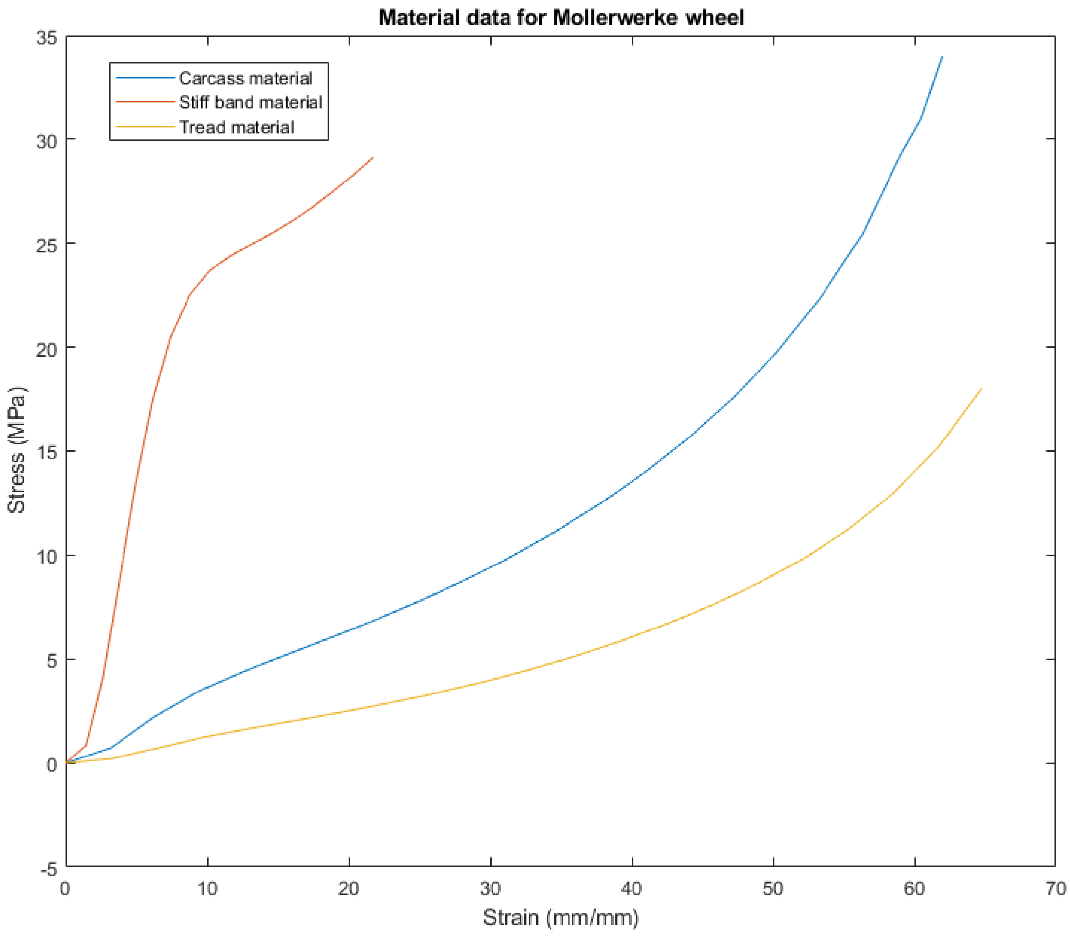

Figure 27: Material data after processing in MATLAB.

5.5.1 Hyperelastic Material Models

Once the data curves are plotted the curve fit can begin to take place. This comprehensive dataset is crucial for the precise calibration of hyperelastic materials, although, for materials exhibiting near or full incompressibility, volumetric data may be overlooked based on the presumption of incompressibility.

Calibration of the hyperelastic model involves selecting a suitable hyperelastic model and curve-fitting it to the empirical data. This process yields constants that are interpreted as material properties. During curve fitting, the objective is to minimize the cumulative discrepancy between the experimental data and the model's prediction, a task achieved through the least squares function. Depending on the model's complexity and the number of material constants involved, nonlinear regression methods are employed to minimize this error function, termed residue, which serves as a metric to evaluate the fit quality between different models.

In practical scenarios, calibration may rely on data from a single deformation mode, though this restricts the model's reliability to that specific mode. Hence, it is advisable to incorporate data from multiple or all deformation modes for enhanced accuracy. Following calibration, the model's validity is evaluated by examining physical plausibility, such as assessing the initial shear modulus which is:

$$\mu_0 = 2 * C_{10} \tag{46}$$

Where C_{10} is the first constant when performing a curve fit.

At this juncture, it is essential to deliberate on the appropriate material model. The available hyperelastic material models are categorized into two primary classes: phenomenological models and micromechanical models. Additionally, these models are differentiated based on their compressibility - namely, Neo-Hookean or fully incompressible, and compressible models. An array of models, with the selection criterion predominantly hinging on the anticipated strain range, which varies across models, extending from 30% up to 800%.

The calibration of hyperelastic material models is a meticulous process necessitating experimental data across various deformation modes, the judicious selection of hyperelastic models, and the careful curve-fitting of this data. The authenticity of the calibrated model is verified through physical plausibility checks and its application in simulations, ultimately ensuring a robust and reliable representation of the material's behaviour under various loading conditions.

5.6 Wheel Design

As seen in Figure *24* and Figure *25*, the wheel design can use 3 different materials. The design of the wheel should take advantage of this variation in materials with its geometry. The wheel design concepts were modelled in Solid Edge. Various wheel design concepts were designed with different aspects in mind. However, the basic dimensions were kept constant as stated below:

Outer diameter of the NPT = 350mm

Thickness of the thread = 3.5mm

Outer shear band diameter= 343mm

Thickness of the shear band = 4mm

Outer carcass diameter= 335mm

Inner carcass diameter= 228.86mm

Width between spokes = 8.86mm

Width of the NPT =120mm

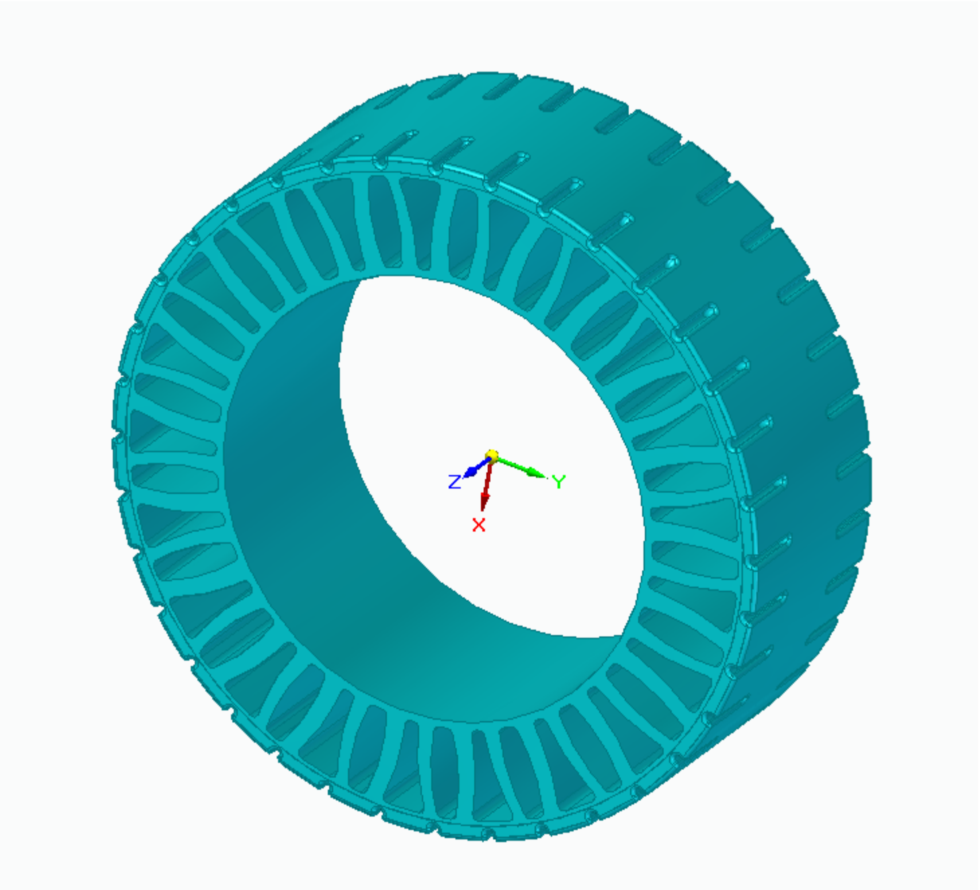

Figure 28: Wheel concept 1.

Figure 28 represents concept 1 which was initially thought of as a round triangle design for strength and minimising stress concentrations. This could provide strength and damping with the variation in spoke thickness.

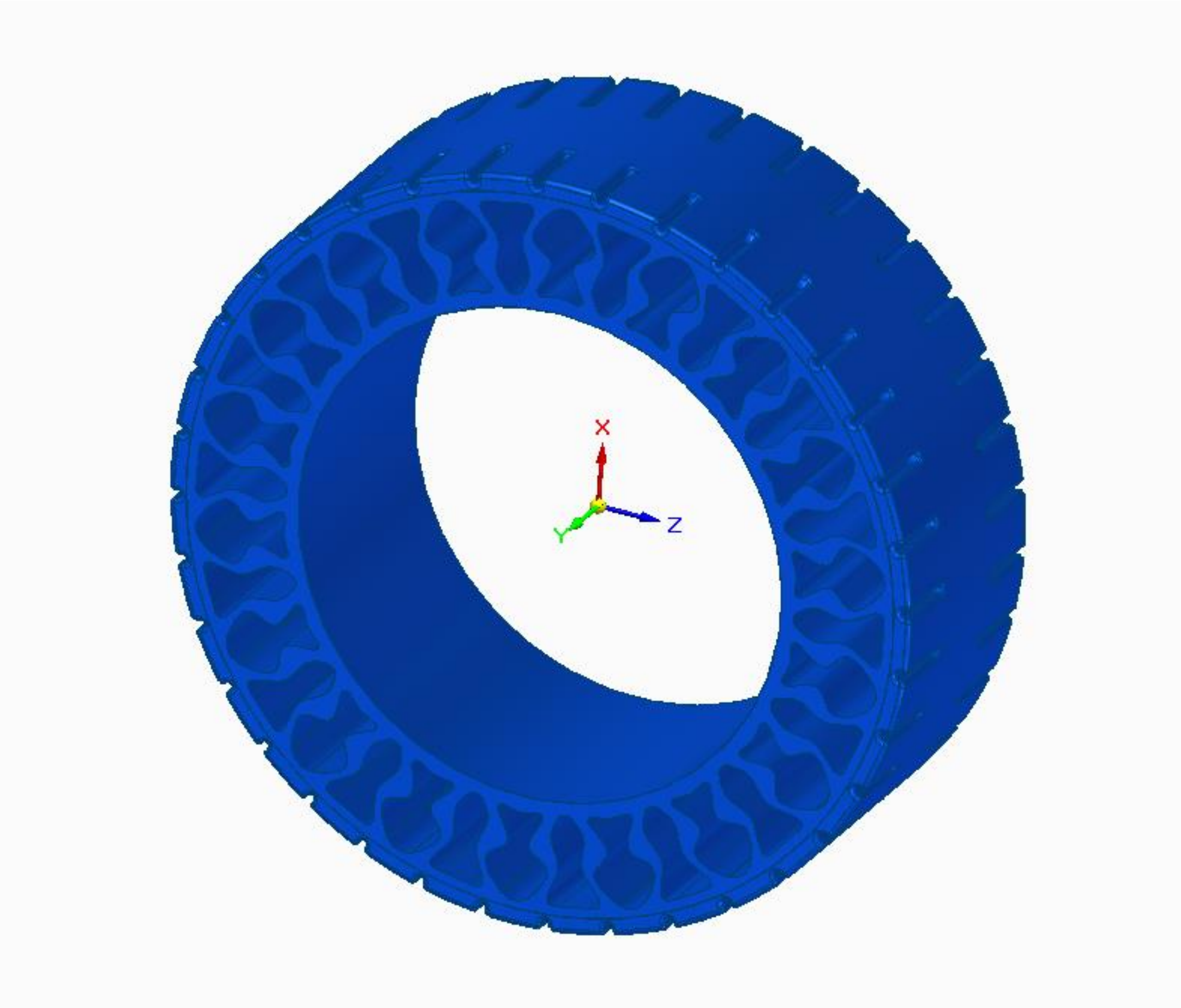

Figure 29: Wheel concept 2.

Figure 29 represents concept 2 which was envisioned to have a thinner spoke on a larger pitch circle diameter (PCD) to deform more and provide greater damping on impact while the thicker sections on a smaller PCD provide more strength.

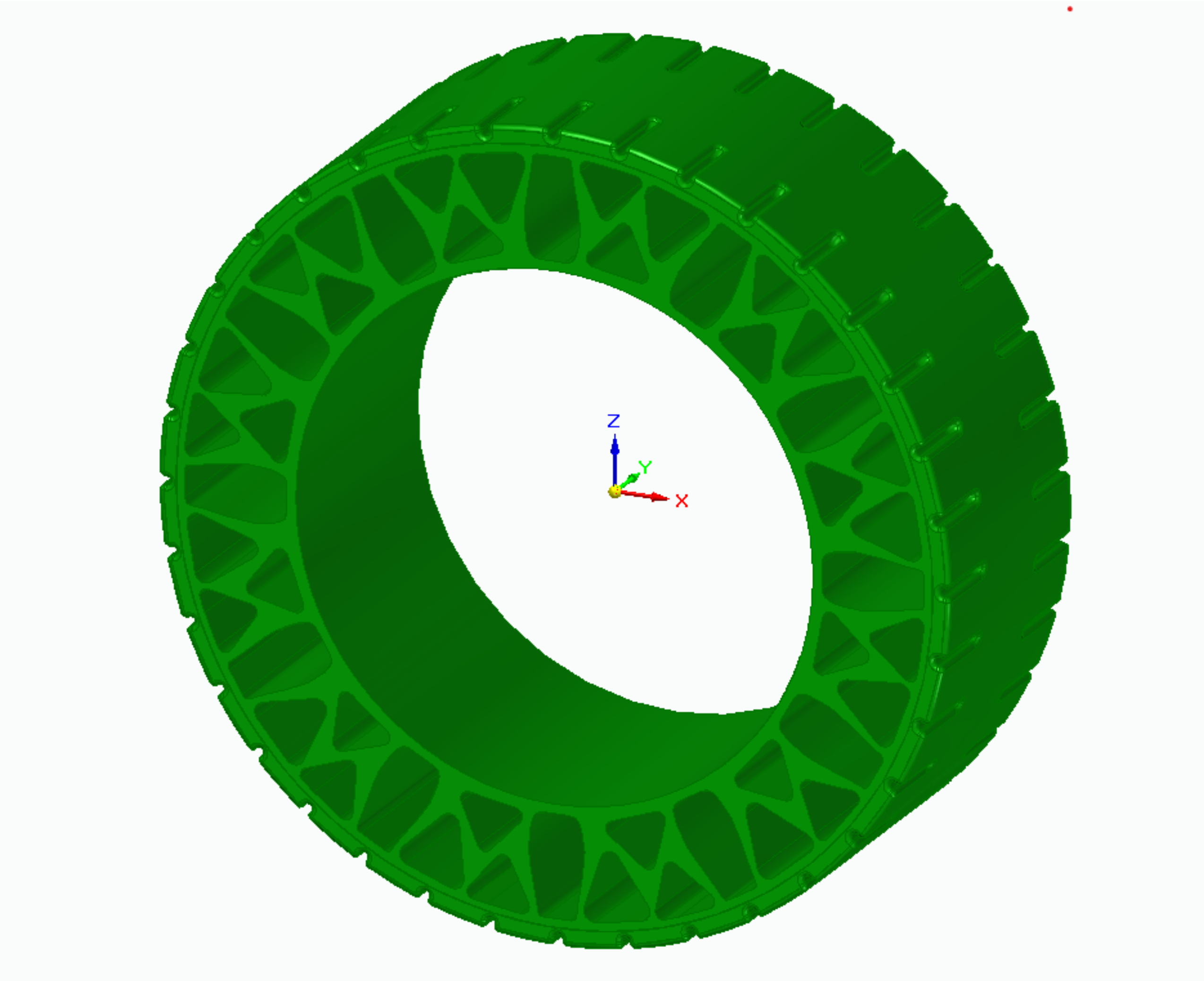

Figure 30: Wheel concept 3.

Figure 30 represents concept 3 which was a triangular design of different sizes together with a rhomboid in-between with the aim of distributing stress through the radii of the wheel from a soft outer to stiff inner.

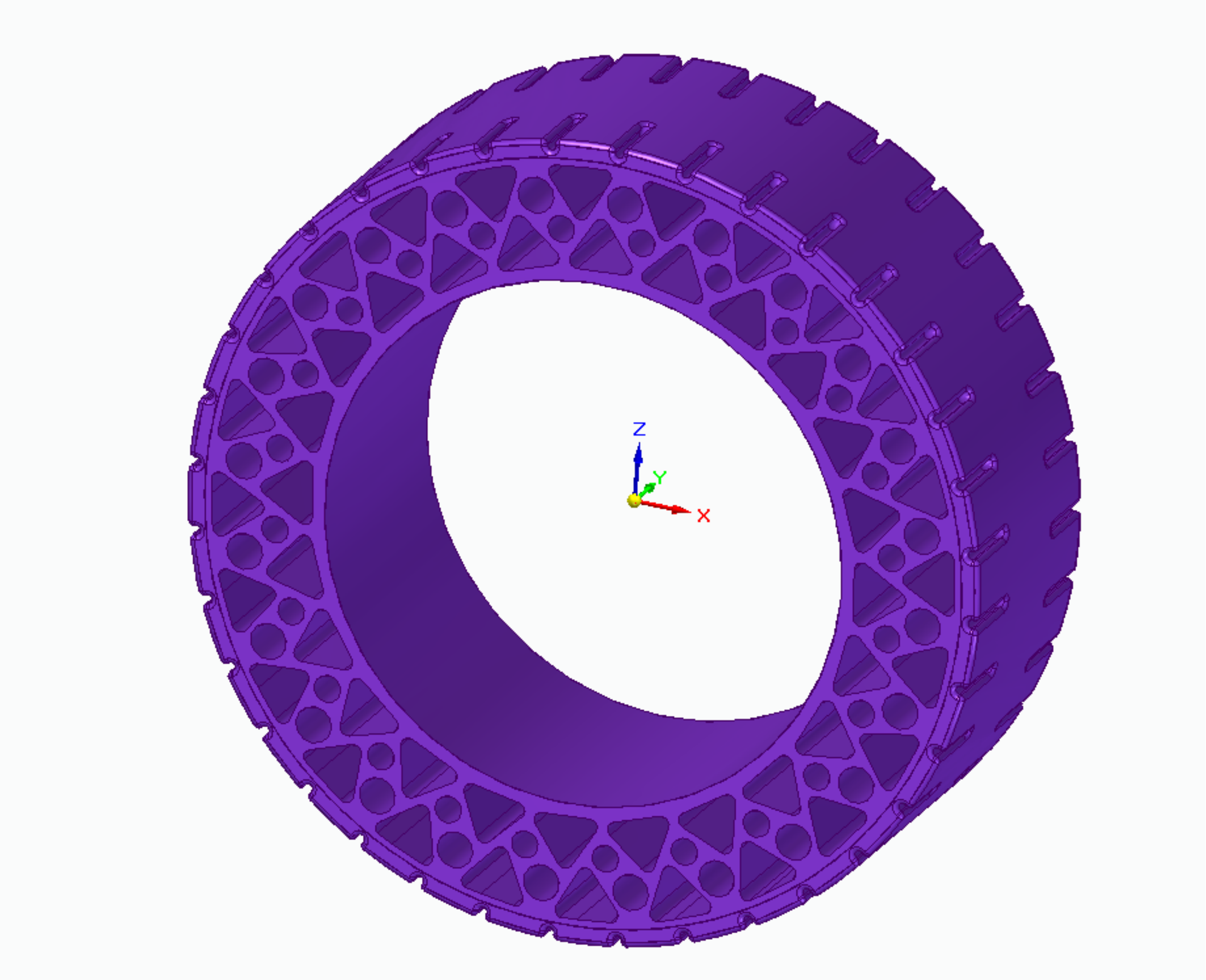

Figure 31: Wheel concept 4.

Figure 31 represents wheel concept 4 which replaces the rhomboid of concept 3 with circles to reduce any stress concentrations.

Figure 32: Wheel concept 5.

Figure *32* represents a rectangle and triangular structure. The thought process for the design was providing strength on larger PCD with the triangular structure while distributing the load with the rectangles. The outer pattern on the thread was added to increase traction but has no influence on the load bearing capabilities of the wheel.

The final design decided of the wheel was concept 5 which can be seen in Figure 24 and Figure *32*. This design has come from the rectangular inner and triangular outer. Concept 5 was chosen for manufacture because of the various shapes to analyse the distribution between the 2 different shapes in FEA.

5.7 Mould Design

To manufacture the wheel out of PU it will have to cast from a mould. To cast wheel at a premium quality without any air entrapment, bubbles without the PU and without any off-ratio material that is well mixed, rotational casting is used. This uses the centrifugal force from spinning a mould cast material from the outer diameter inward. This also aids in reducing the bubbles in the PU. The PU will also be cast from a Baulé machine, which heats up the prepolymer and curative to a set temperature. The machine also uses a vacuum to degas the material before mixing it at a specific ratio of prepolymer and curative.

To manufacture the mould a negative of the part will have to be designed and then CNC machined out of Al alloy 7075-T6. This is the same Al alloy as the rim which ensure uniform heating such that the outside temperature of the mould can be measured during heating and can be regarded as the inside temperature with a good degree of certainty due to the same thermal conductivity of the Al alloy 7075-T6.

Firstly, a bush and flange are design to hold the rim within a mould:

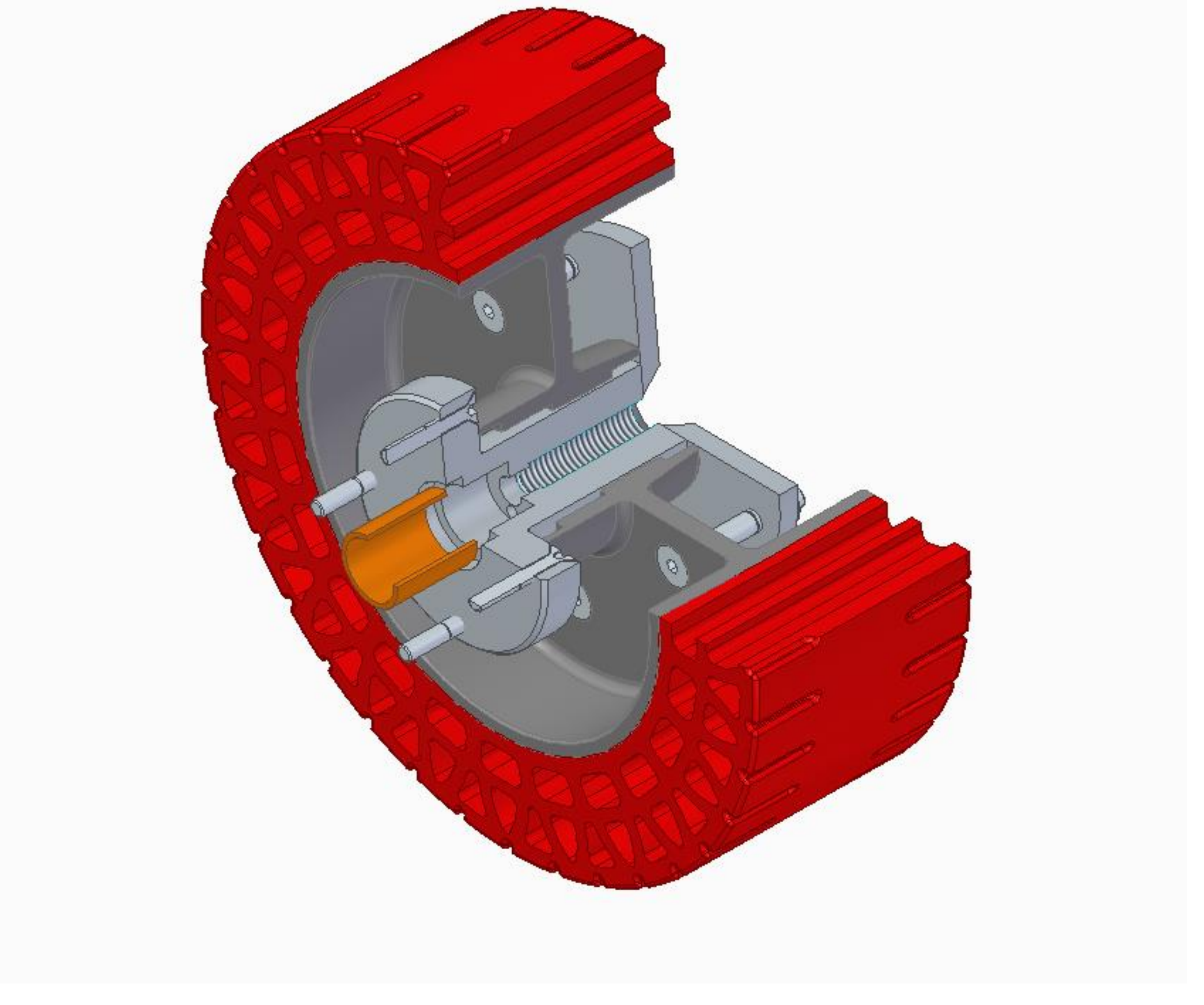

Figure 33: Holding the rim in place with a bush and flange.

Machined inserts which provide the structured pattern of the rectangular and triangular shape will be CNC machined individually to fit into an outer mould. These will be held in place by a bolt that fits on a solid circular plate. Three individual inserts can be seen together in Figure 35. All these inserts will be pieced together around the mould and the bolt holes running through them can be seen in Figure 34.

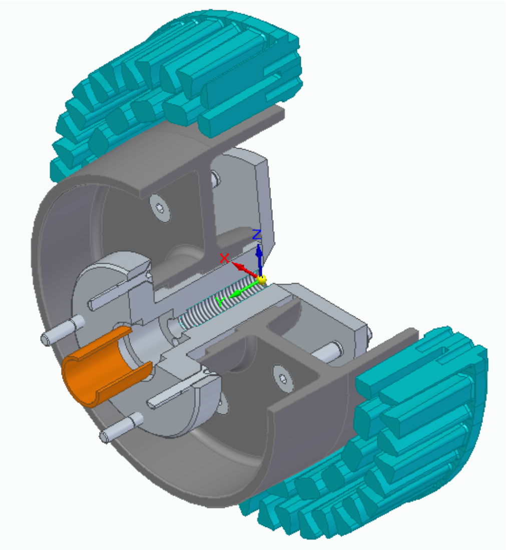

Figure 34: Structured inserts in mould

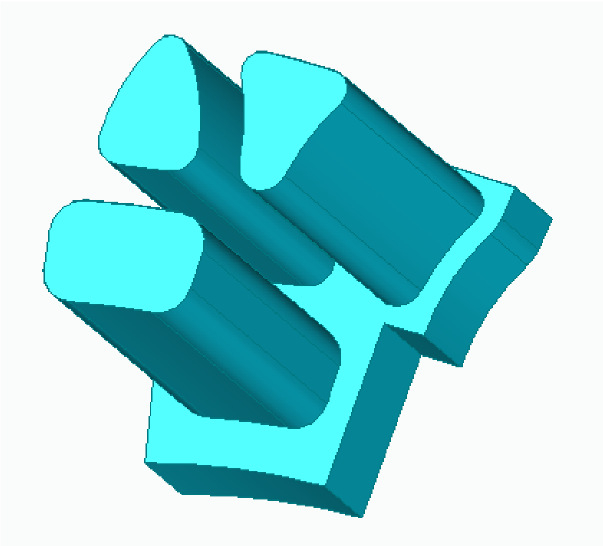

Figure 35: Structured insert.

The outer most shell of the mould will be CNC machined to provide the thread pattern of the wheel. This outer section will also hold in place all the inner mould pieces. The outer mould piece has holes on its back face to attach onto a flanged shaft to spin the mould during casting.

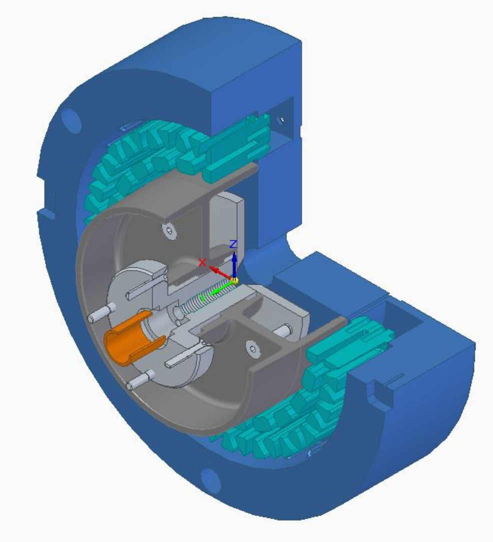

Figure 36: Outer casing of mould

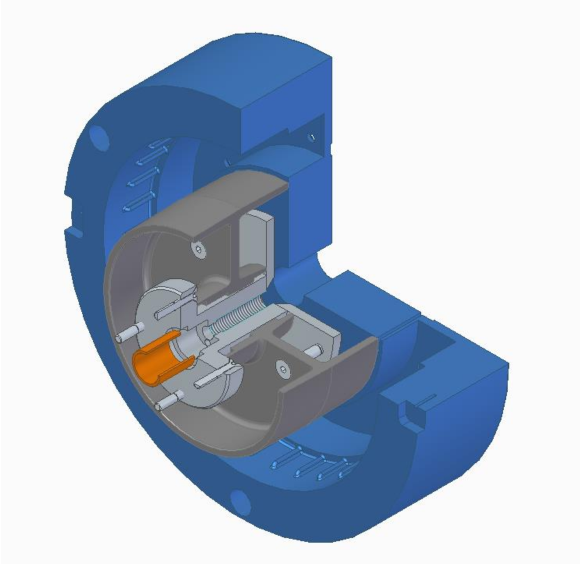

Figure 37: Outer casing of mould with thread design machined in it.

In the assembly shown in Figure 38, the adaptor plate (a circular, gold-toned component) serves a pivotal role within the manufacturing and service life of the mould. Positioned between the outer mould (depicted in blue) and the internal mould inserts (illustrated in turquoise), the adaptor plate mitigates the necessity for multiple drilled holes in the large aluminium segment of the mould. This strategic placement of the adaptor plate not only preserves the structural integrity of the mould but also introduces a modular aspect to the mould design. By facilitating the interchangeability of the turquoise inserts, the adaptor plate enables alterations in the wheel's configuration without the requirement for extensive re-machining of the entire mould, a process that is notably cost-prohibitive. The integration of the adaptor plate into the mould assembly is achieved through bolting, ensuring a secure attachment, and it incorporates designated apertures to accommodate the wheel inserts, thereby streamlining the mould modification process.

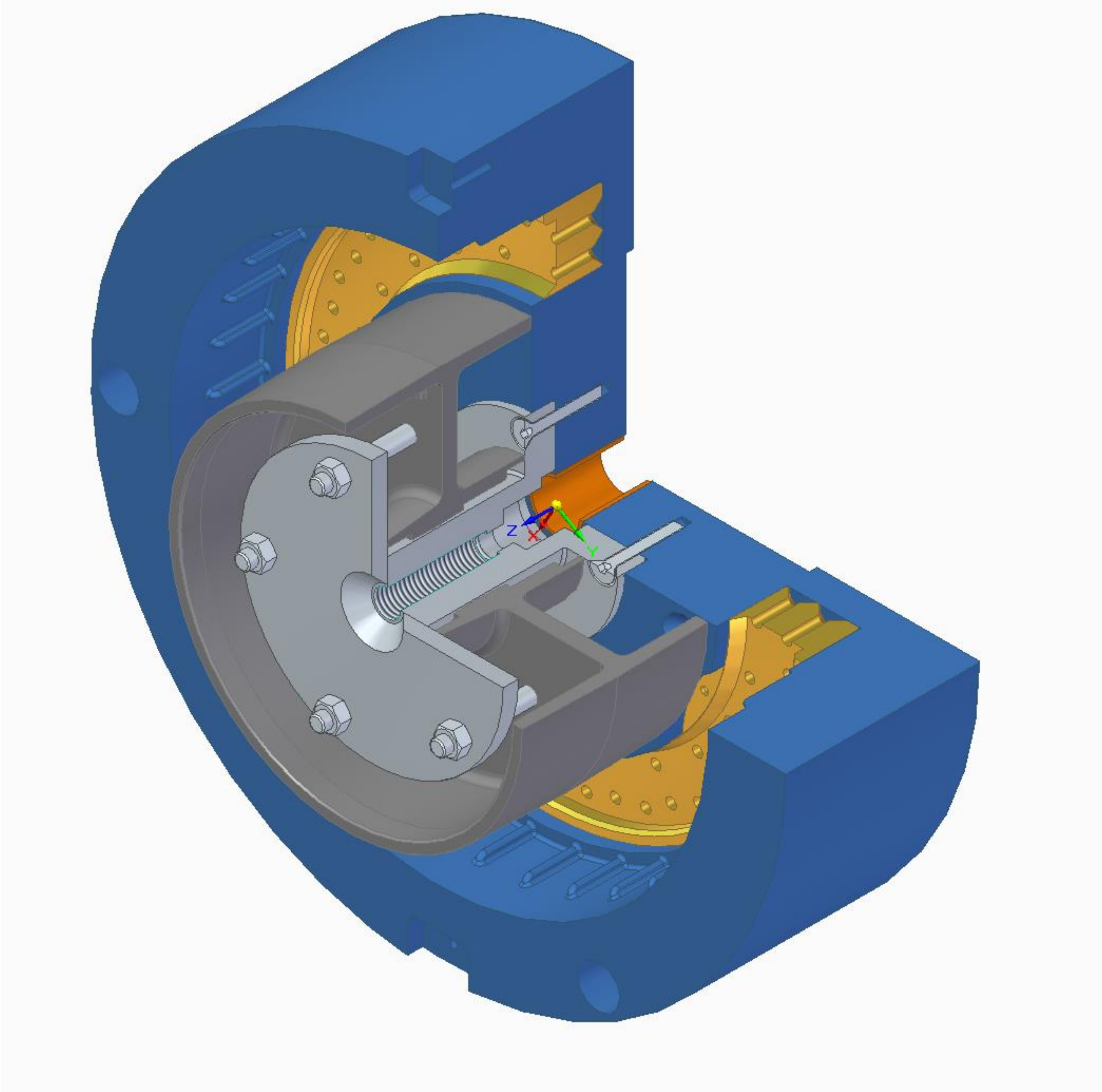

Figure 38: Plate used to bolt the insets in.

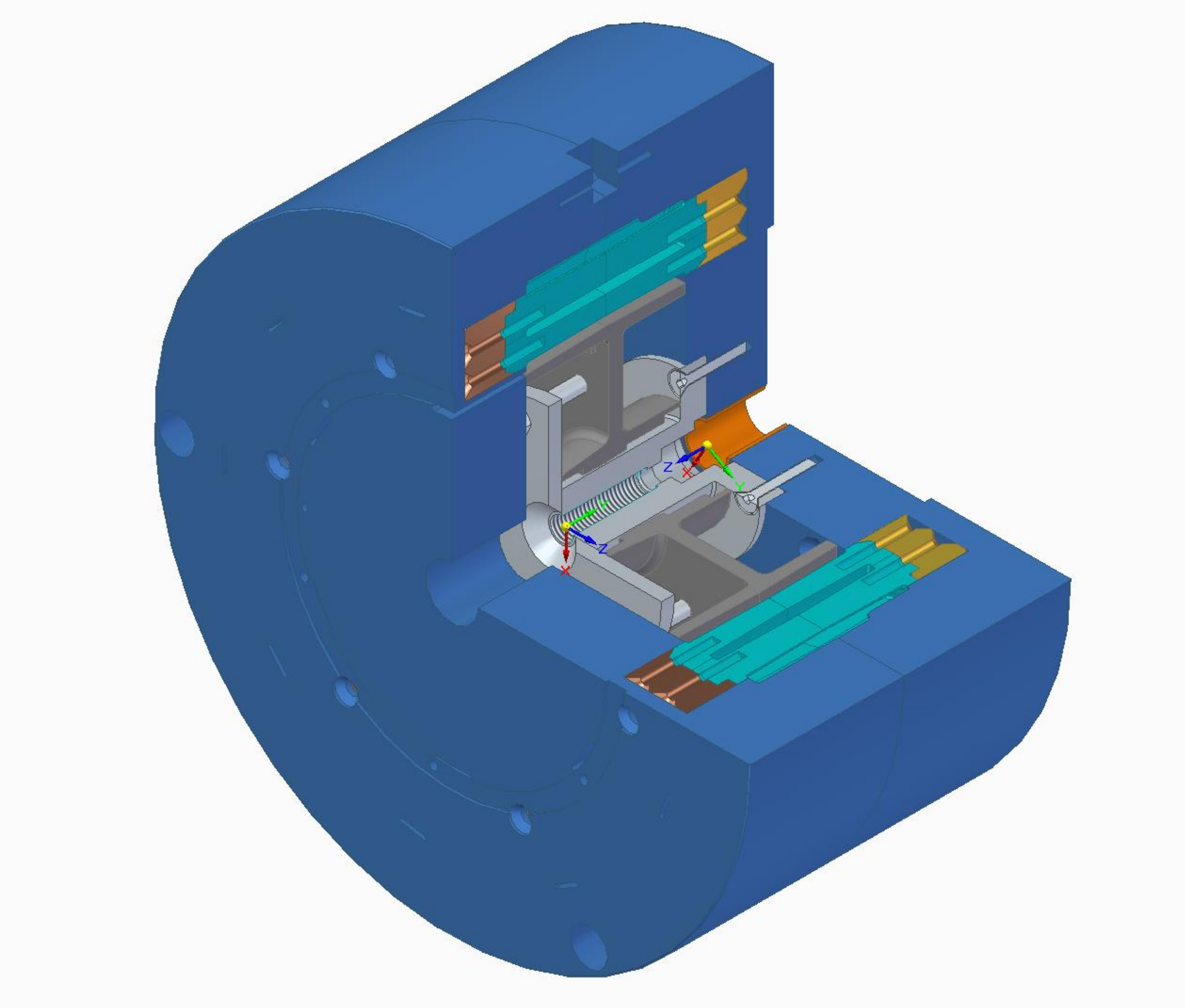

Figure 39: Mould is mirrored due to symmetry.

Within the structural configuration of the mould, filling apertures are strategically situated at the frontal section as seen in Figure 40. These apertures are essential for the introduction of PU into the mould, a process that is executed concurrently with the mould's rotational movement for the centrifugal casting. The design ensures that PU is first introduced through the apertures located on the larger diameter using a casting plate seen in Figure 43, a method primarily dedicated to the casting of the thread and the stiff shear band. Subsequent to this initial phase, the filling process advances towards the carcass, utilizing apertures positioned on a smaller pitch circle diameter (PCD) seen in Figure 42.

The dimensional precision of the mould design is critical, particularly concerning the PCD of the inner filling apertures. These apertures are meticulously positioned slightly beneath the rim, with a specified clearance of approximately <1mm seen in Figure 40. This precise placement is instrumental in achieving complete casting of the wheel, ensuring optimal adhesion and integration with the rim structure, a factor paramount in the overall functionality and performance of the wheel assembly.

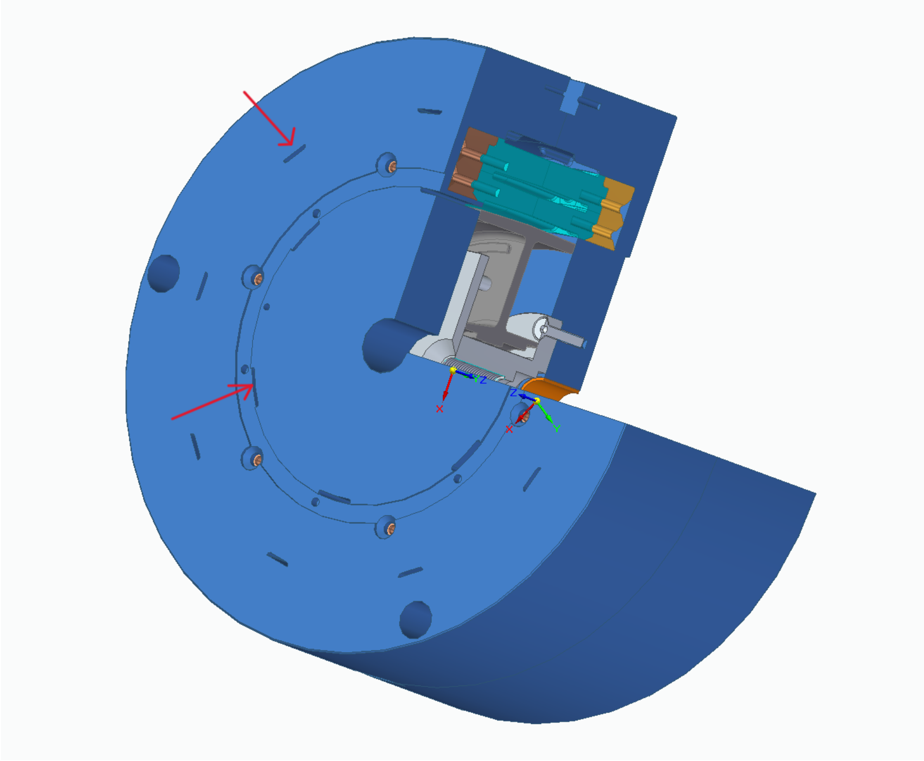

Figure 40: Filling ports where PU will fill through on front of the mould.

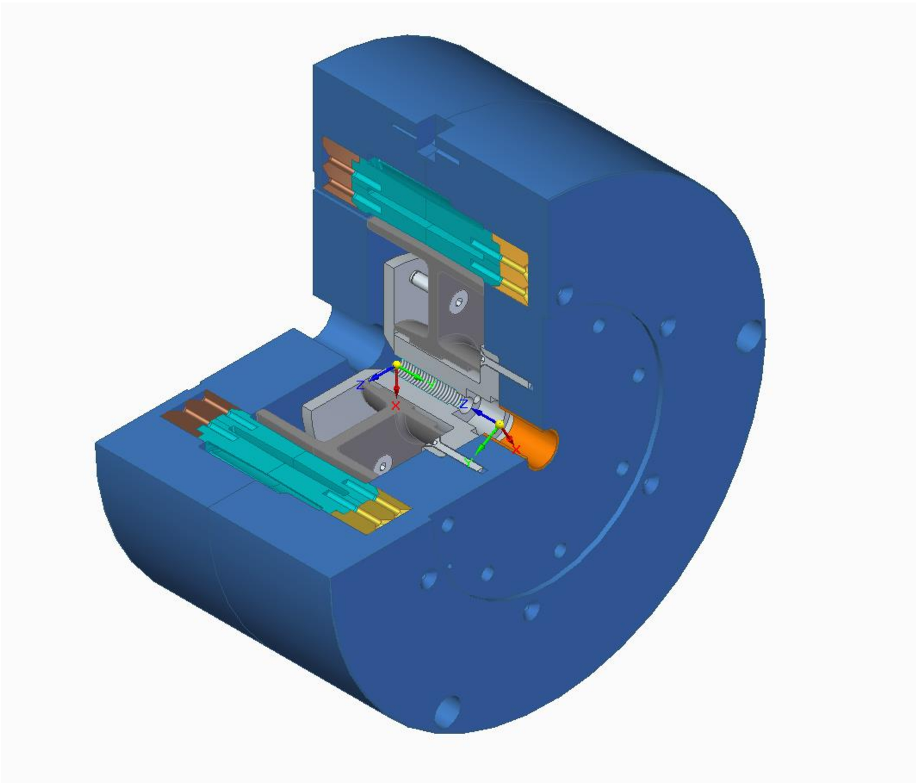

Figure 41: Back of the mould which bolts onto a shaft and motor to spin.

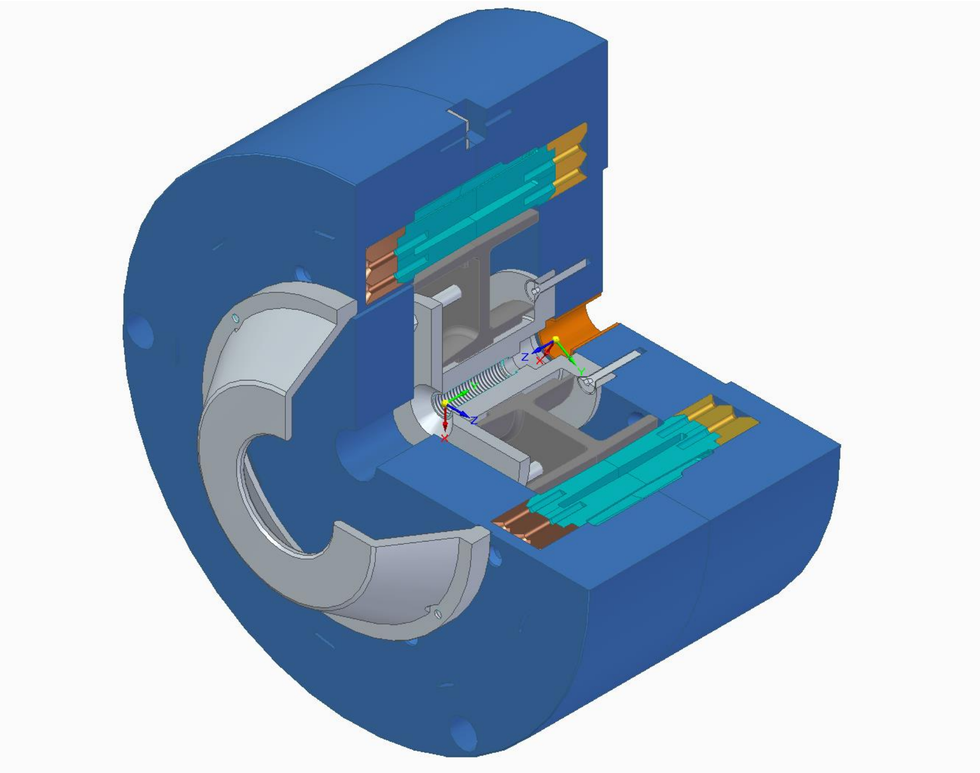

Figure 42: Inner filling plate.

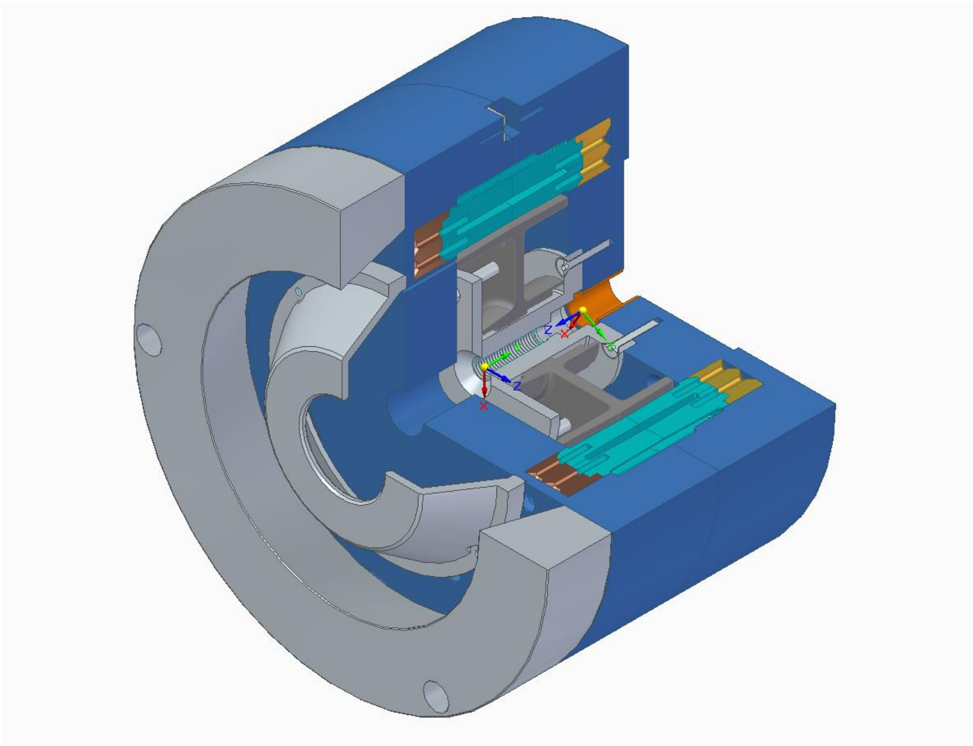

Figure 43: Outer filling plate.

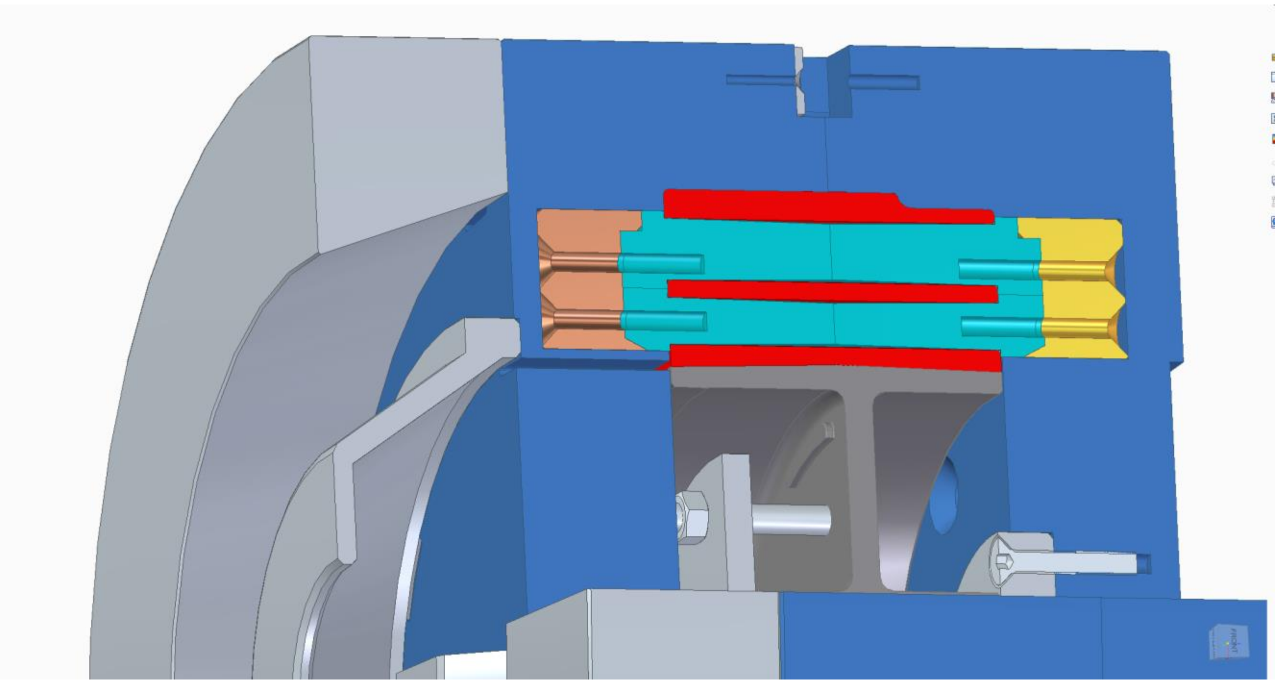

Figure 44: Filling plates in relation to the casting hole.

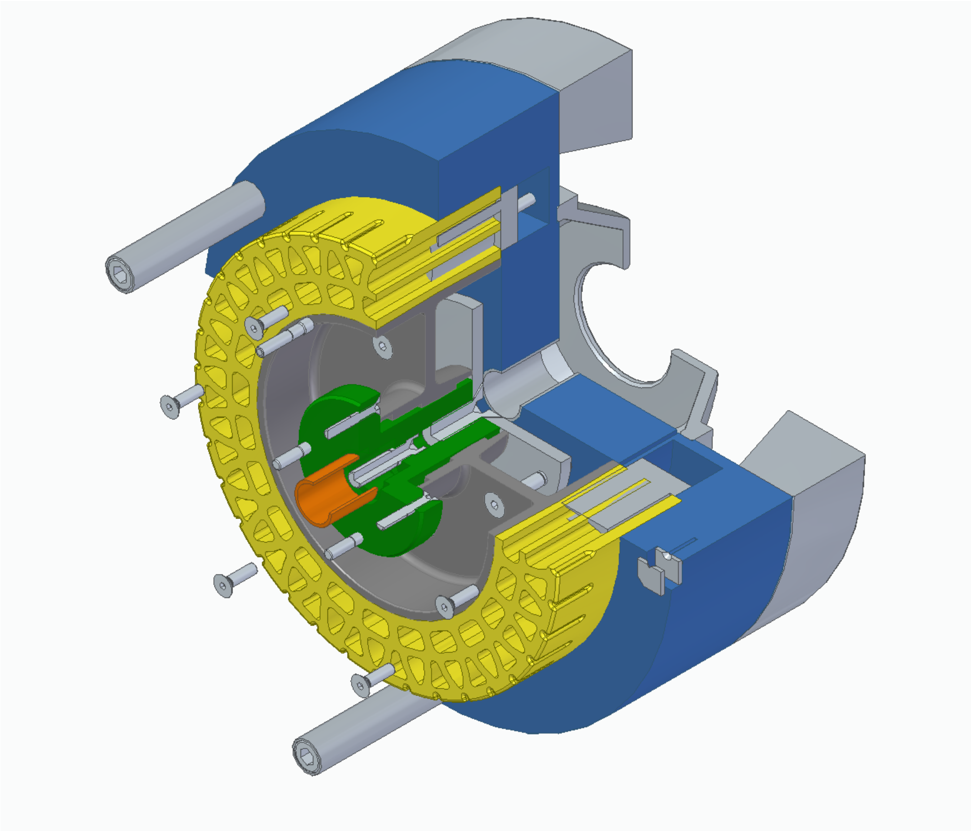

Figure 45: All mould pieces run on roller bearing for alignment.

As described in 5.4 material selection on page 35, the mould was subjected to a precise Computer Numerical Control (CNC) machining process to ensure a superior surface finish as seen in Figure 46, Figure 47, Figure 48 and Figure 49. This meticulous finish on the mould is projected to enhance the quality of the final polyurethane product, providing it with an aesthetically pleasing and functionally superior surface.

Figure 46: CNC machined parts out of Al alloy.

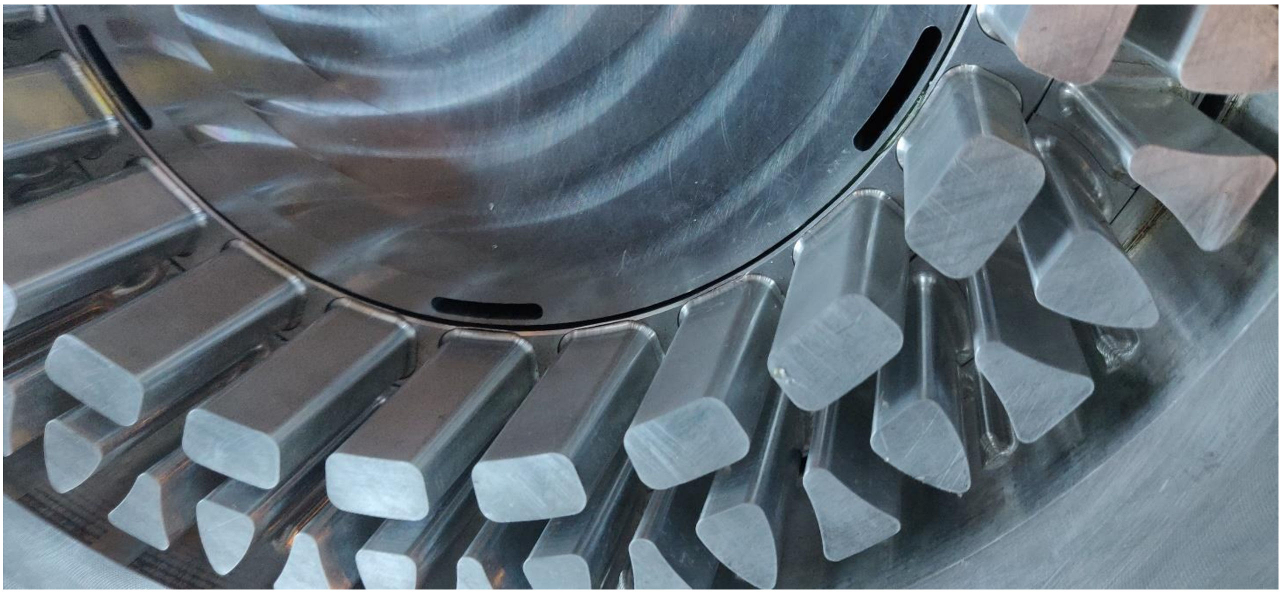

Figure 47: Mould casting holes.

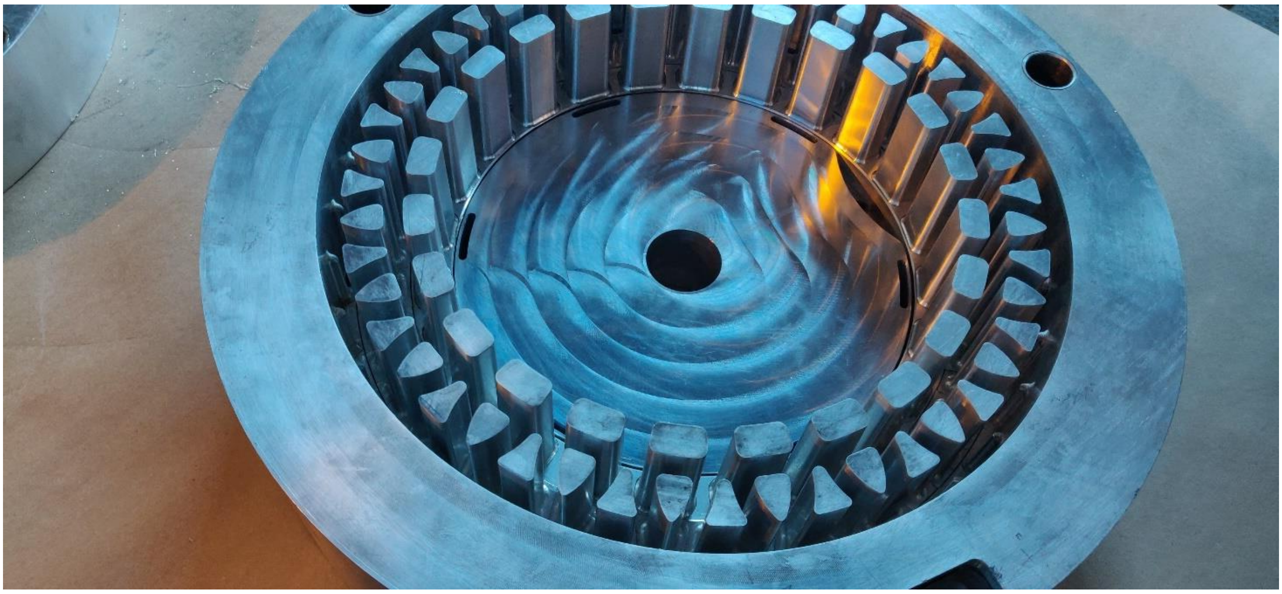

Figure 48: Al mould for wheel.

Figure 49: Mould on alignment rods in spinning oven.

5.8 Casting

The fabrication process of the wheel was carefully executed, utilizing the specified materials for the thread, stiff shear band, and carcass, yielding exceptional results from the mould. Notably, the dimensional precision of the mould, particularly pertaining to the interface between structured inserts, demonstrated potential for improvements. A reduction in the manufacturing tolerances from 0.3mm to 0.1mm is recommended, aiming to mitigate the incidence of PU flashing. This phenomenon, characterized by the minor overflow of PU into the mating surfaces of the mould. This excess flashing necessitates subsequent removal from the final product.

Furthermore, attention is drawn to the optimization of CNC machining operations, with a specific focus on enhancing the repeatability aspect. Observations indicate variability in the fit quality across mirrored planes of certain components, suggesting a need for rigorous refinement in the quality control protocols associated with the machining processes.

It is also noteworthy that the wheel's distinctive yellow/orange hue is not a result of pigment application but rather is inherent to the natural colouration of the PU material employed in the manufacturing process. This aspect underscores the material's intrinsic aesthetic properties, contributing to the wheel's visual appeal without the necessity for additional coloration agents.

Figure 50: PU wheels cast next to the mould.

Figure 51: A total of 5 wheels were cast for testing.

Figure 52: Cast PU final product.

5.9 Simulation

ANSYS emerges as a versatile and comprehensive simulation computational tool, designed to facilitate multi-disciplinary simulations encompassing a wide spectrum of physical phenomena, including structural mechanics, vibrational analysis, fluid dynamics, thermal conductivity, and electromagnetism. This powerful software suite empowers engineers to meticulously replicate and scrutinize the complex interplay of various physical factors in a cohesive virtual environment. By enabling the simulation of real-world conditions and operational tests prior to the physical prototyping of products, ANSYS significantly enhances the design process. This not only allows for the identification and refinement of potential vulnerabilities within the design but also enables predictive analytics regarding the product's performance, longevity, and susceptibility to potential issues, all within a three-dimensional simulated context.

The focal point of this research is the development and refinement of a simulation model through ANSYS, with the primary objective of conducting a comprehensive FEA. This analysis aims to accurately assess the load-bearing capabilities of PU wheels. Additionally, the research aims to conduct a modal analysis, thereby evaluating the efficacy and precision of FEA in modelling hyperelastic materials. These materials are characterized by their significant non-linear elastic response to applied forces, presenting a complex analytical challenge due to their inherent non-linearities and the presence of multiple material constituents, each governed by distinct material models.

The pursuit of this research is to not only validate the robustness of FEA in the context of hyperelastic materials but also to delve into the intricacies of simulating multifaceted material behaviours. This includes understanding the interactions between different material models and the resultant implications on the predictive accuracy of the FEA in reflecting the real-world performance of PU wheels under varying load conditions. Through this investigation, the research aims to push the boundaries of current simulation capabilities, fostering advancements in the predictive modelling and analysis of complex material systems for real world applications.

5.10 Experimental testing

Experimental testing constitutes a critical phase for corroborating and substantiating the FEA methodologies. The validation protocol involves subjecting either individual components or assembled products to a rigorously constructed testing apparatus. For this research the wheel and rim assembly will be tested completely as it is impossible to cast the wheel without the rim in the current mould configuration. To test the wheel, operational loads and specified boundary conditions are carefully imposed. Subsequently, the empirical outcomes are compared with the FEA predictions, thereby furnishing a comprehensive validation of not only the finite element model but also the authenticity of the applied load states and boundary constraints.

The experimental framework is accurately designed for the validation of the wheel model, with particular emphasis on a bearing loading as the principal deformation mode. In the FEA analysis force will be uniformly ramped as a loading condition in order to match the experimental testing conditions. This approach facilitates a comparative analysis of the load versus displacement outcomes.

5.11 Verification and Validation

Criteria For Validation

Validation is a more dynamic process that investigates the discrepancy between the numerical simulation and the experimental data to see if the computational simulation agrees with the physical phenomenon. While validation offers proof of how exactly the mathematical model corresponds to experimental tests, verification offers information on whether the computational model is solved correctly and accurately.

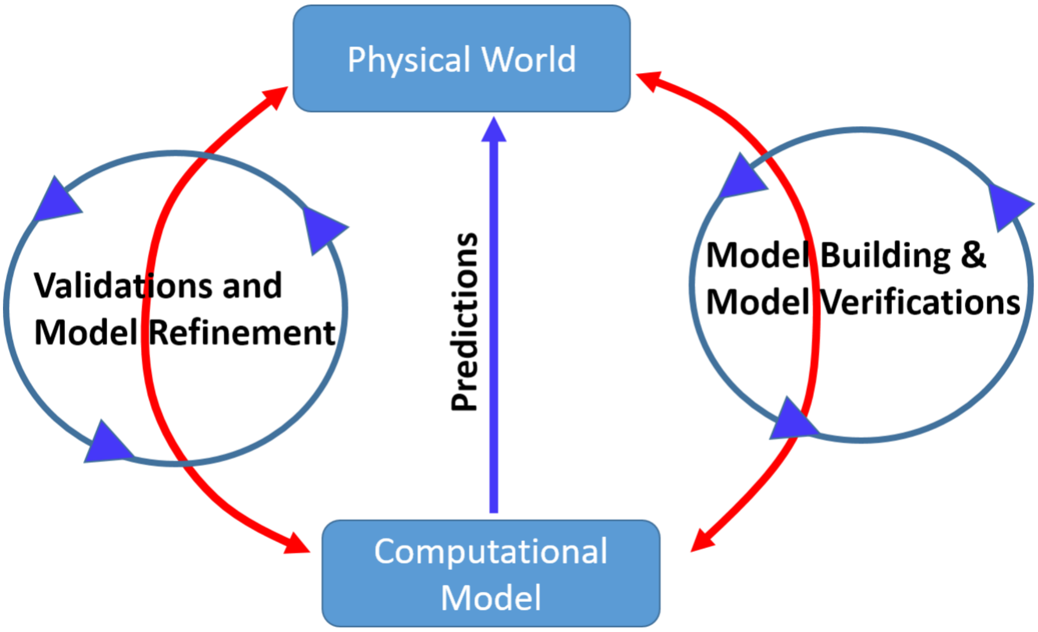

Figure 53: Verification and Validation Procedure for FEA [29]

It is crucial to remember that creating a computational model and comparing it to the physical world requires an iterative process in which all hypotheses, approximations, and their effects on the quality of the computational model are evaluated to create the computational model that is best suited to representing the physical world. The criteria that will be evaluated is the deformation of the wheel as it is the simplest to record experimentally.

The wheel will also then undergo design optimisation in which the criteria for this will be the quantity of PU used. The least amount of PU used to meet the design requirements will yield the most cost-effective design and will provide ease of manufacturing for the mould.

6. Experimental testing

Based on the budget and machines available for testing it was decided that the best experimental tests to perform was load deformation for stiffness characterization on a Polyurethane (PU) tyre. The wheel was subjected to 20 load-controlled tests with a constant ramp rate of 166.6N/s and 2 000N/s. The test conditions were set up to replicate the FEA conditions to validate an in-house developed FEA model.

6.1 Test Procedure

Characterization tests were carried out on the University of Pretoria's 100kN Schenck Hidropuls in November 2023. A total of 20 load-controlled tests were executed with two different ramp rates. A load of 10kN was applied at a constant ramp rate on two different triangle orientations located on the contact patch of the tyre with test parameters listed in

Table 14: Test parameters

Ramp rate (N/s)	**Load application position**	**Loading time (s)**	**De-loading time (s)**	**Quantity of tests**
2000	Triangle apex	5	5	5
166.6	Triangle apex	60	60	5
2000	Triangle flat/bottom	5	5	5
166.6	Triangle flat/bottom	60	60	5

6.2 Test Setup

A special jig was designed and manufactured to attach the specimen to the 100kN Hidropuls. The test setup for the tyre characterization tests was commissioned with the following components and layout:

- Specially designed and manufactured U-shape test fixture to attach the tyre to the load transducer.
- Specially designed and manufactured rigid load spreader in order to distribute load evenly across the contact patch of the tyre.
- Data logger to record force and displacement feedback.
- Incorporation of a laser displacement transducer in order to measure the displacement of the load spreader device.
- Incorporation of a 20kN load transducer in order to obtain accurate load feedback and control.

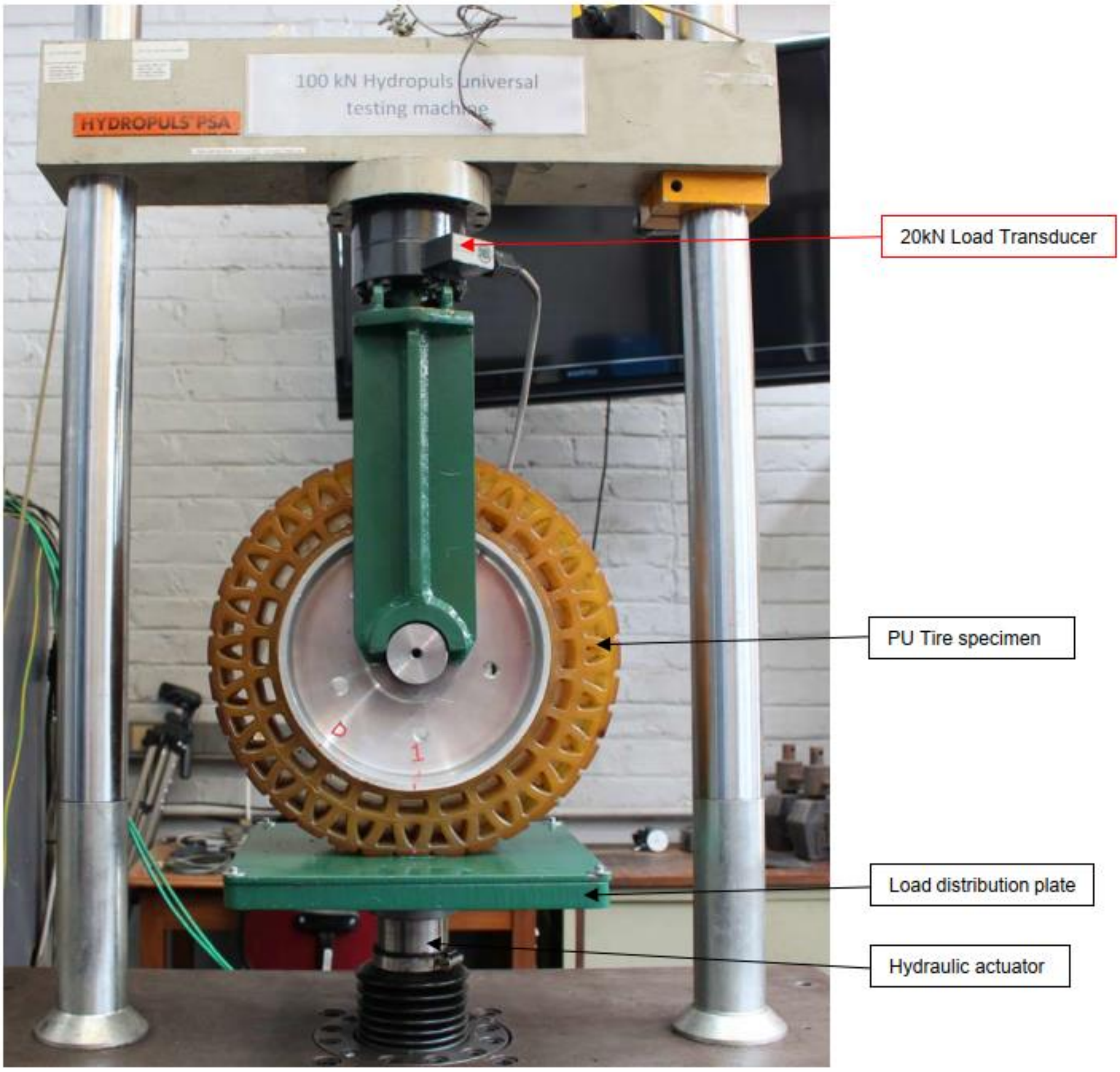

Figure 54: Test setup.

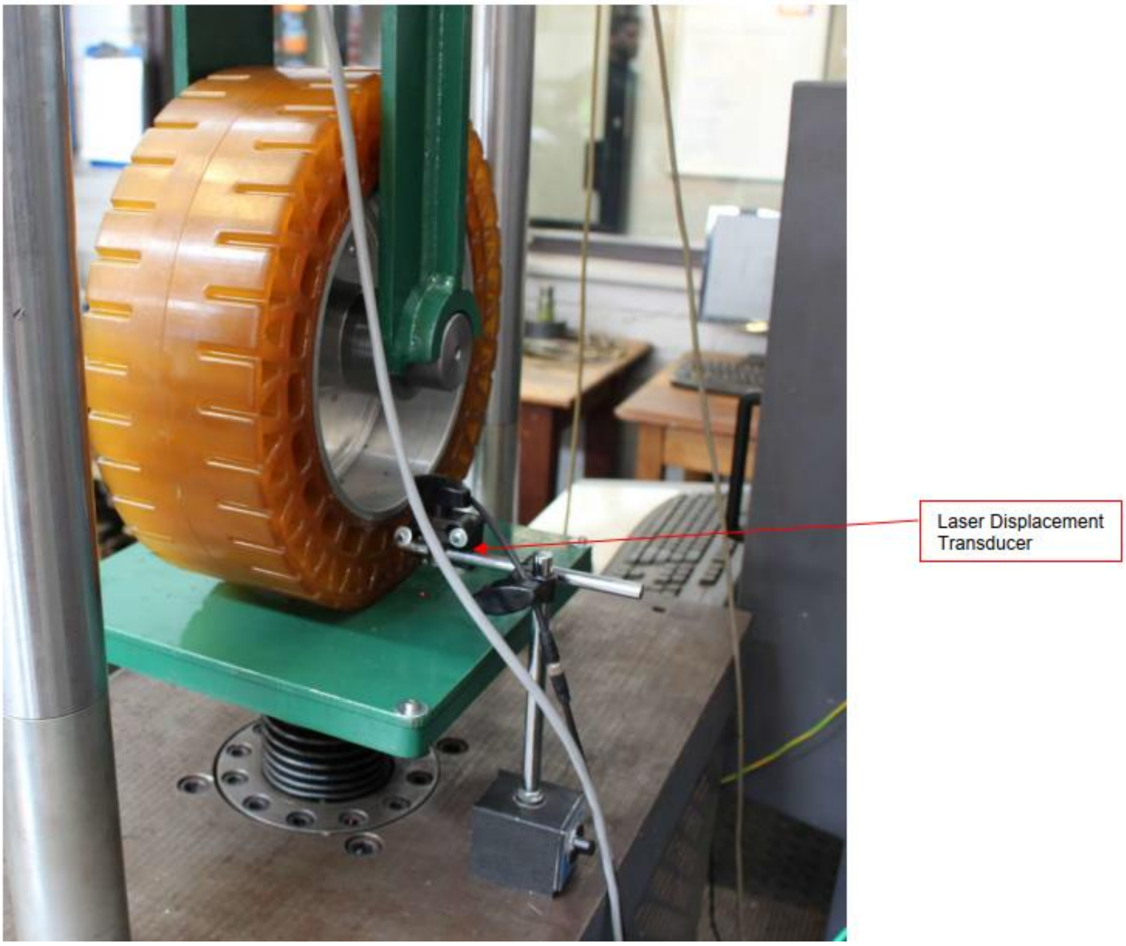

Figure 55: Test setup with laser displacement transducer.

6.3 Results

Tests on the PU tyre was successfully carried out for the two ramp rates and both contact patch locations. The tyre stiffness is calculated using a linear fit through the loading and unloading regions of the test data, respectively. The gradient of the linear fit is the tyre stiffness in kilonewtons per millimetre. The tyre stiffness is estimated for each data set, and the average is calculated for all data sets. The stiffness estimates for loading and unloading are shown in Figure 57, Figure 61, Figure 65 and Figure 69 as the dotted black lines.

The goodness of fit is provided in the form of coefficient of determination, $RR2$, and is calculated using the following formula:

$$R^2 = 1 - \frac{\sum_{i=1}^{n}(y_i - \hat{y}_i)^2}{\sum_{i=1}^{n}(y_i - \bar{y})^2} \tag{47}$$

In the above equation, $\hat{y}$ are the calculated values of the linear fit to the test data (y), and $\bar{y}$ is the mean of y. R^2 falls between 0 and 1, with a value close to 1 indicating the linear fit is good at estimating the stiffness.

Table 15: Triangle Apex, 5 seconds duration of loading and unloading the tyre to 10 kN, respectively.

Run Number	**Loading Stiffness [kN/mm]**	**R2 Loading**	**Unloading Stiffness [kN/mm]**	**R2 Unloading**	**R2**
1	2.596	0.9995	2.71	0.9883	-
2	2.5577	0.9997	2.6564	0.9911	-
3	2.5624	0.9991	2.6761	0.9912	-
4	2.4381	0.9991	2.6139	0.9928	-
5	2.5175	0.9992	2.6564	0.9898	-
Average	2.5343	-	2.6626	-	-

Table 16: Triangle Apex, 60 seconds duration of loading and unloading the tyre to 10 kN, respectively.

Run Number	**Loading Stiffness [kN/mm]**	**R2 Loading**	**Unloading Stiffness [kN/mm]**	**R2 Unloading**	**R2**
1	2.1759	0.9995	2.3352	0.9842	-
2	2.2259	0.9987	2.3483	0.9853	-
3	2.2651	0.9986	2.3608	0.9891	-
4	2.2598	0.9982	2.3164	0.9881	-
5	2.2266	0.9986	2.3521	0.9881	-
Average	2.2307	-	2.3426	-	-

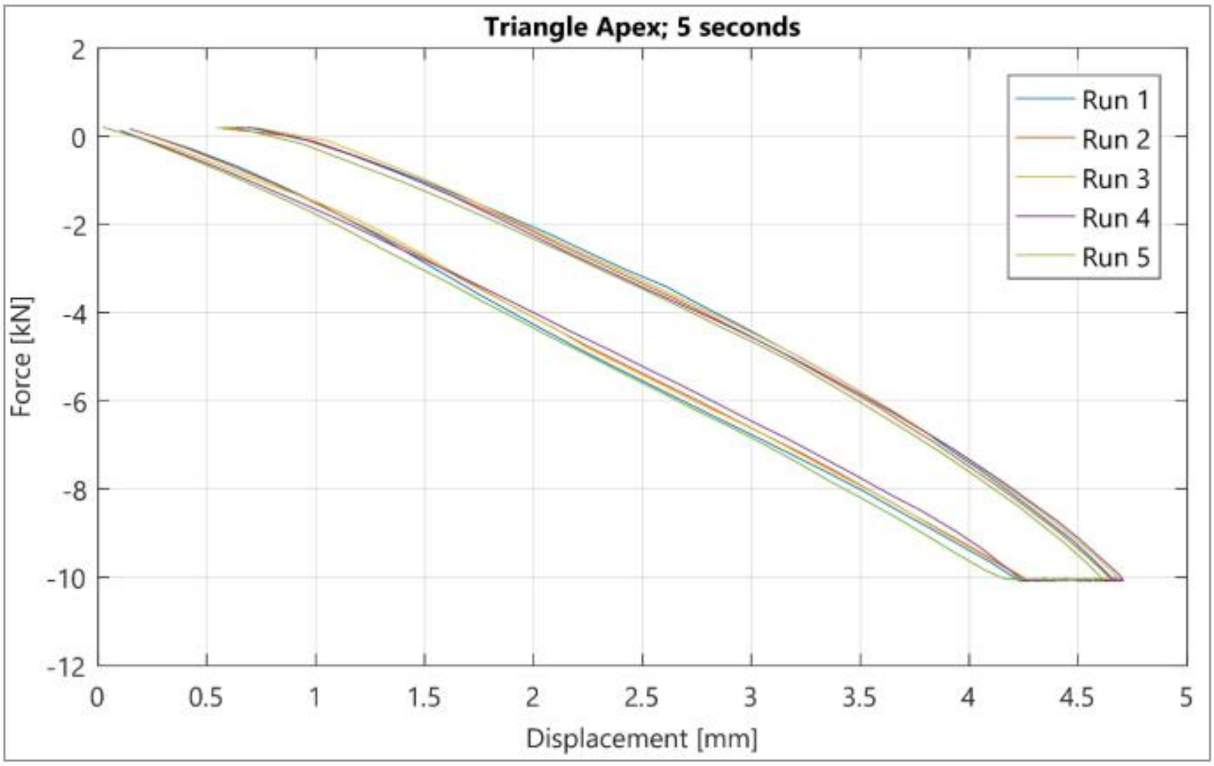

Figure 56: Stiffness results for T-apex, 5s.

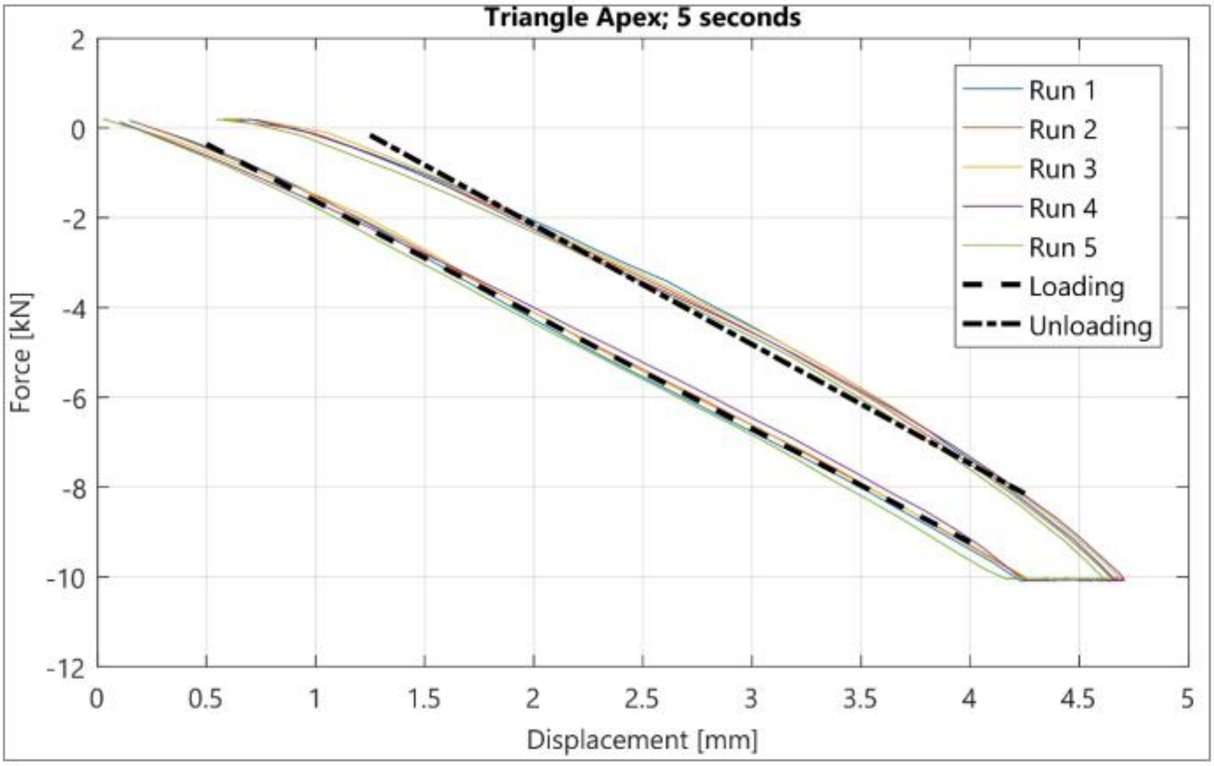

Figure 57: Stiffness results for T-apex, 5s with linear fit.

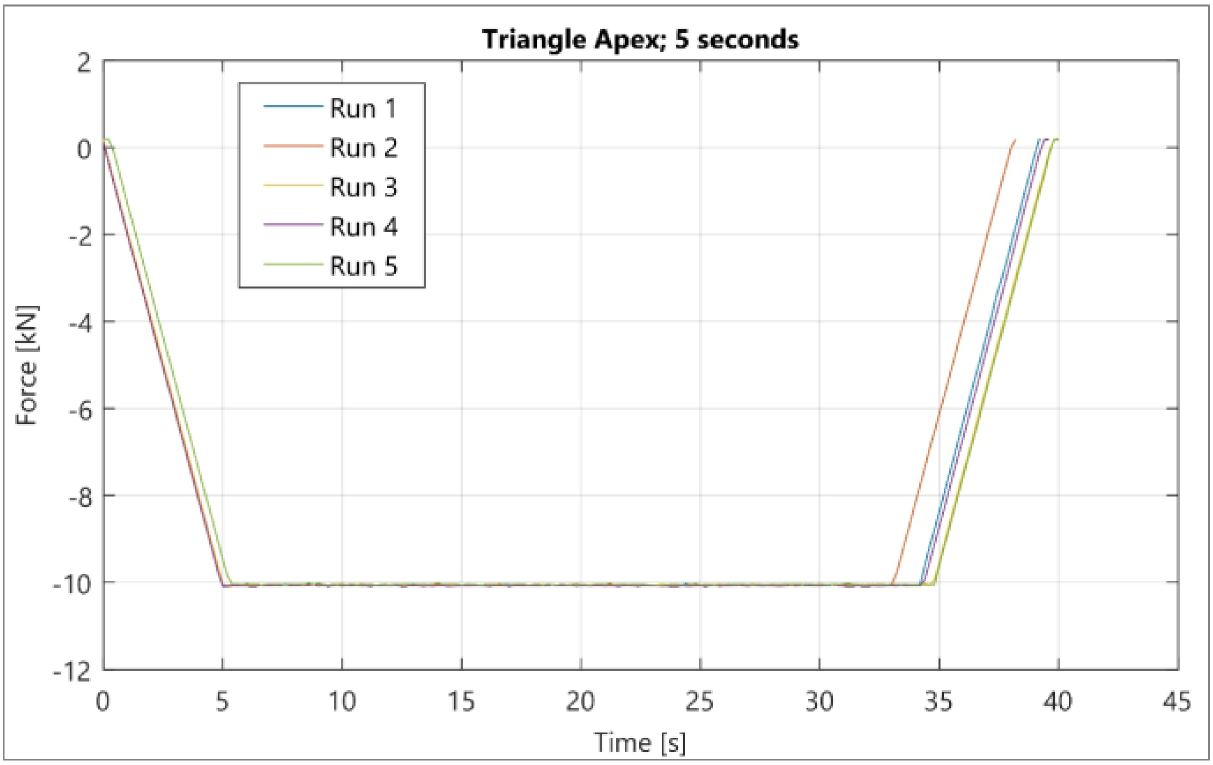

Figure 58: Load results for T-apex, 5s.

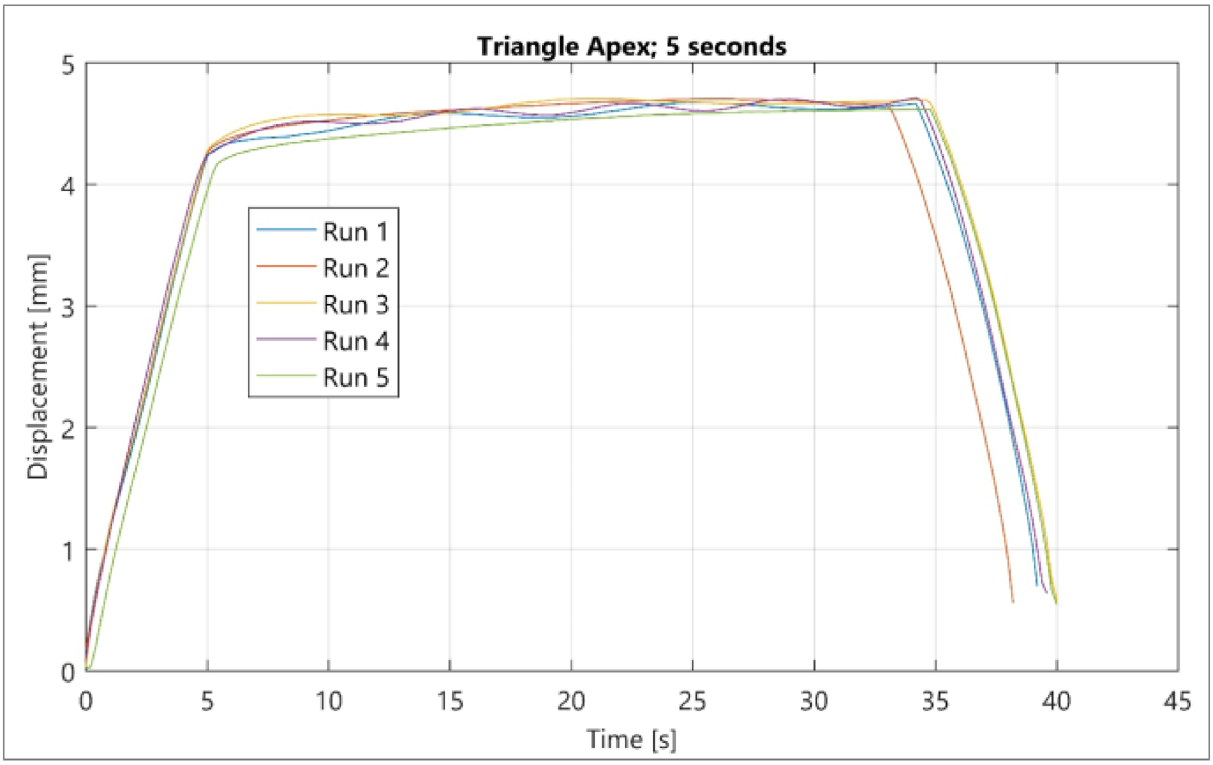

Figure 59: Displacement results for T-apex, 5s

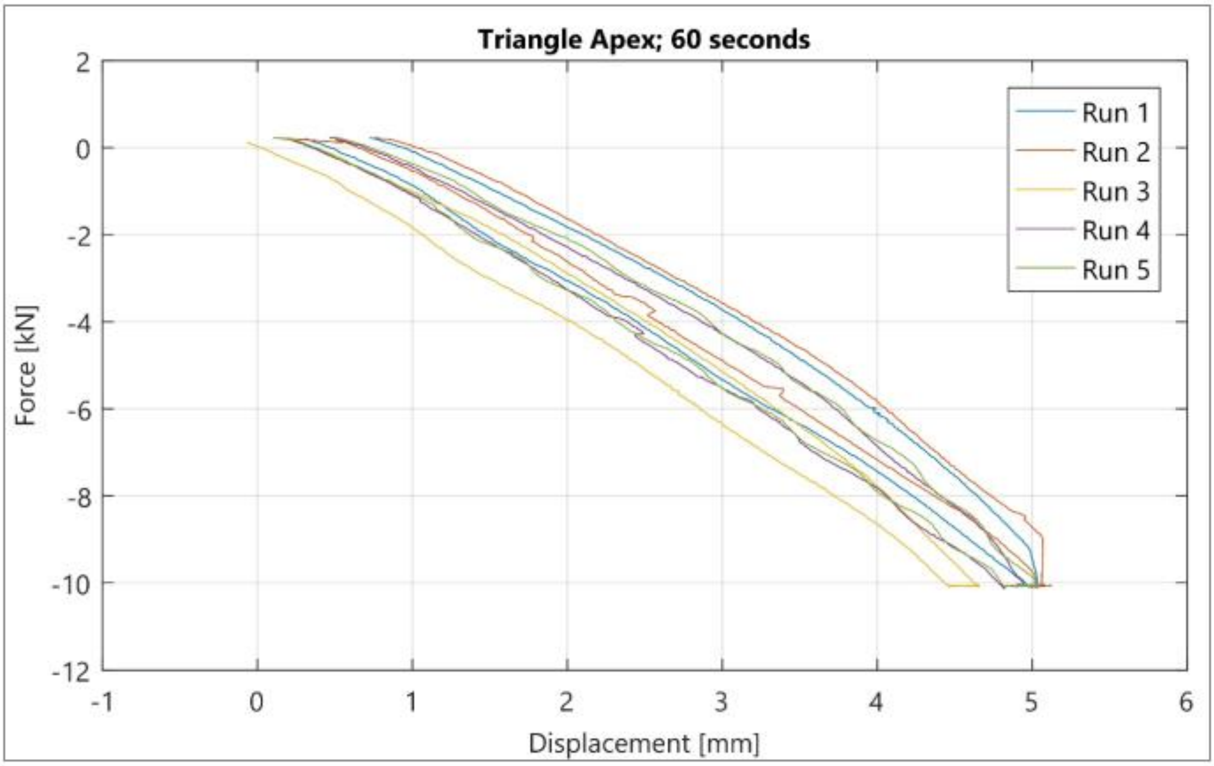

Figure 60: Stiffness results for T-apex, 60s.

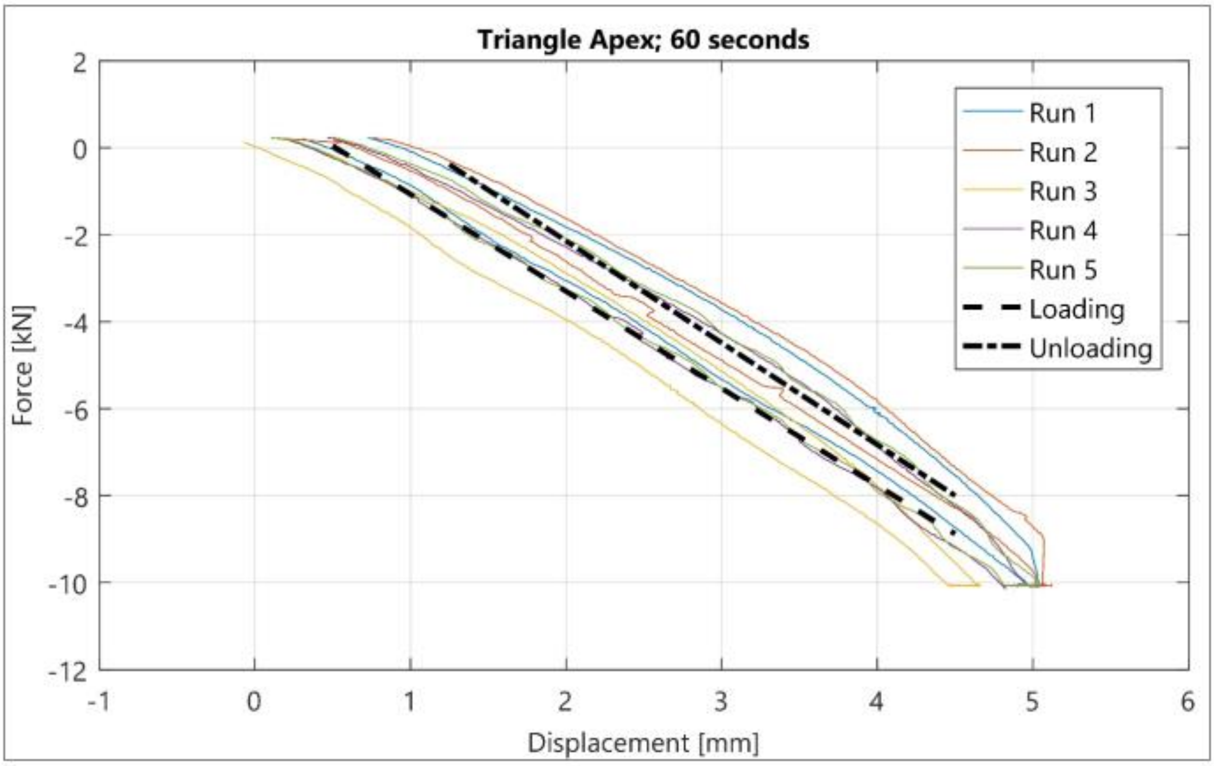

Figure 61: Stiffness results for T-apex, 60s with linear fit.

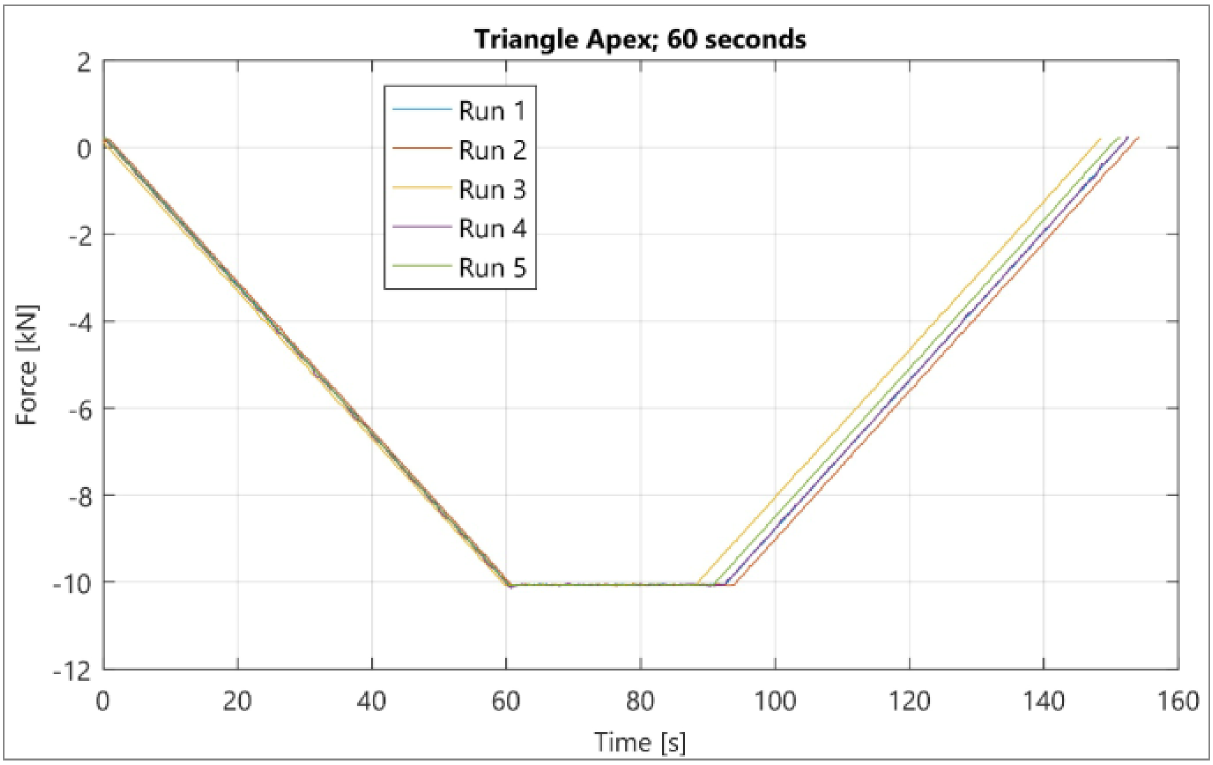

Figure 62: Load results for T-apex, 60s.

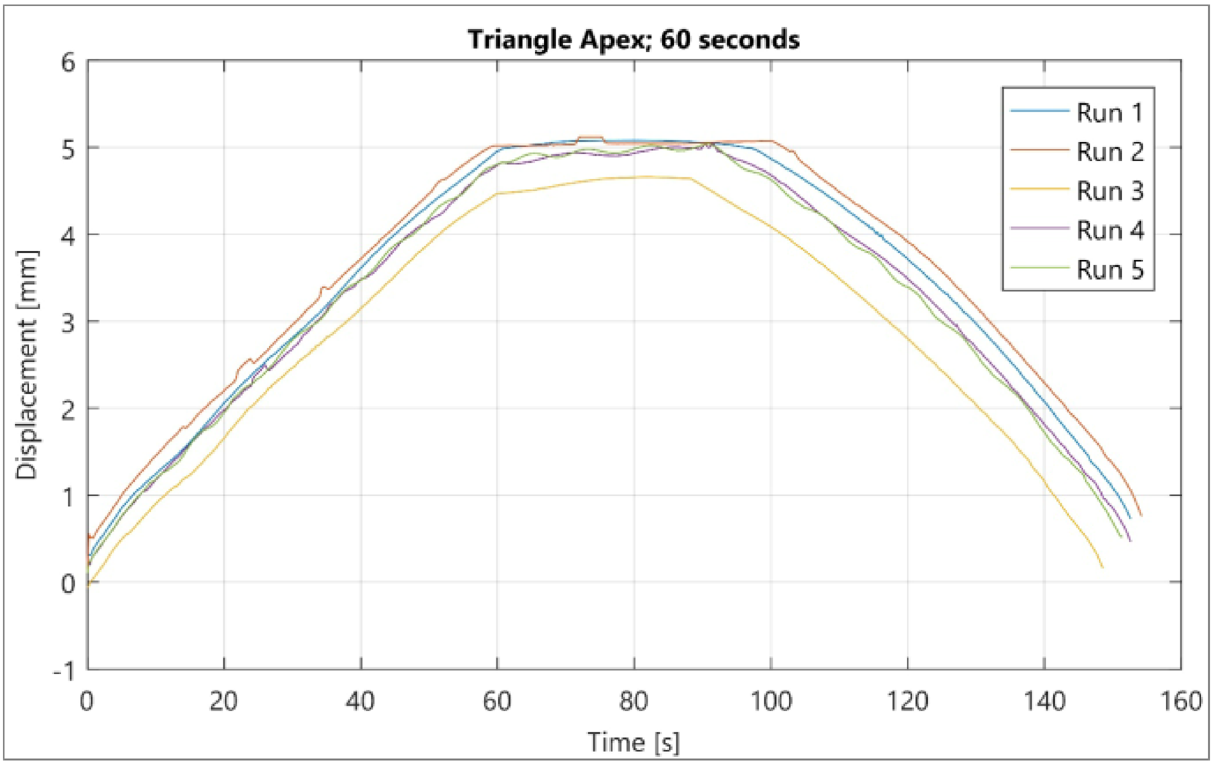

Figure 63: Displacement results for T-apex, 60s

Table 17: Triangle Bottom, 5 seconds duration of loading and unloading the tyre to 10 kN, respectively.

Run Number	Loading Stiffness [kN/mm]	R2 Loading	Unloading Stiffness [kN/mm]	R2 Unloading	R2
1	2.859	0.9964	2.9461	0.9906	-
2	2.6614	0.994	2.9438	0.987	-
3	2.938	0.9966	3.0486	0.9837	-
4	2.7529	0.9921	3.0621	0.9796	-
5	2.6917	0.991	3.0867	0.9871	-
Average	2.7806	-	3.0175	-	-

Table 18: Triangle Bottom, 60 seconds duration of loading and unloading the tyre to 10 kN, respectively.

Run Number	Loading Stiffness [kN/mm]	R2 Loading	Unloading Stiffness [kN/mm]	R2 Unloading	R2
1	2.5698	0.9952	2.6852	0.9851	-
2	2.4771	0.9941	2.713	0.9881	-
3	2.3864	0.9923	2.7276	0.976	-
4	2.5134	0.9938	2.711	0.9836	-
5	2.4813	0.9937	2.6991	0.9861	-
Average	2.4856	-	2.7072	-	-

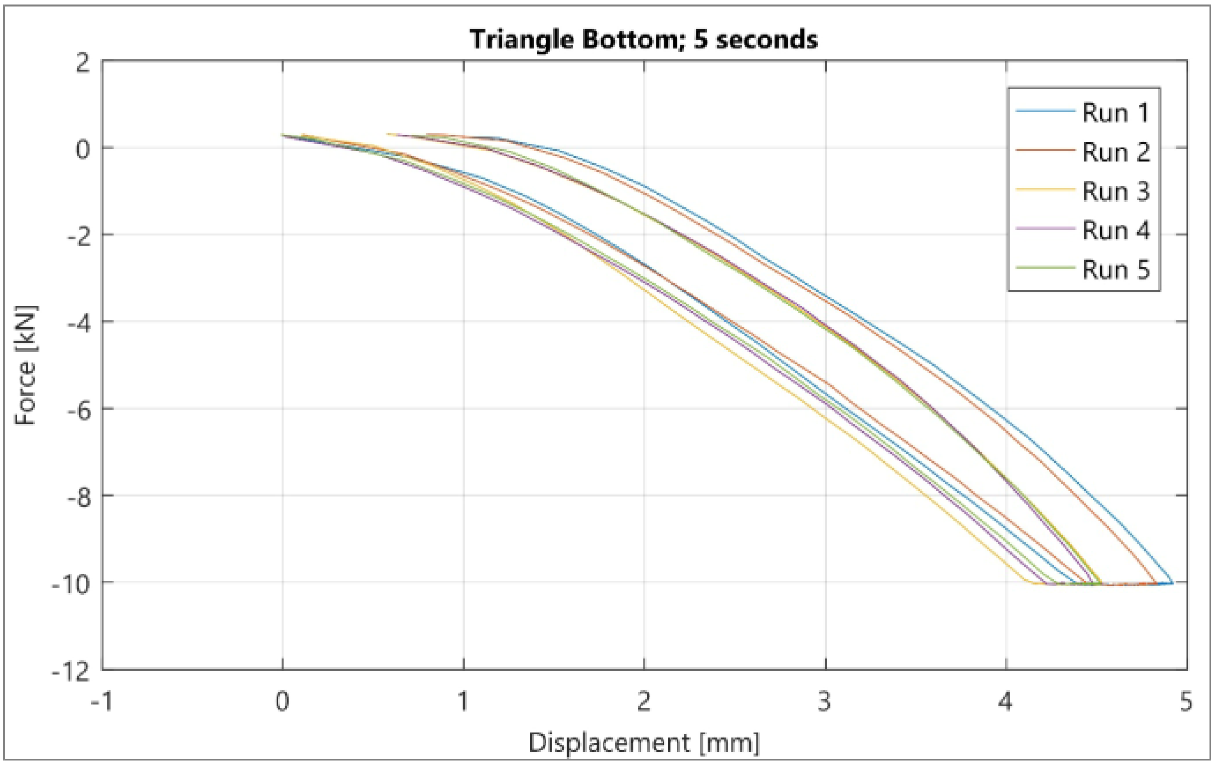

Figure 64: Stiffness results for T-bottom, 5s.

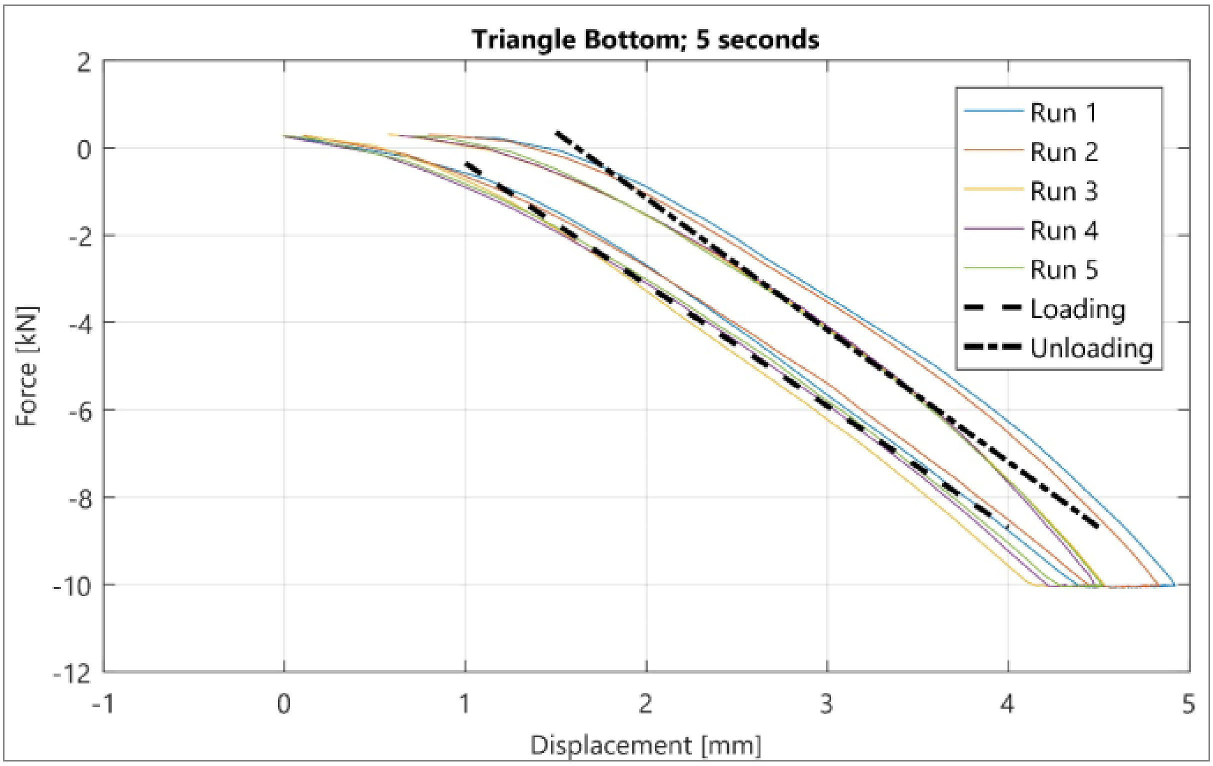

Figure 65: Stiffness results for T-bottom, 5s with linear fit.

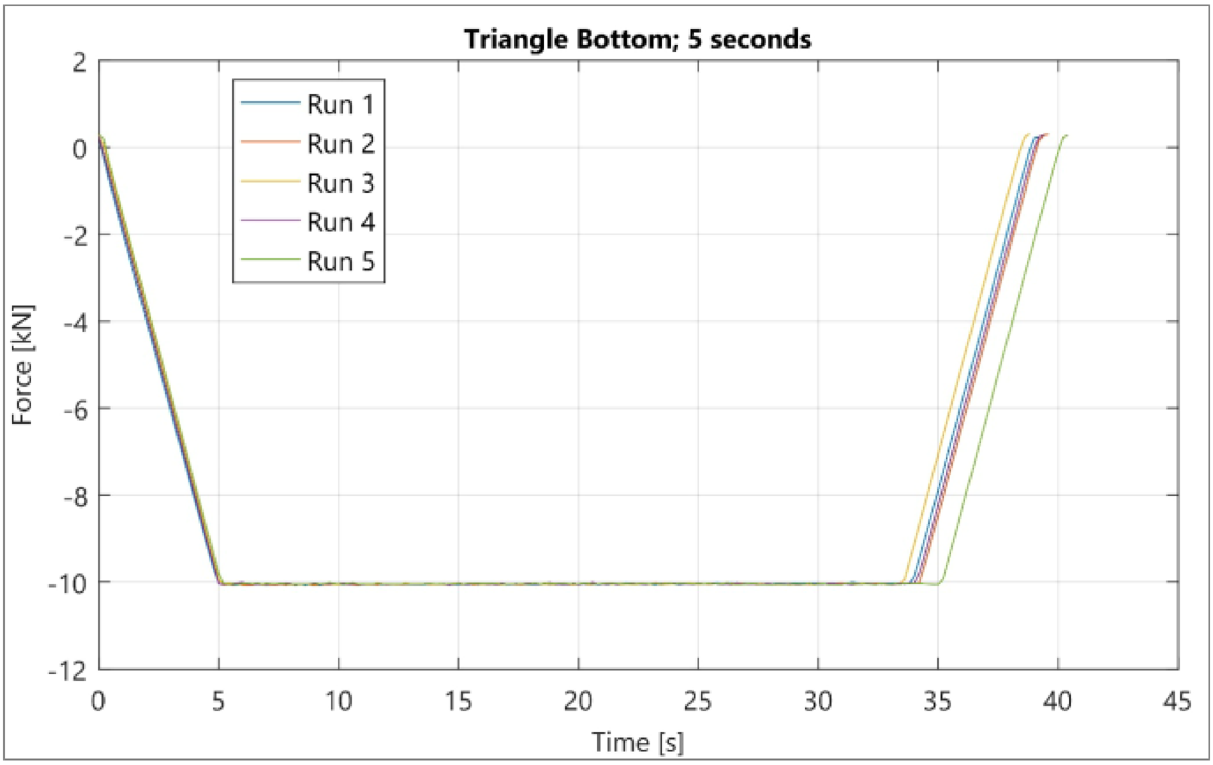

Figure 66: Load results for T-bottom, 5s.

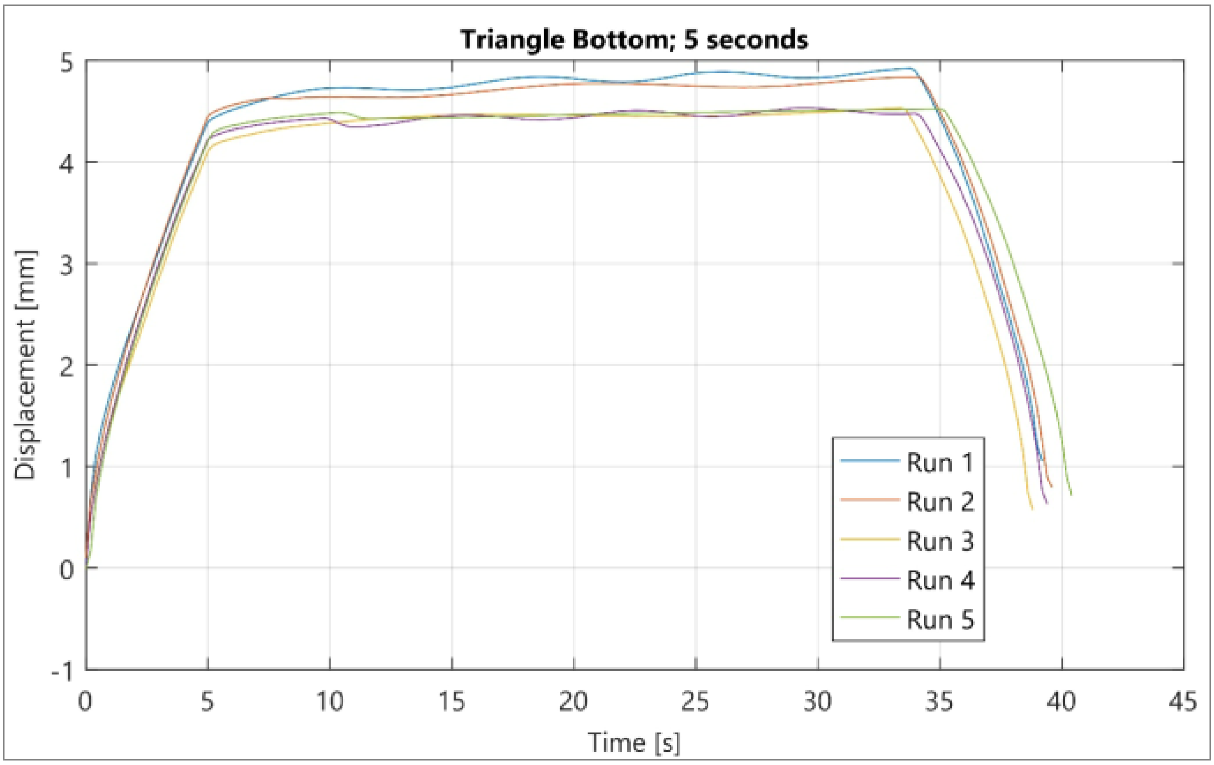

Figure 67: Displacement results for T-bottom, 5s.

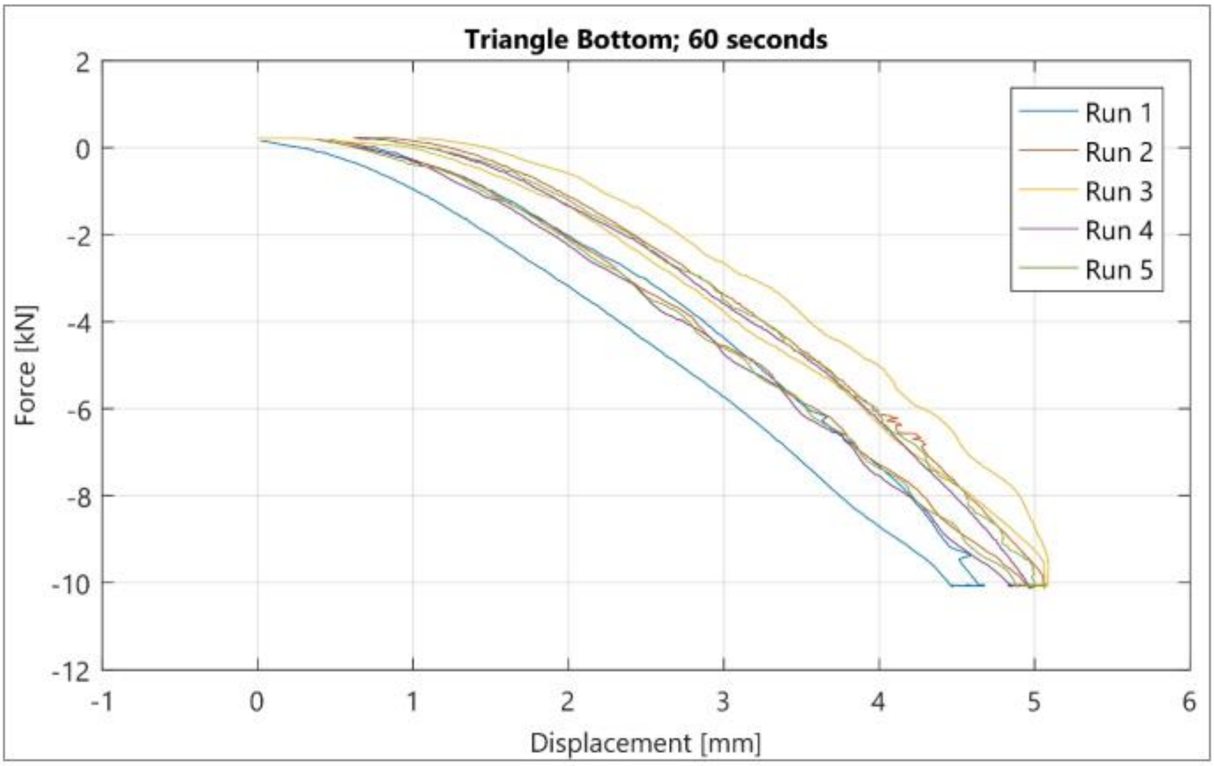

Figure 68: Stiffness results for T-bottom, 60s.

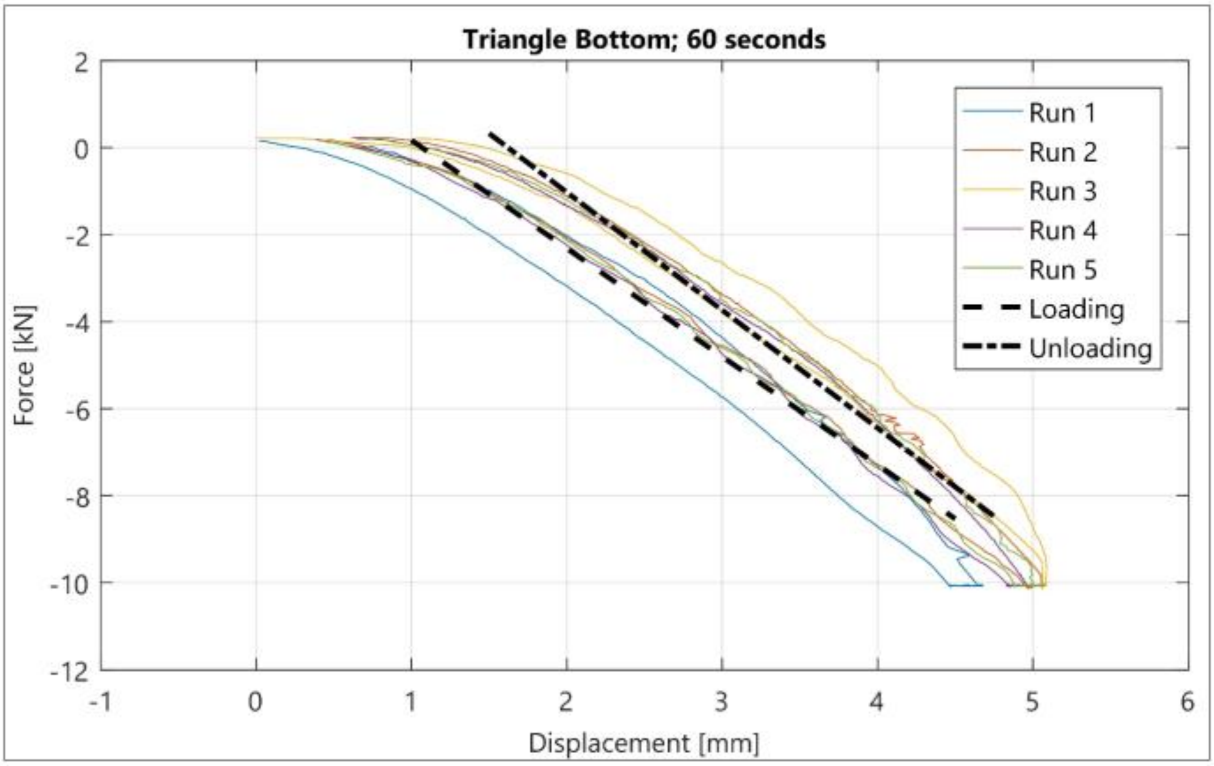

Figure 69: Stiffness results for T-bottom, 60s with linear fit.

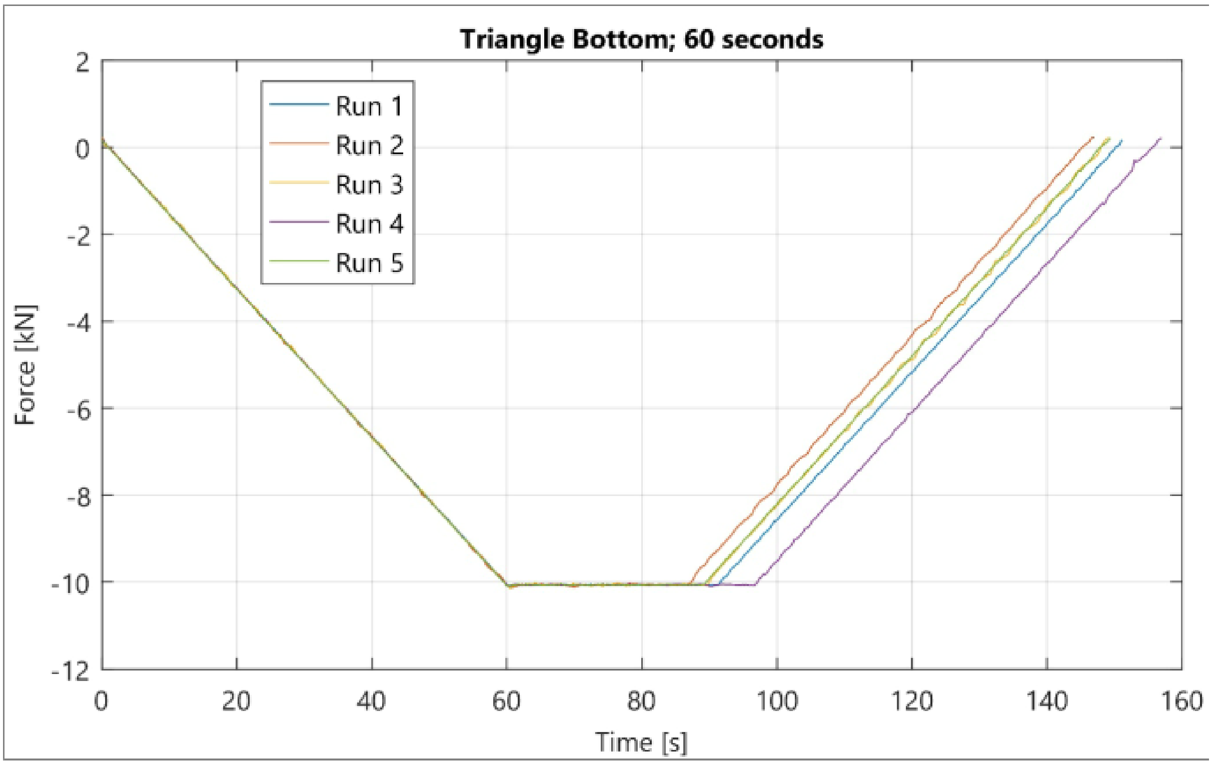

Figure 70: Load results for T-bottom, 60s.

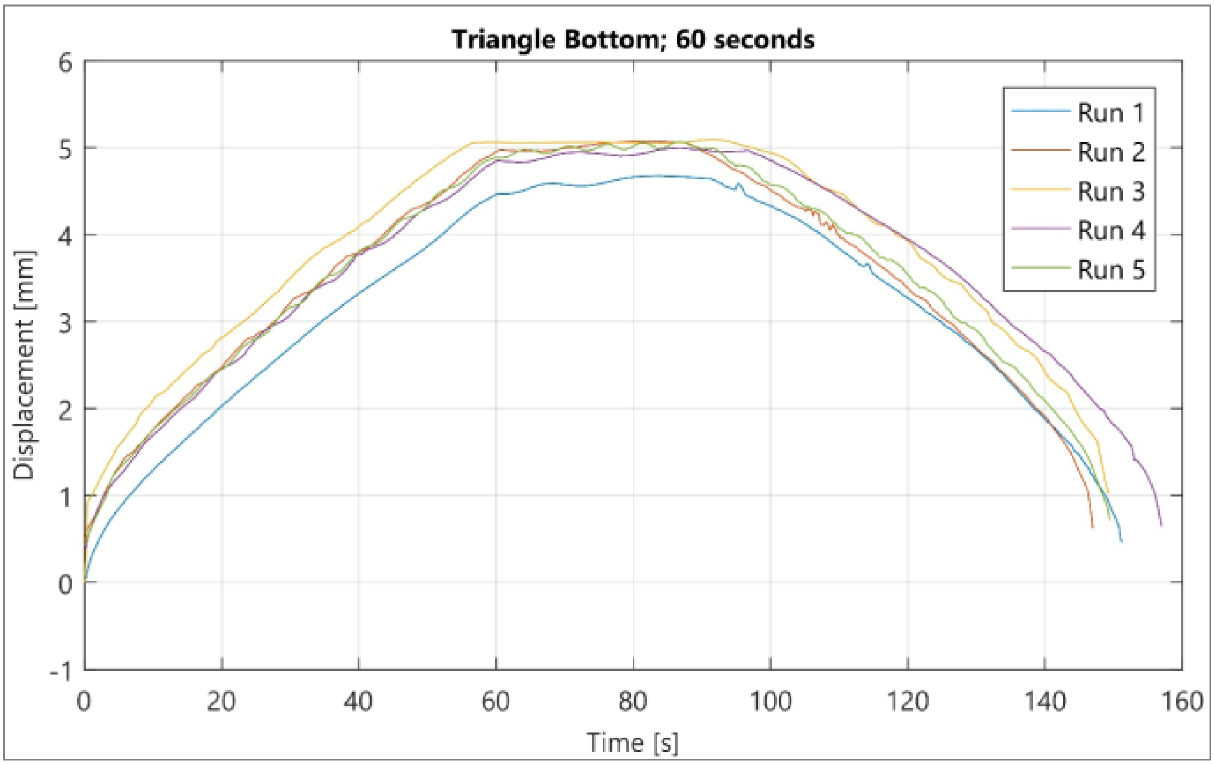

Figure 71: Displacement results for T-bottom, 60s.

Table 19: Summary of Results

Data Set	**Average Stiffness [kN/mm]**	
	Loading	Unloading
Triangle Apex; 5s	2.5343	2.6626
Triangle Apex; 60s	2.2307	2.3426
Triangle Bottom; 5s	2.7806	3.0175
Triangle Bottom; 60s	2.4856	2.7072

7. FEA Approach

7.1 Engineering Data (Material Modelling and Curve Fitting)

All the non-PU materials were assigned as aluminium 7075-T6 with properties from with ANSYS material guide which is highlighted in Table 1.

Using the hyperelastic material testing data and employing advanced numerical processing techniques facilitated by MATLAB, as delineated in Annexure A. The process of curve fitting, a statistical method used to construct a curve that best fits the data points needs to be conducted.

The overarching challenge lies in the determination of specific coefficients within the constitutive equations that characterize the material properties under examination. These coefficients are pivotal in capturing the complex, non-linear behaviour exhibited by hyperelastic materials.

While it is feasible to calibrate hyperelastic models using experimental data from a singular mode of deformation, such an approach may limit the model's predictive accuracy to that specific mode of deformation. Consequently, it is prudent to employ data from multiple or all three deformation modes to enhance the model's robustness and reliability.

The calibration process entails the selection of an appropriate hyperelastic model and its subsequent curve-fitting against the gathered experimental data. This procedure yields constants that are interpreted as the material's inherent properties. Within the ANSYS Mechanical framework, there are plenty of hyperelastic material models are available for selection, each accommodating curve fitting within the Engineering Data module as seen in Figure 72.

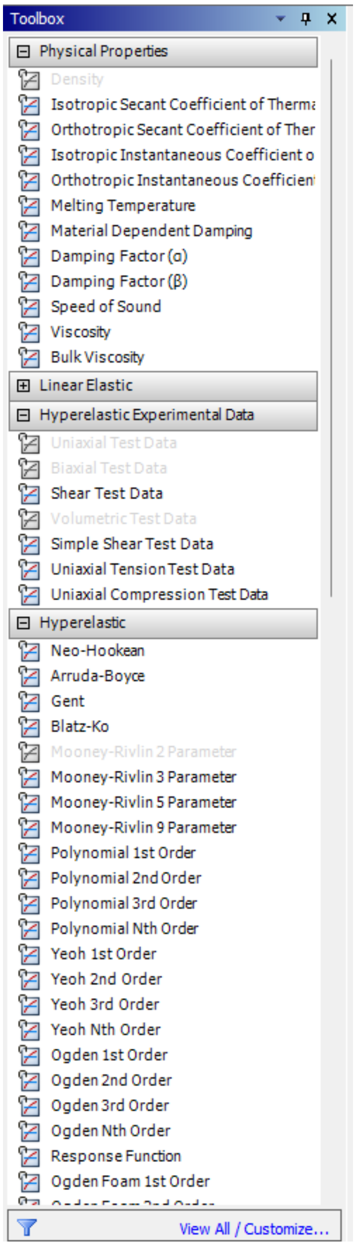

Figure 72: ANSYS selection of material models.

Curve fitting is essentially an optimization process, minimizing the cumulative discrepancy between the experimental data and the model's predictions. This discrepancy is quantified through an error function, typically the least squares function, and is minimized using either linear or non-linear regression methods based on the model's complexity and the number of material constants involved.

The minimized value of this error function, referred to as the residue, serves as a metric for evaluating the quality of the fit between the model predictions and the experimental data. The subsequent Figure 81, Figure 83 and Figure 84 show the curve fitting in ANSYS Workbench using the Engineering Data module, utilizing an elastomer sample's data inclusive of uniaxial tension, compression and shear.

This comprehensive approach to material testing and model calibration, involving data processing, model selection, and curve fitting, is instrumental in advancing the understanding and predictive capabilities of hyperelastic material behaviour. It underlines the intricate interplay between empirical data and computational modelling, ultimately facilitating the development of more accurate and reliable material models.

7.1.1 Carcass material (LF950A)

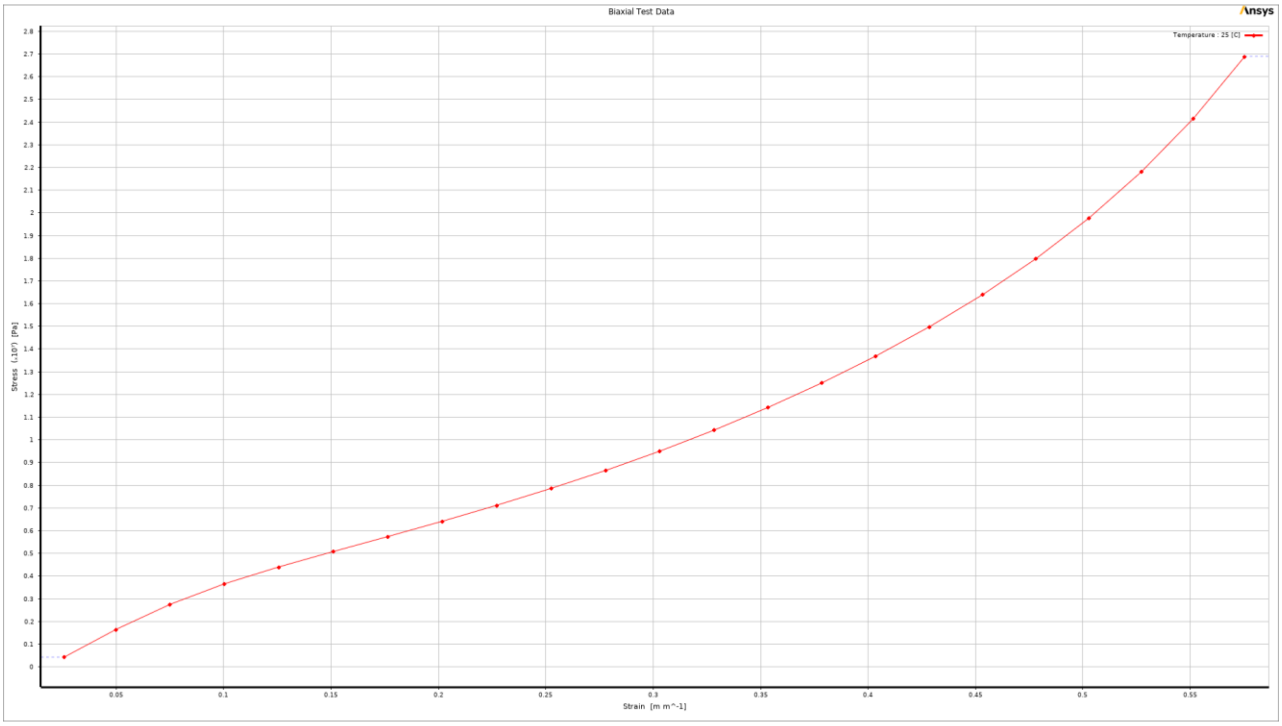

Figure 73: LF950 Compression testing after processing raw data at room temperature.

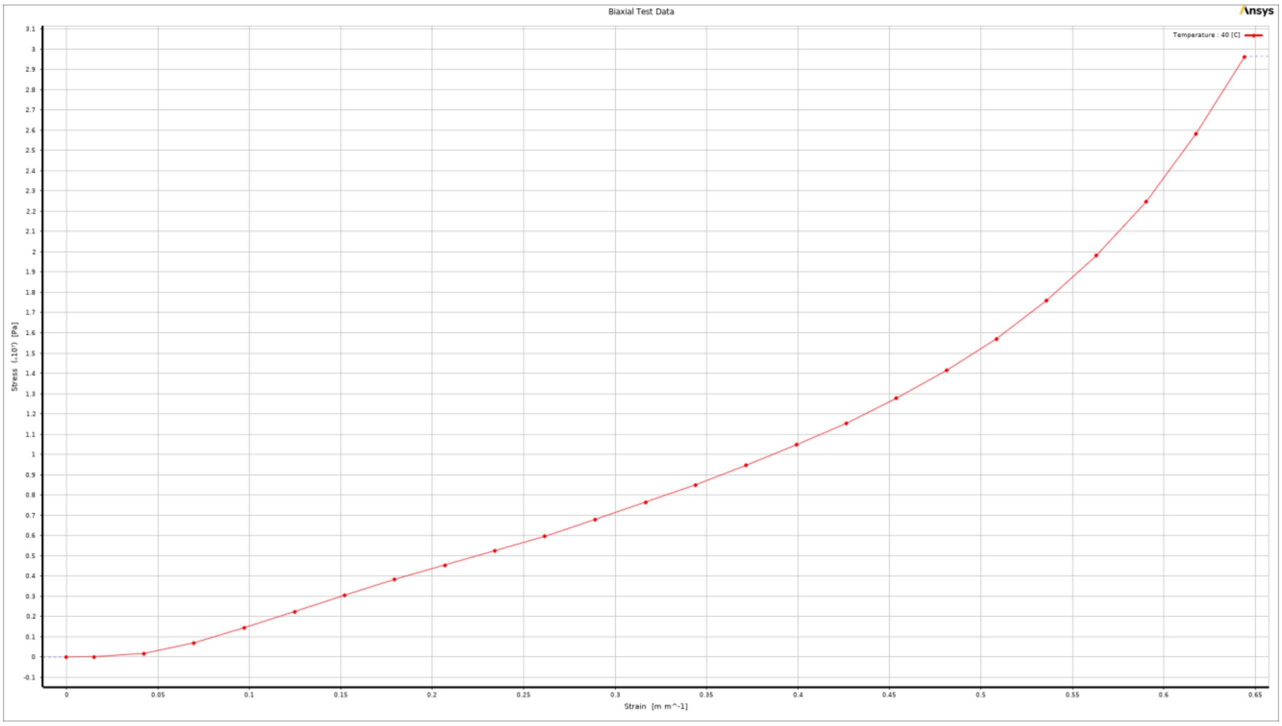

Figure 74: LF950 Compression testing after processing raw data at 40℃

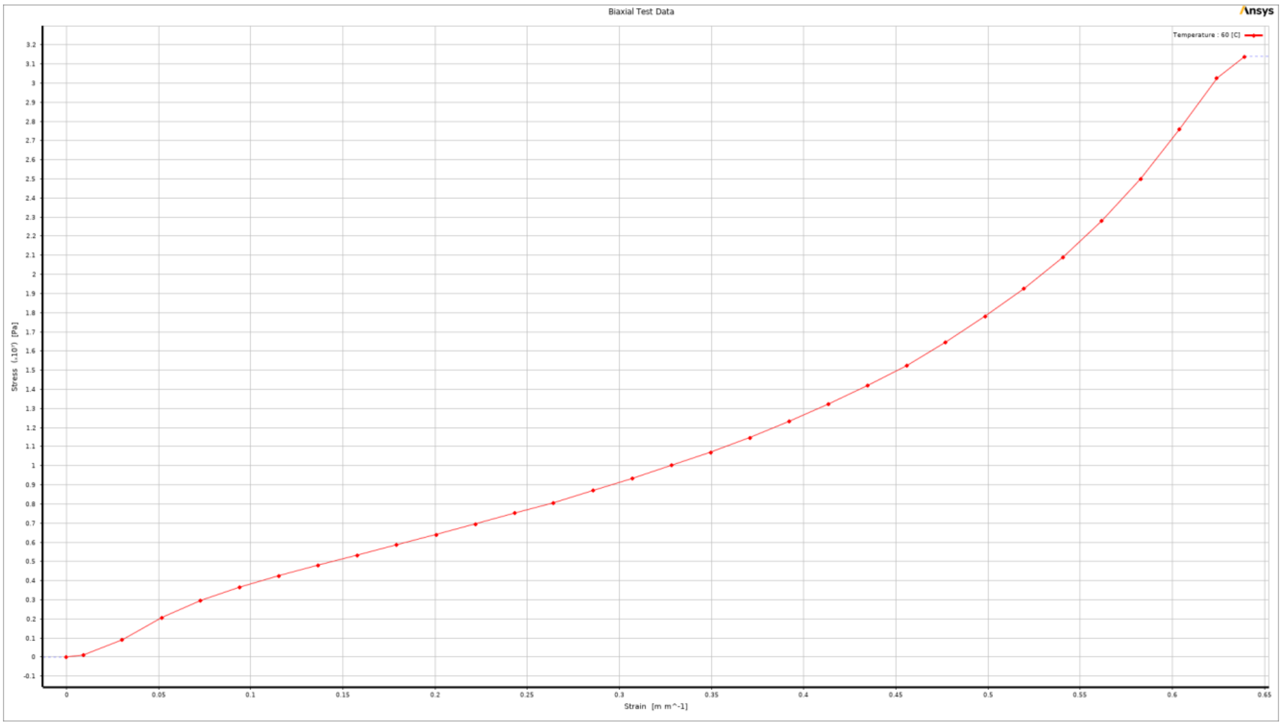

Figure 75: LF950 Compression testing after processing raw data at 60℃

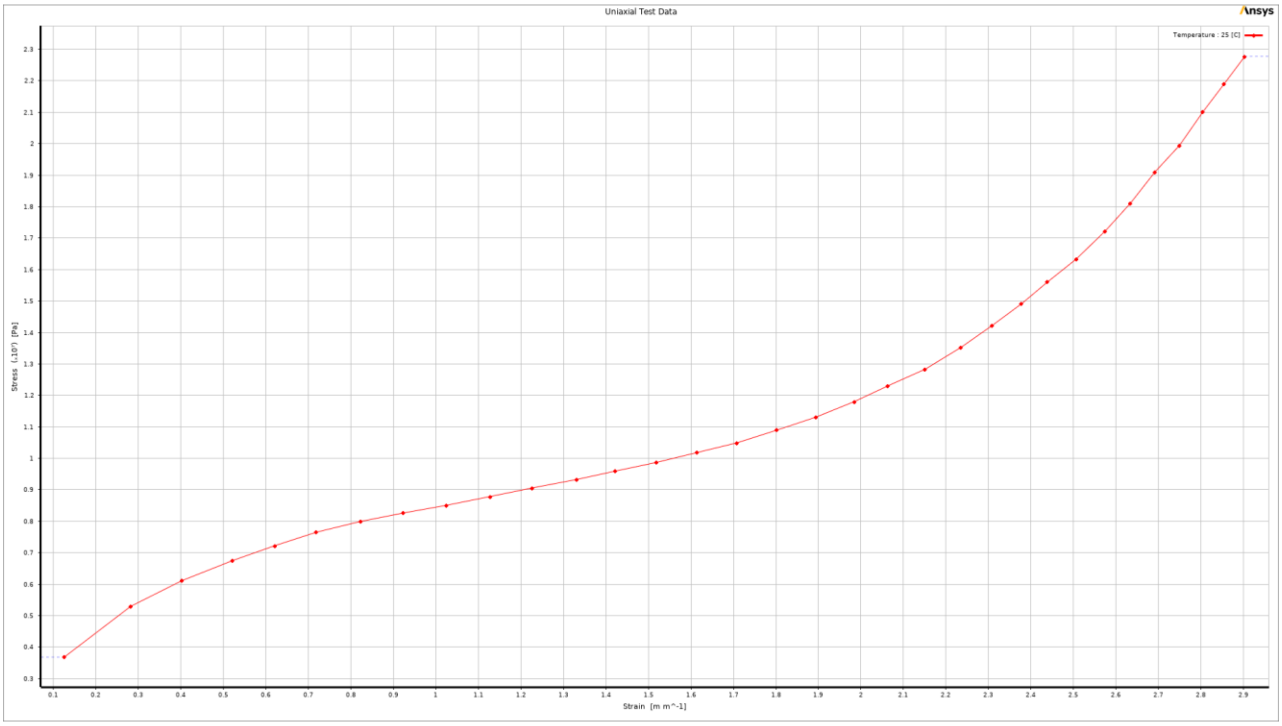

Figure 76: LF950 Uniaxial tensile testing after processing raw data at room temperature.

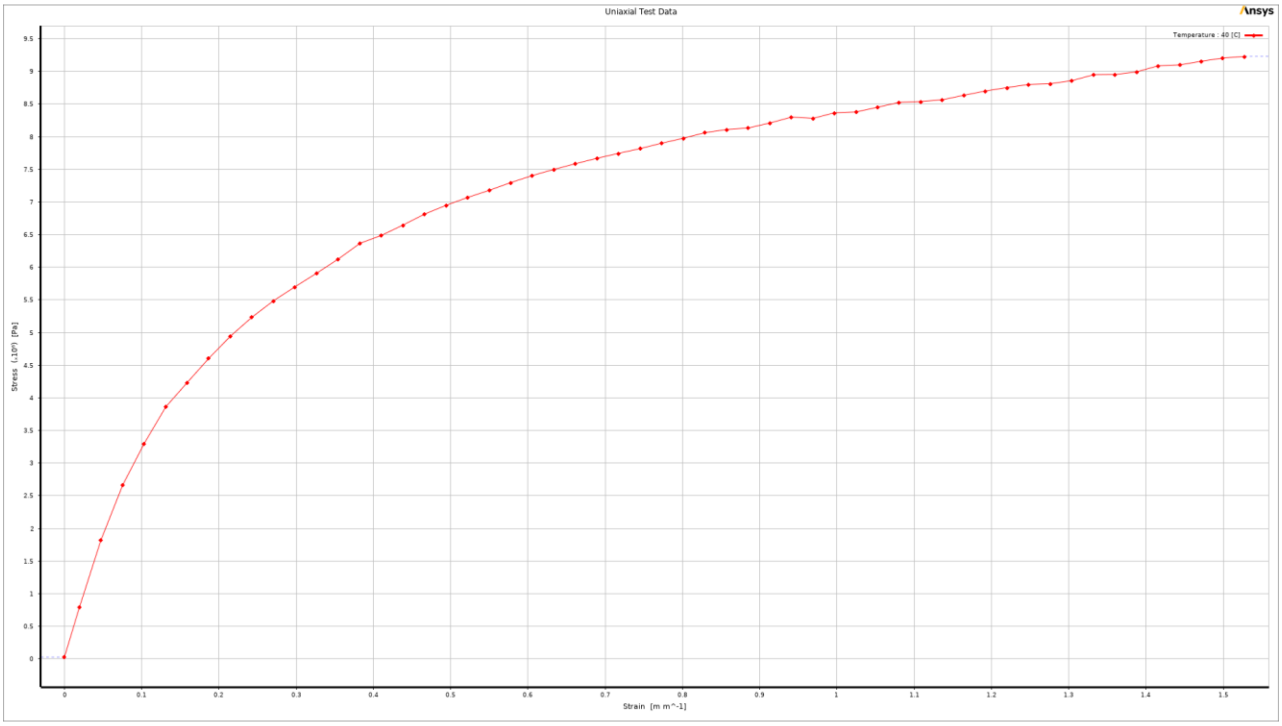

Figure 77: LF950 Uniaxial tensile testing after processing raw data at 40℃.

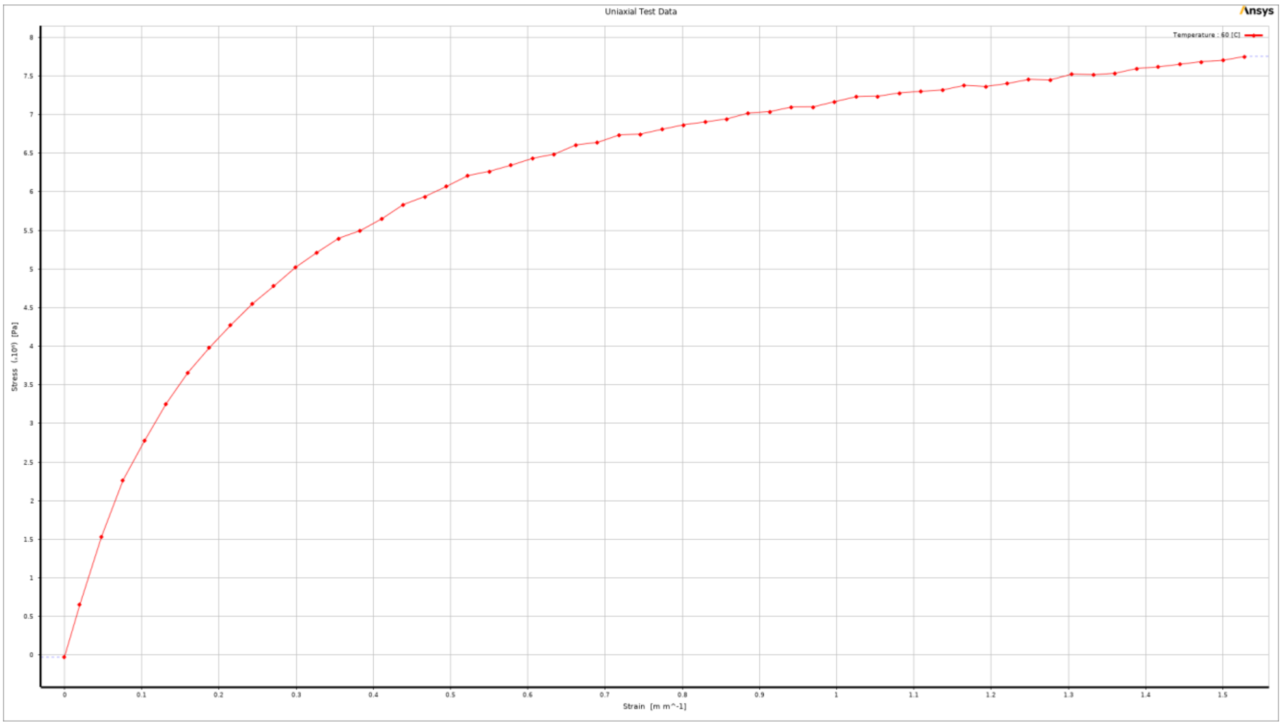

Figure 78: LF950 Uniaxial tensile testing after processing raw data at 60℃

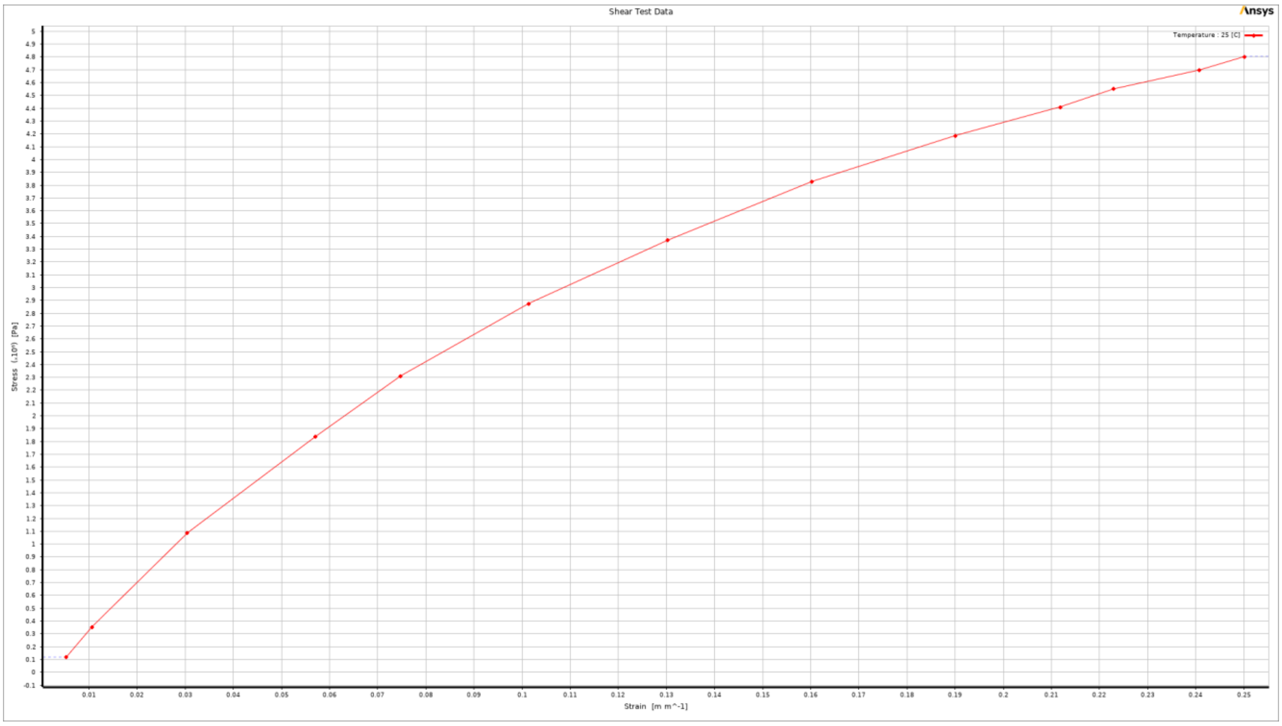

Figure 79: LF950 testing after processing raw data at room temperature.

*In the context of evaluating the mechanical properties of hyperelastic materials, a notable impediment was encountered during the attempt to procure shear data at higher temperatures. Specifically, the specimens under examination consistently evaded secure retention by the clamping jaws of the testing apparatus, resulting in slippage. This phenomenon prevented the effective application of shear forces, thereby rendering the acquisition of empirical shear data unfeasible.

The propensity of the samples to disengage from the jaw clamps of the testing device may be attributed to a multitude of factors intrinsic to the material's characteristics or stemming from the experimental setup machine. Hyperelastic materials, known for their extensive elasticity and substantial deformation capabilities, may present unique challenges in maintaining a firm grip within the confines of conventional clamping mechanisms. This issue underscores the necessity for a meticulous reassessment of the test fixture design or the exploration of alternative methods for securing the samples, ensuring an unyielding engagement conducive to the precise application of shear forces.

It was decided that the room temperature data would be sufficient to characterise the material.

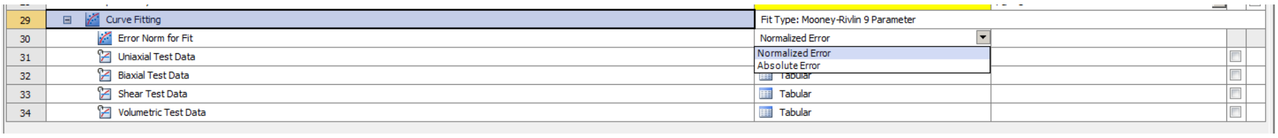

Figure 80: Curve fitting setting in ANSYS.

The same approach was used for the 3 different materials used. The absolute error model was used with the closest curve fit as seen in Figure 73 to Figure 84.

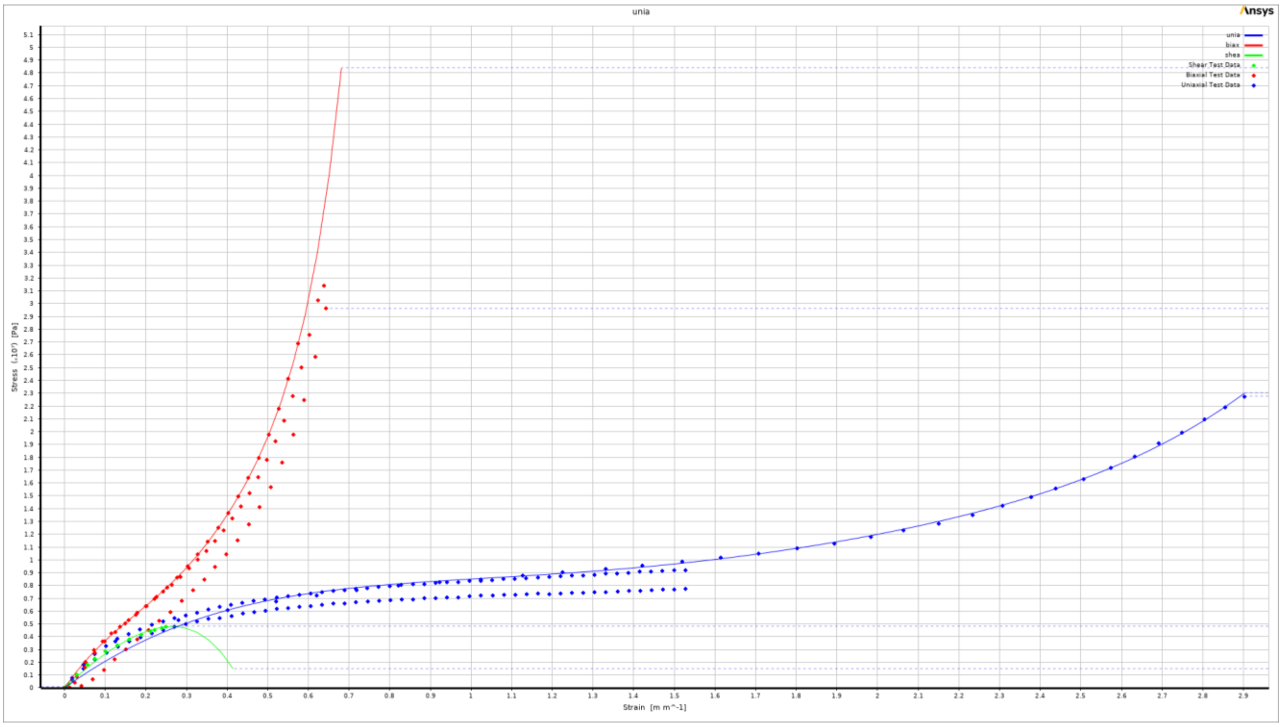

Figure 81: All 3 sets of data fitted with the Mooney-Rivlin 9 model.

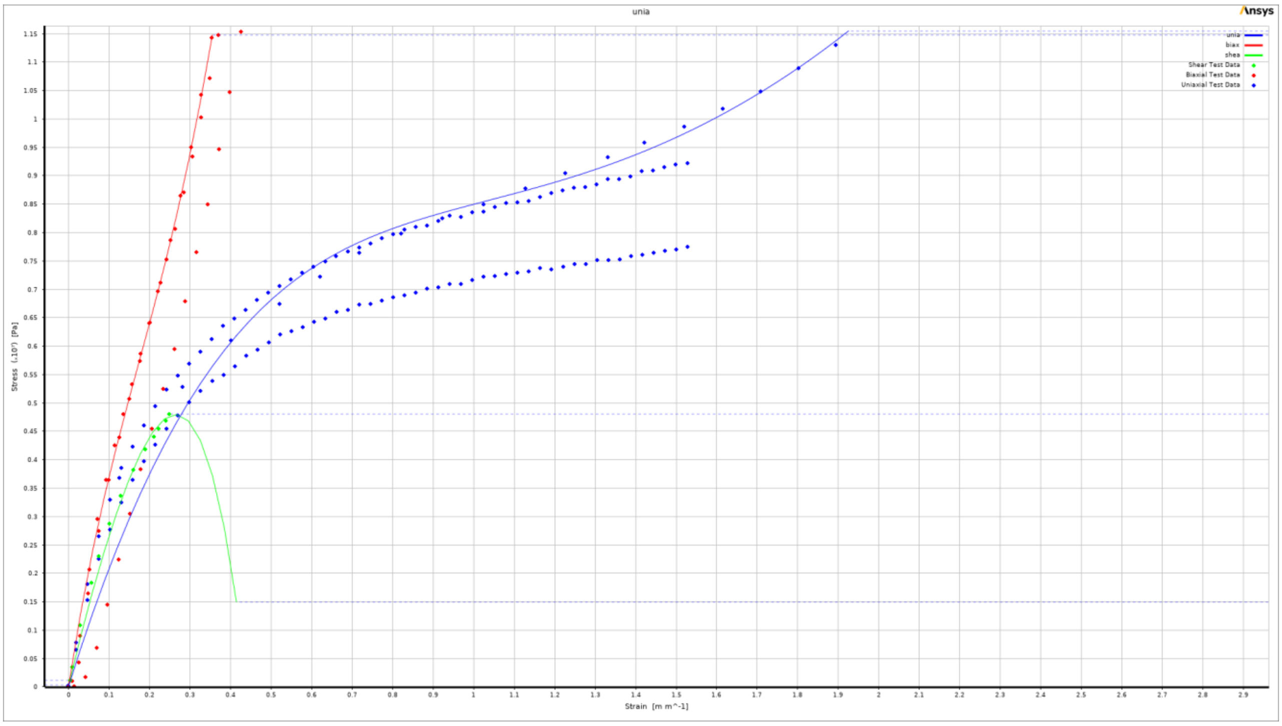

Figure 82: Closer look at the material curves at lower strains.

Table 20: Calculated Material constants of LF950A with Mooney-Rivlin 9 model

Temperature (℃)	Material Constant C10 (Pa)	Material Constant C01 (Pa)	Material Constant C20 (Pa)	Material Constant C11 (Pa)	Material Constant C02 (Pa)	Material Constant C30 (Pa)	Material Constant C21 (Pa)	Material Constant C12 (Pa)	Material Constant C03 (Pa)	Incompressibility Parameter D1 (Pa^-1)
25	3625892	214432.4	25240400	-5.2E+07	26583933	132350.7	-1028675	-3466577	713977.1	6.11E-10
40	6847008	-3311531	-1.3E+07	20940635	-8736193	-1378849	5795442	-3553149	864541.3	8.55E-10
60	3155831	969050	33298748	-6.9E+07	34412484	177587.6	-1640333	-3823603	704519.8	8.85E-10

7.1.2 Stiff Shear Band (LF750D)

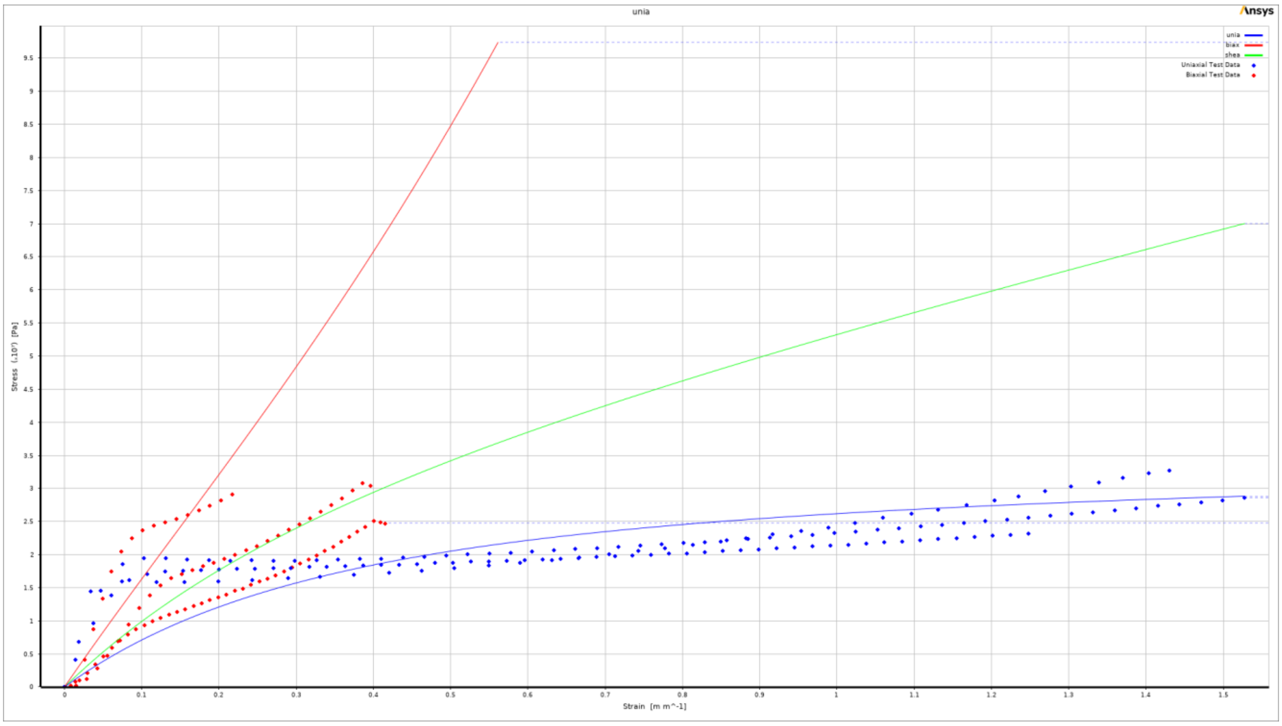

Figure 83: All 3 sets of data fitted with the Mooney-Rivlin 2 model.

Table 21: Calculated Material constants of LF750D with Mooney-Rivlin 2 model

Temperature (C)	Material Constant C10 (Pa)	Material Constant C01 (Pa)	Incompressibility Parameter D1 (Pa^-1)
25	765489.9	13431063	5.57E-10
40	4515538	4903745	8.62E-10
60	5550511	2451921	7.26E-10

7.1.3 Soft Thread (V6060)

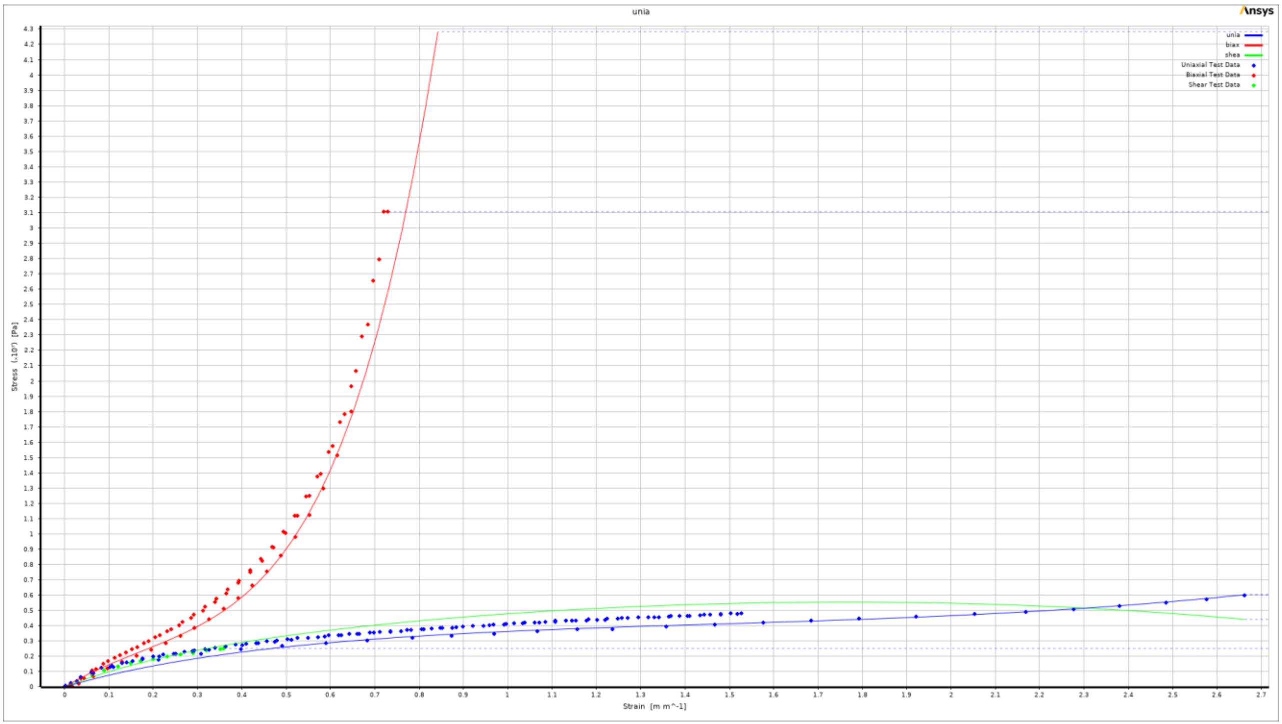

Figure 84: All 3 sets of data fitted with the Mooney-Rivlin 5 model.

Table 22: Calculated Material constants of V6060 with Mooney-Rivlin 5 model

Temperature (°C)	**Material Constant C10 (Pa)**	**Material Constant C01 (Pa)**	**Material Constant C20 (Pa)**	**Material Constant C11 (Pa)**	**Material Constant C02 (Pa)**	**Incompressibility Parameter D1 (Pa^-1)**
25	1047497	391864.1	99177.58	-433467	298046.6	5.63E-10
40	1264599	701882.6	345180.8	-1113732	537024.4	8.34E-10
60	1235473	744975.7	373805.3	-1181748	564999	8.50E-10

7.2 Geometry

The geometry used is the wheel design concept 5 highlighted in Figure 32, however the rim was simplified to reduce simulation complexity.

A geometry without a rim was also used to eliminate the meshing of the rim completely. The use of the rim will be discussed in more detail through the setup of the simulation. A plate was added to the bottom of the wheel measuring 300x120x2mm which will be used to simulate the rigid road conditions.

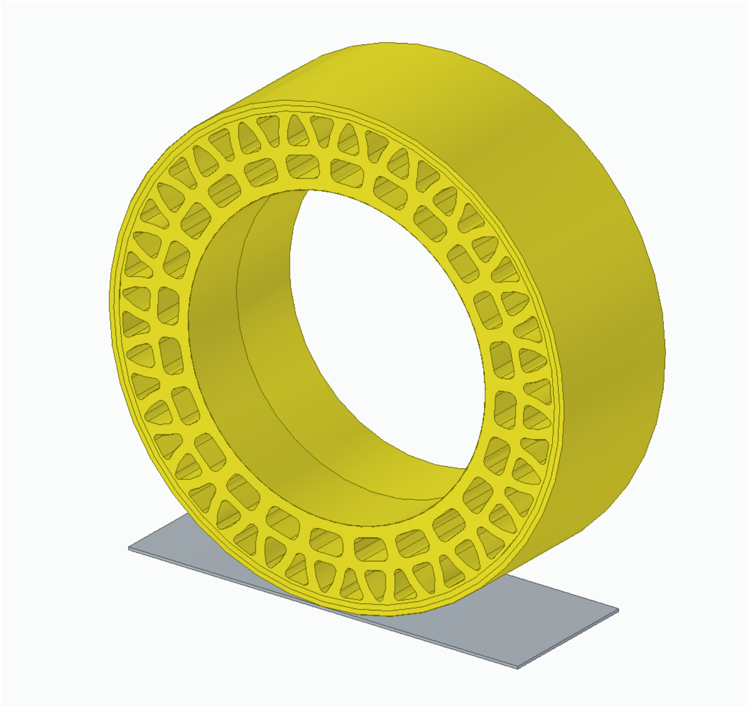

Figure 85: PU wheel without rim.

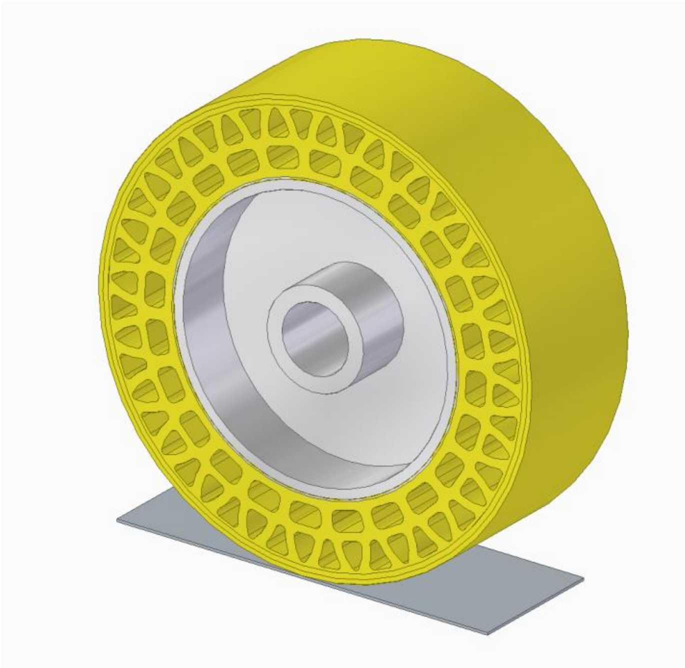

Figure 86: PU wheel with simplified rim.

7.3 Contact Definitions

The simplest contact definition is to input the bottom surface of the plate as a fixed support. This will ensure that the plate "road surface" remains fixed in position. The upper surface of the plate is not selected as this will be a contact surface with the thread of the wheel. If one surface is selected with two different definitions, then the following error will usually occur: "One or more remote boundary conditions is scoped to a large number of elements which can affect solver performance. Consider using the pinball setting to reduce the number of elements included in the solver".

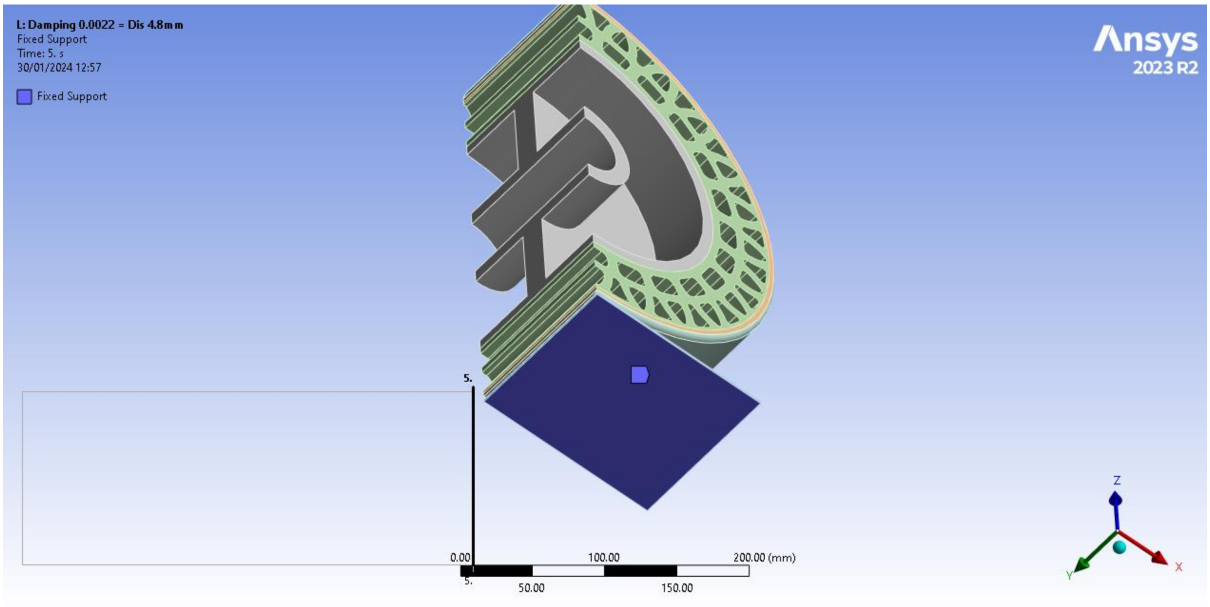

Figure 87: Fixed surface of the plate.

Symmetry was then applied to split the wheel in through the XZ place i.e. in half to reduce the mesh size and therefore the runtime. This however did not work as there was impractical, unconverged results. Instead of acting as a symmetry place, elements on the PU wheel (excluding the elements on the Al rim) in contact with the plane was acting as the plane was a fixed support. The idea was developed that if a used a cutting place through the centre XZ plane of the wheel and use a frictionless support only on the rim it will act as a symmetry plane as seen in Figure 88. Excluding the PU elements allowed the solution to converge however the results as seen in Figure 89 were impractical as compared to experimental testing. The cutting/symmetry plane through the XZ plane was therefore abandoned due to these results.

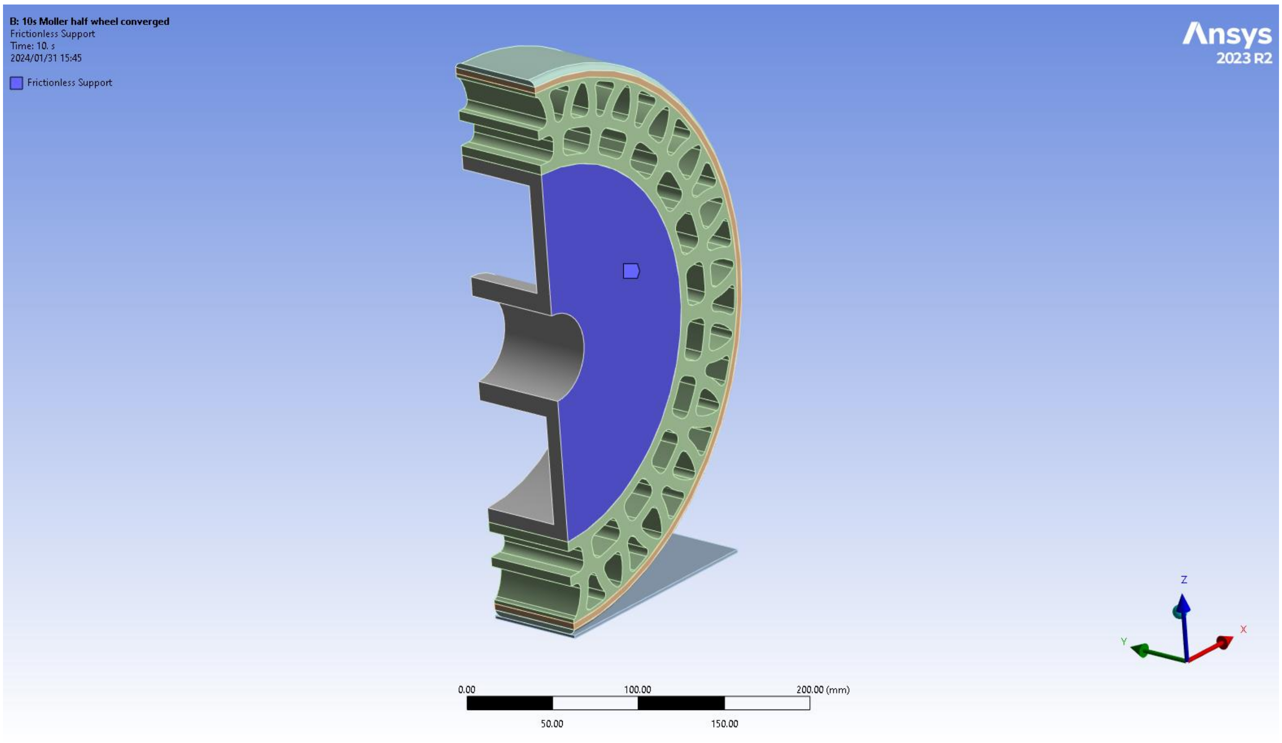

Figure 88: Frictionless support to represent a symmetry plane.

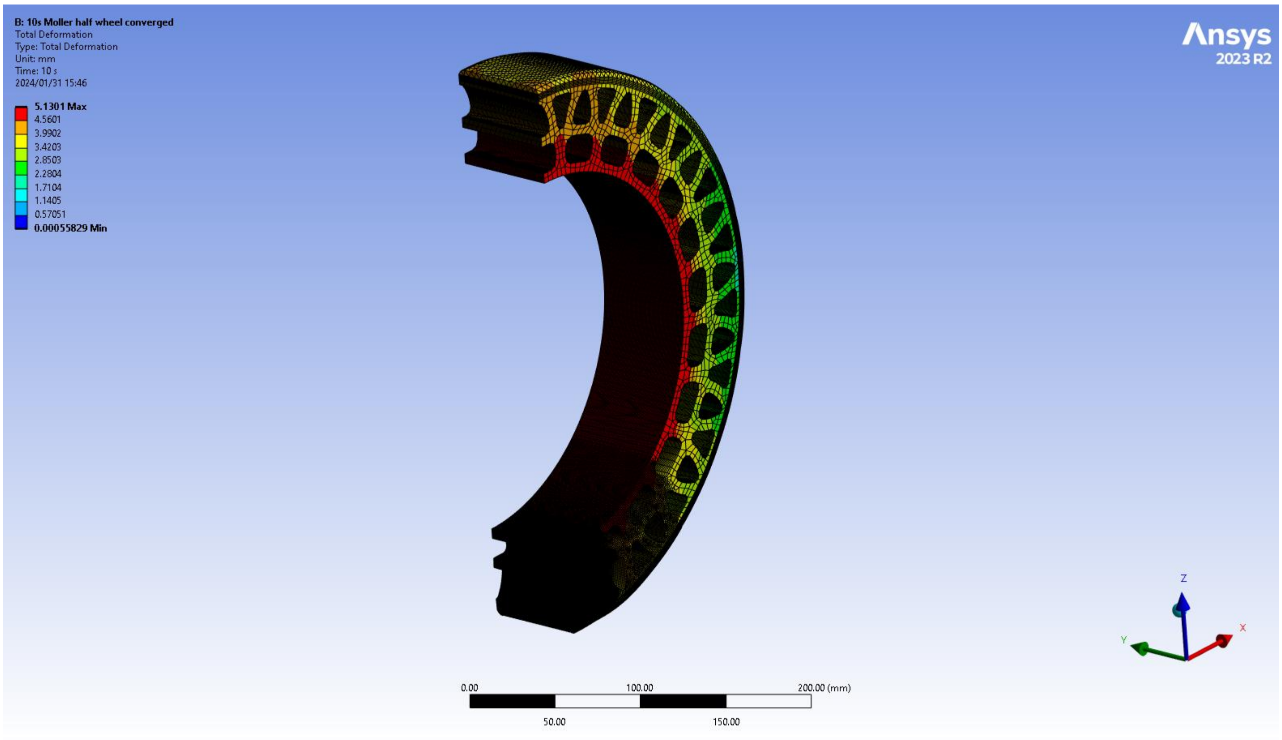

Figure 89: Deformation when using a frictionless support as a symmetry plane.

Symmetry could be applied through the YZ plane as seen in Figure 90 as the wheel geometry is completely symmetrical in this plane as well as the loading been symmetrical as well. This is an important factor to realise as a symmetry plane in the XY plane was initially used due to the geometric symmetry however the loading conditions are not symmetrical and therefore cannot be used.

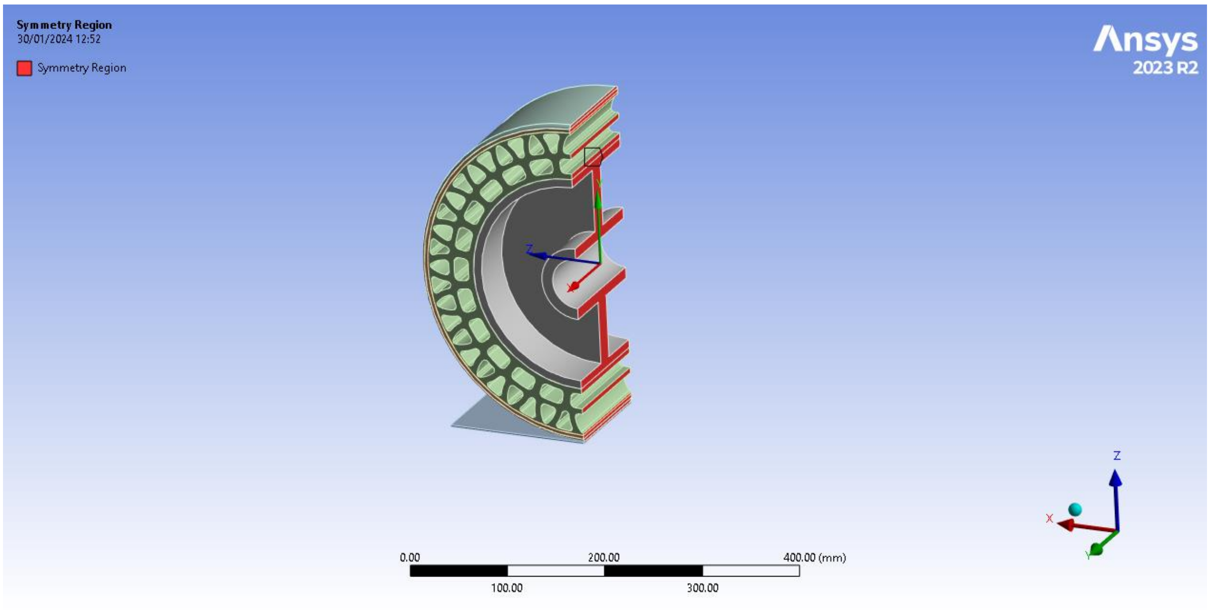

Figure 90: Symmetry applied through YZ plane.

7.3.1 Contact between the wheel and plate (road)

Addressing Contact as a Nonlinear Constraint creates further complexity in modelling.

Contact represents a nonlinear boundary value conundrum, primarily because during the interaction phase, both the contact forces and the contact surface area are subject to variation. Given the large strain nature of PU, these alterations in contact area are notably pronounced and present substantial modelling obstacles, particularly when put together with earlier material non-linearities. The transmission of contact stress predominantly occurs in the normal direction (Z); however, in the presence of friction, shear stress transmission is also a factor.

From a mathematical standpoint, the contact challenge manifests as a constrained optimization issue, where the conditions of contact are encapsulated as inequalities, commonly referred to as Kuhn-Tucker conditions [30]. Within the finite element method framework, several strategies have been employed to model frictional contact and enforce the nonpenetration constraint, effectively preventing the overlap of contact bodies. Noteworthy among these are Penalty Methods, Lagrange Multipliers, Augmented Lagrangian methods, Perturbed Lagrangian techniques, Hybrid Methods, Gap Elements, Interface Elements, the direct application of contact forces, and Solver Constraints. In essence the Penalty formulation models contact as a spring, preventing penetration through contact stiffness, influenced by material properties, geometry, and kinematics. The Lagrange formulation treats contact as a constraint, aiming for zero penetration without requiring contact stiffness.

A critical observation is that the employment of any interface elements necessitates a prior knowledge of the contact location. The inherent flexibility of PU compounds this challenge, often leading to inaccurately estimated contact areas and consequentially incorrect force transmission across surfaces. In Penalty Methods, an inappropriate selection of the penalty parameter can result in penetration (if the penalty is too low) or numerical instability (if the penalty is excessively high). The Lagrange multiplier approach, while robust, introduces an elevated computational cost due to additional variables for contact pressure, coupled with potential numerical instability.

After testing, MPC, Augmented Lagrangian and Pure Penalty formulations, Normal Lagrange formulation worked in terms of preventing penetration of PU elements through the road surface. It was decided to use Normal Lagrange contact formulation for this reason.

The type of contact was selected was a no separation contact as it is a linear contact to simplify the non-linearities of the materials. For a dynamic simulation a frictional contact should be selected with the PU dynamic coefficient of 0.3 as stated previously used. However, in this load bearing analysis, the no separation contact will be sufficient for the correct physics to apply.

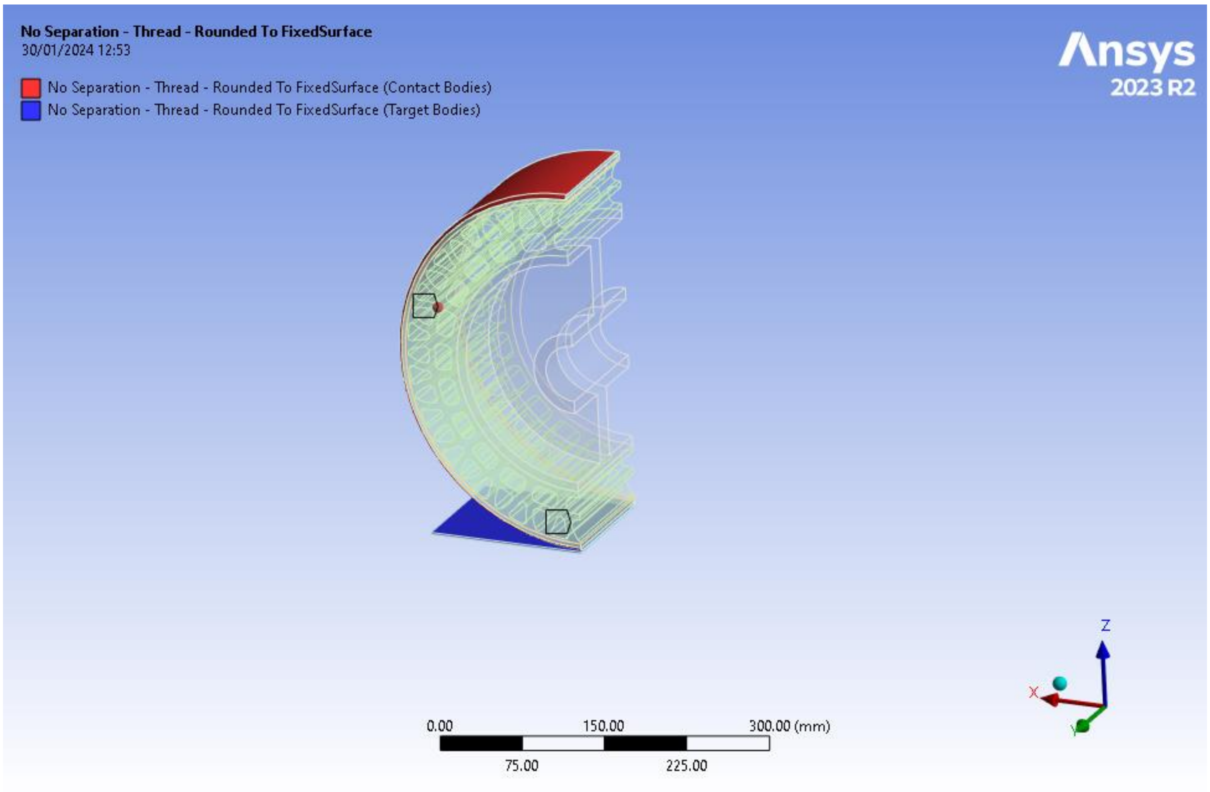

Figure 91: Thread layer selected as contact for plate.

Details of "No Separation - Thread - Rounded To FixedSurface"

Scope	
Scoping Method	Geometry Selection
Contact	3 Faces
Target	1 Face
Contact Bodies	Thread - Rounded
Target Bodies	FixedSurface
Protected	No
Definition	
Type	No Separation
Scope Mode	Manual
Behavior	Asymmetric
Trim Contact	On
Trim Tolerance	1. mm
Contact APDL Name	
Target APDL Name	
Suppressed	No
Display	
Element Normals	No
Advanced	
Formulation	Normal Lagrange
Small Sliding	Program Controlled
Detection Method	Program Controlled
Pinball Region	Radius
Pinball Radius	5. mm
Geometric Modification	
Contact Geometry Correction	None
Target Geometry Correction	None

Figure 92: Contact details.

7.4 Boundary Conditions

The force applied will be tested to 1-ton or 10 000N. Therefore, a ramped force of 10 000N is applied to the inner surface of the rim. It is important to note that this is the exact face which was loaded during the experimental testing.

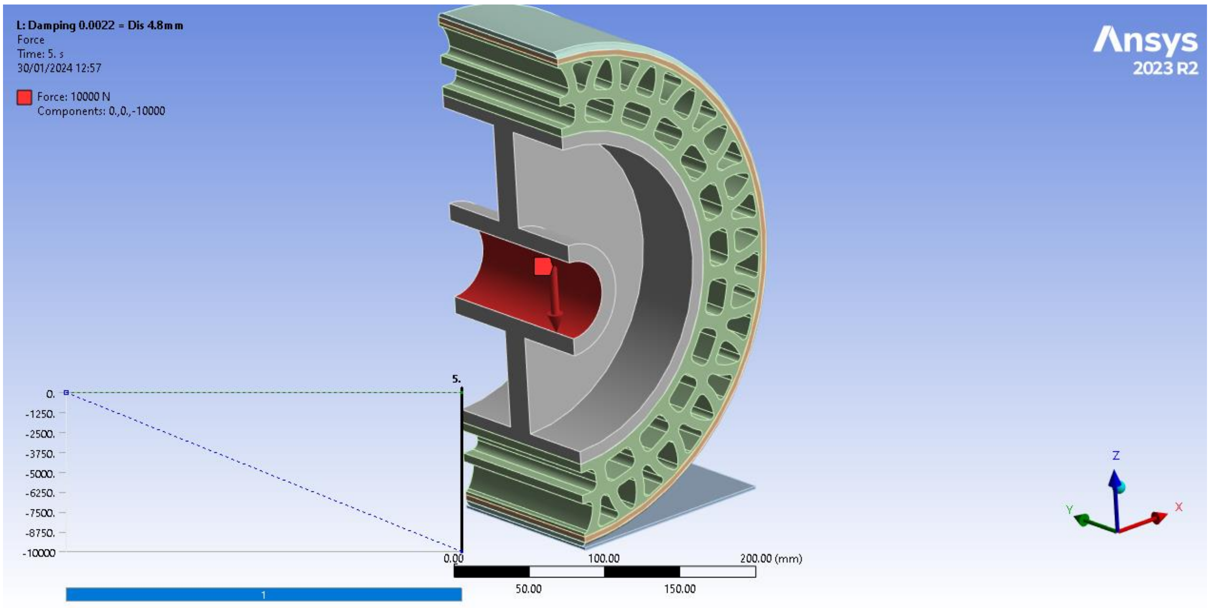

Figure 93: Ramped force applied.

In experimental testing the wheel was constrained in from sliding in the Y direction with bushes on the machine. To replicate this in simulation, a remote displacement was added with would only allow motion in the Z direction thereby stopping any unwanted slipping or sliding in the Y direction as seen in Figure 94 and Figure 95.

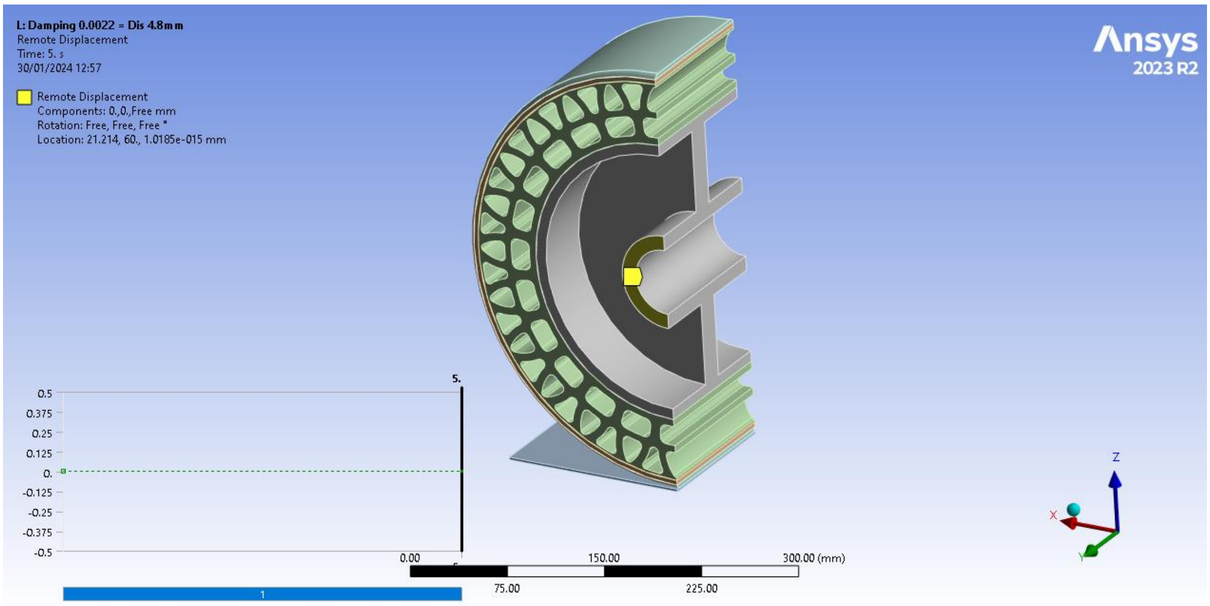

Figure 94: Remote displacement applied to the rim.

Details of "Remote Displacement"

Scope	
Scoping Method	Geometry Selection
Geometry	1 Face
Coordinate System	Global Coordinate System
X Coordinate	21.214 mm
Y Coordinate	60. mm
Z Coordinate	1.0185e-015 mm
Location	Click to Change
Definition	
Type	Remote Displacement
X Component	0. mm (ramped)
Y Component	0. mm (ramped)
Z Component	Free
Rotation X	Free
Rotation Y	Free
Rotation Z	Free
Suppressed	No
Behavior	Deformable
Advanced	

Figure 95: Remote displacement details.

7.5 Meshing

As a start a relatively course mesh was selected however convergence would not even make 20% of the load required. It was then clear that a fine mesh would have to be produced from the start for this analysis.

A nonlinear mechanical mesh was selected with body sizing applied on all components with the following values:

- Rim = 15mm
- Carcass = 10mm
- Stiff Shear band = 10mm
- Thread = 10 mm
- Plate = 15 mm

A sphere of influence was added to the bottom section of the PU portion of the wheel as the area of deformation most concerned with and where distortions was highlighted. The sphere of influence can be seen in Figure 96.

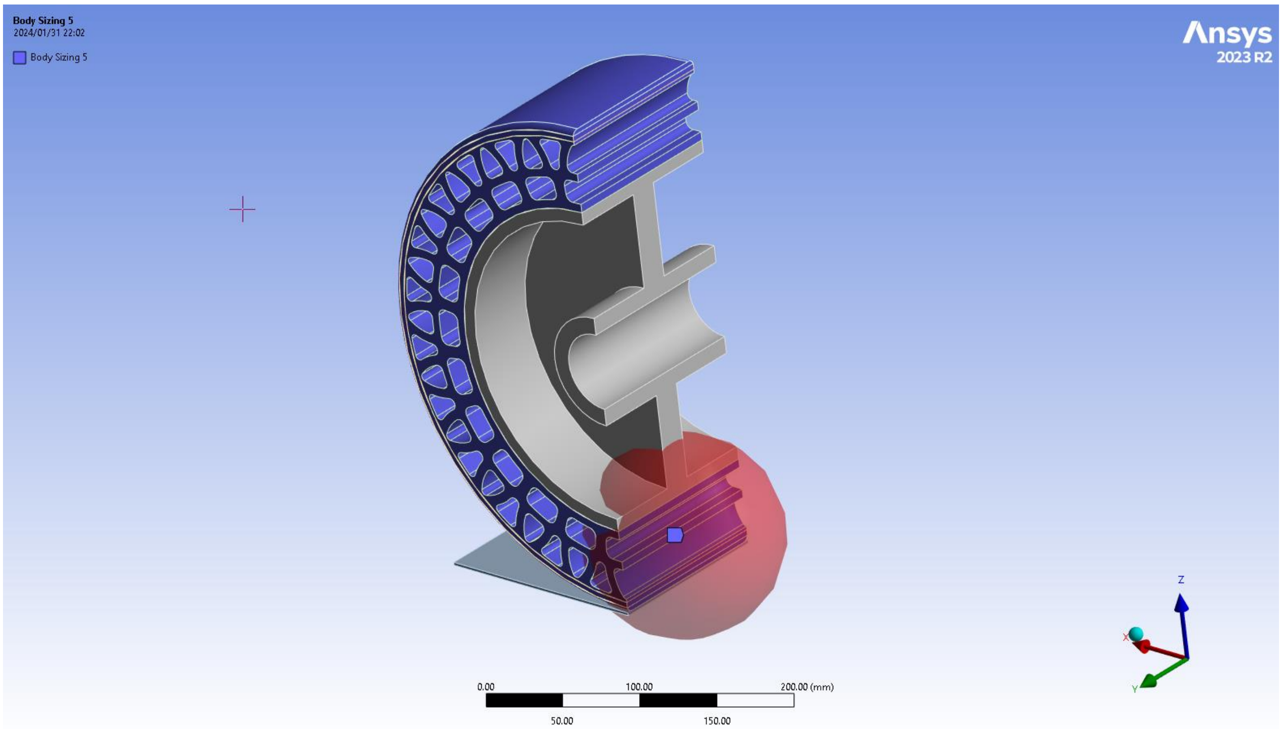

Figure 96: Sphere of influence.

Face meshing was then applied to the thread layer for a more constant mesh. An aspect ratio of 0.8 was desired, the reasoning for this was when large deformation would occur then the elements will deform to produce an aspect ratio of 1 preventing large distortion errors.

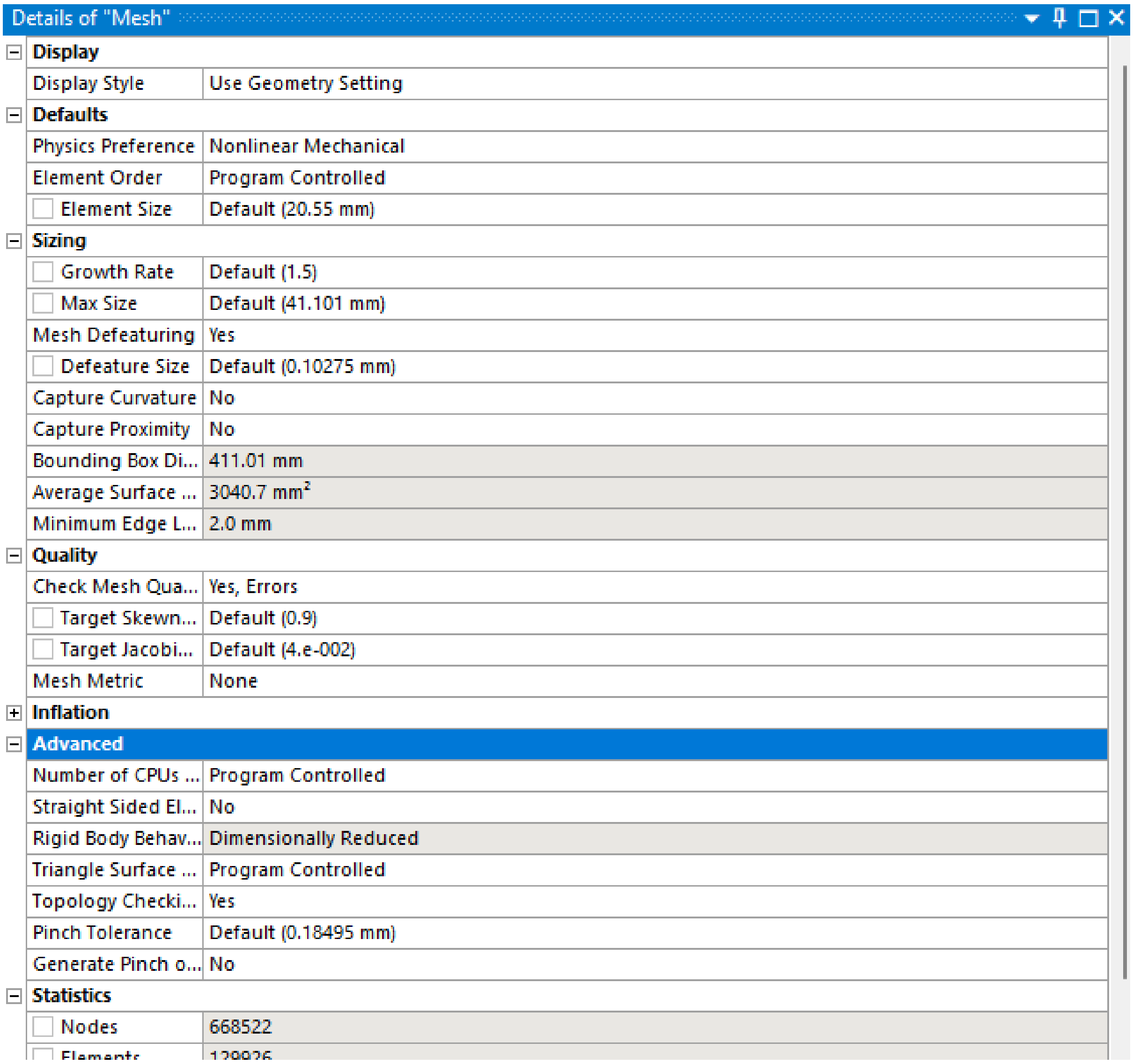

Details of "Mesh"	
Display	
Display Style	Use Geometry Setting
Defaults	
Physics Preference	Nonlinear Mechanical
Element Order	Program Controlled
Element Size	Default (20.55 mm)
Sizing	
Growth Rate	Default (1.5)
Max Size	Default (41.101 mm)
Mesh Defeaturing	Yes
Defeature Size	Default (0.10275 mm)
Capture Curvature	No
Capture Proximity	No
Bounding Box Di...	411.01 mm
Average Surface ...	3040.7 mm²
Minimum Edge L...	2.0 mm
Quality	
Check Mesh Qua...	Yes, Errors
Target Skewn...	Default (0.9)
Target Jacobi...	Default (4.e-002)
Mesh Metric	None
Inflation	
Advanced	
Number of CPUs ...	Program Controlled
Straight Sided El...	No
Rigid Body Behav...	Dimensionally Reduced
Triangle Surface ...	Program Controlled
Topology Checki...	Yes
Pinch Tolerance	Default (0.18495 mm)
Generate Pinch o...	No
Statistics	
Nodes	668522
Elements	129926

Figure 97: Mesh details.

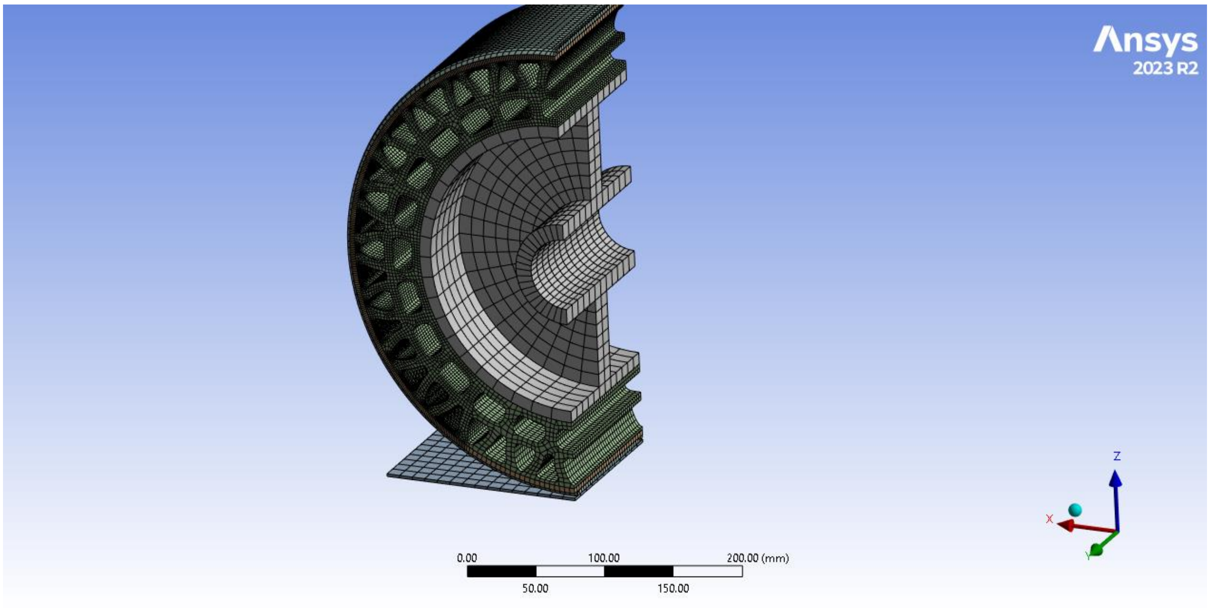

Figure 98: Mesh of wheel.

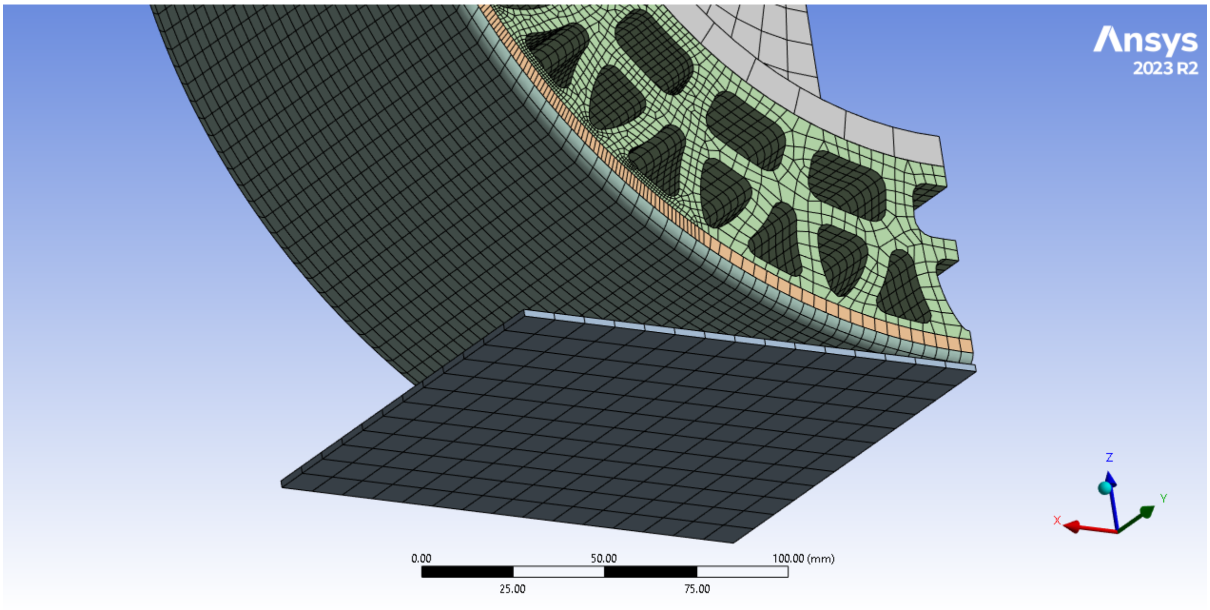

Figure 99: Face meshing of thread region.

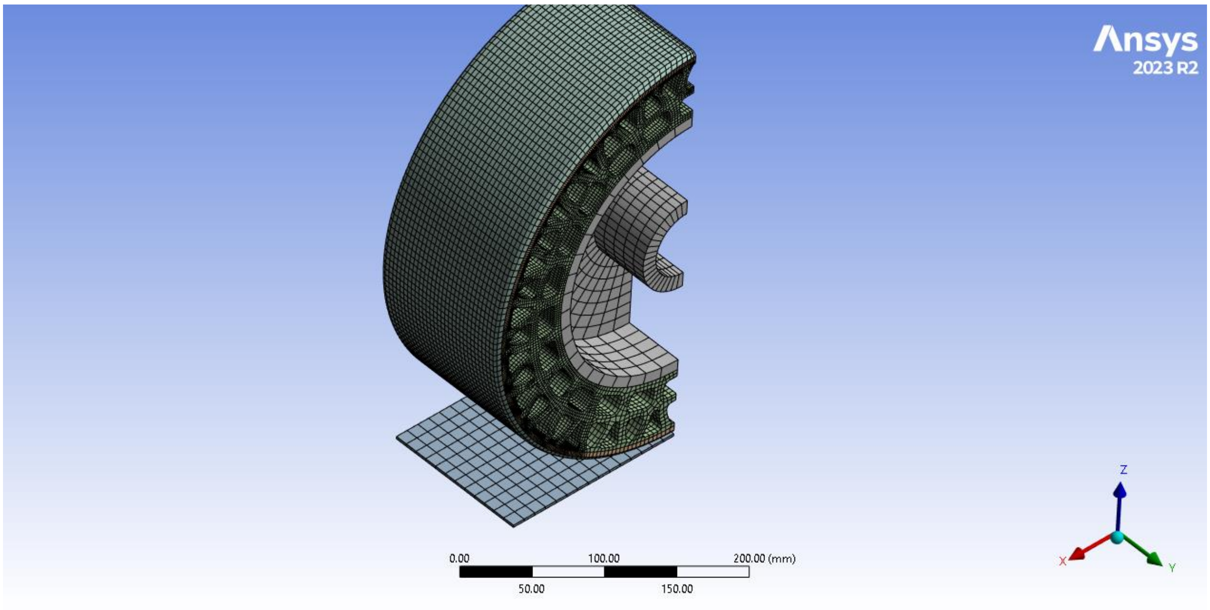

Figure 100: Face meshing of thread region 2.

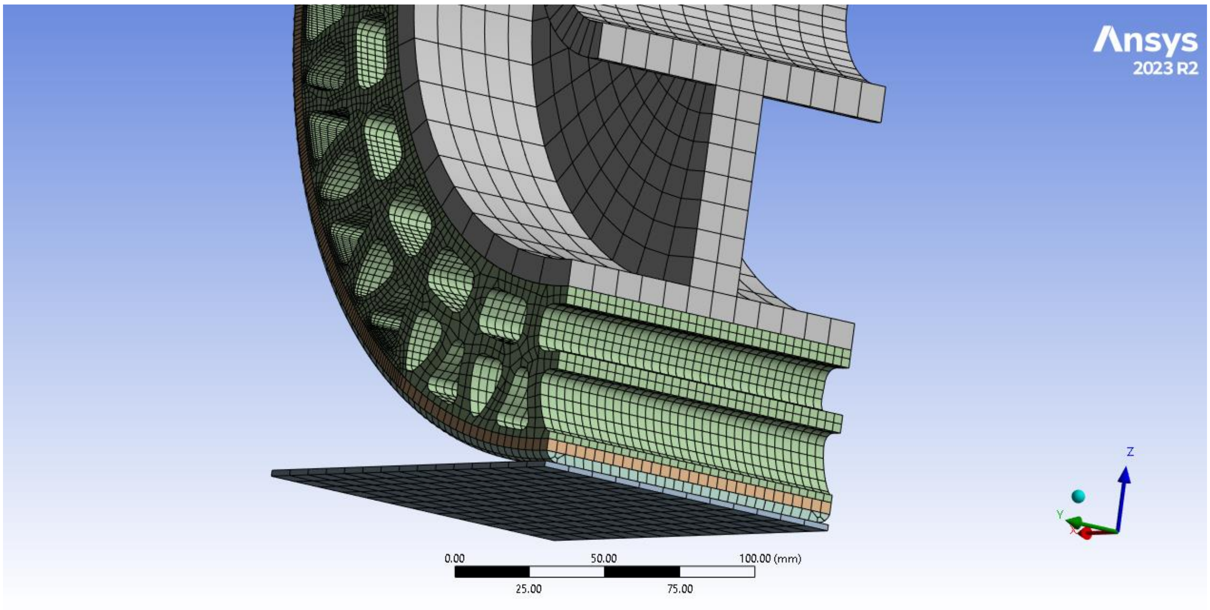

Figure 101: Mesh of different regions.

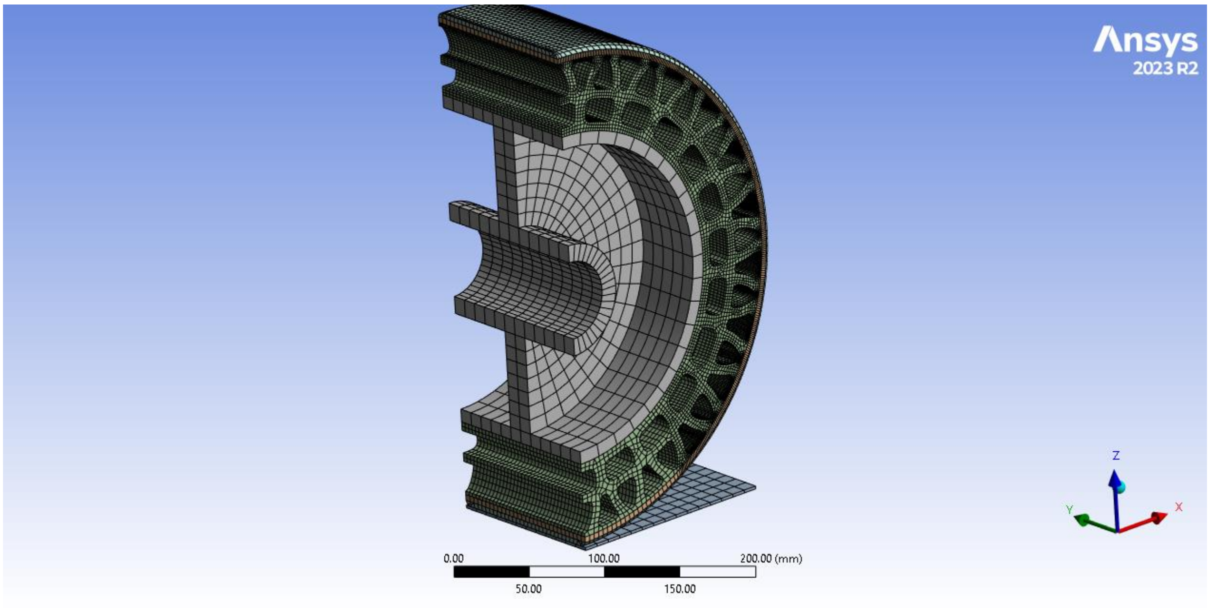

Figure 102: Mesh of different regions 2.

7.6 Analysis Setting

The analysis setting is the most critical setting in non-linear simulations. Substepping is turned on and was used split or bisect force steps to make it easier and more possible to achieve a converged solution. Large deformation is turned on as it is more than likely a hyperelastic material will exhibit large deformations. The Newton-Raphson Option will be selected on Full as a non-linear control. The Newton-Raphson method in ANSYS is a numerical technique used to solve nonlinear equations and is particularly useful for solving nonlinear finite element analyses.

When dealing with a nonlinear problem in ANSYS, the relationship between the input force and output displacement is not linear. Newton-Raphson allows an iteratively refinement of the solution, aiming to reduce the residual between the predicted and actual behaviour until this difference is within an acceptable tolerance.

Newton-Raphson method behaviour used for this non-linear analysis in ANSYS:

- Iteration and Incrementation: Nonlinear problems often require the solution to be approached in small steps or increments. The solution is assumed to be a path that's followed incrementally, and the Newton-Raphson method helps in finding the solution at each of these increments.
- Linearization of Nonlinear Equations: At each increment, the nonlinear equations are linearized around the current state. This involves computing the stiffness matrix and the load vector, considering the current state of deformation, material properties, and boundary conditions.
- Solution of Linear Equations: The linearized equations are solved to compute an increment in the displacement.
- Update and Convergence Check: The solution is updated with the increment, and the difference between the predicted and actual behaviour is checked by monitoring the residuals in the force convergence. If the residual is larger than a specified tolerance, the process is repeated; the equations are linearized again based on the updated solution, and a new increment is computed.
- Convergence Criteria: The iteration continues until the solution converges, meaning the changes in the solution variables and the residuals are smaller than specified tolerances. These tolerances are crucial and need to be set carefully to ensure that the solution is accurate without demanding unnecessary computational effort.

The various parameters of the Newton-Raphson method can be specified for simulation:

- Convergence Tolerances: Defines how close the solution needs to be to the actual solution before it is considered converged.
- Maximum Number of Iterations: Limits the number of iterations to prevent endless computation if the solution does not converge.

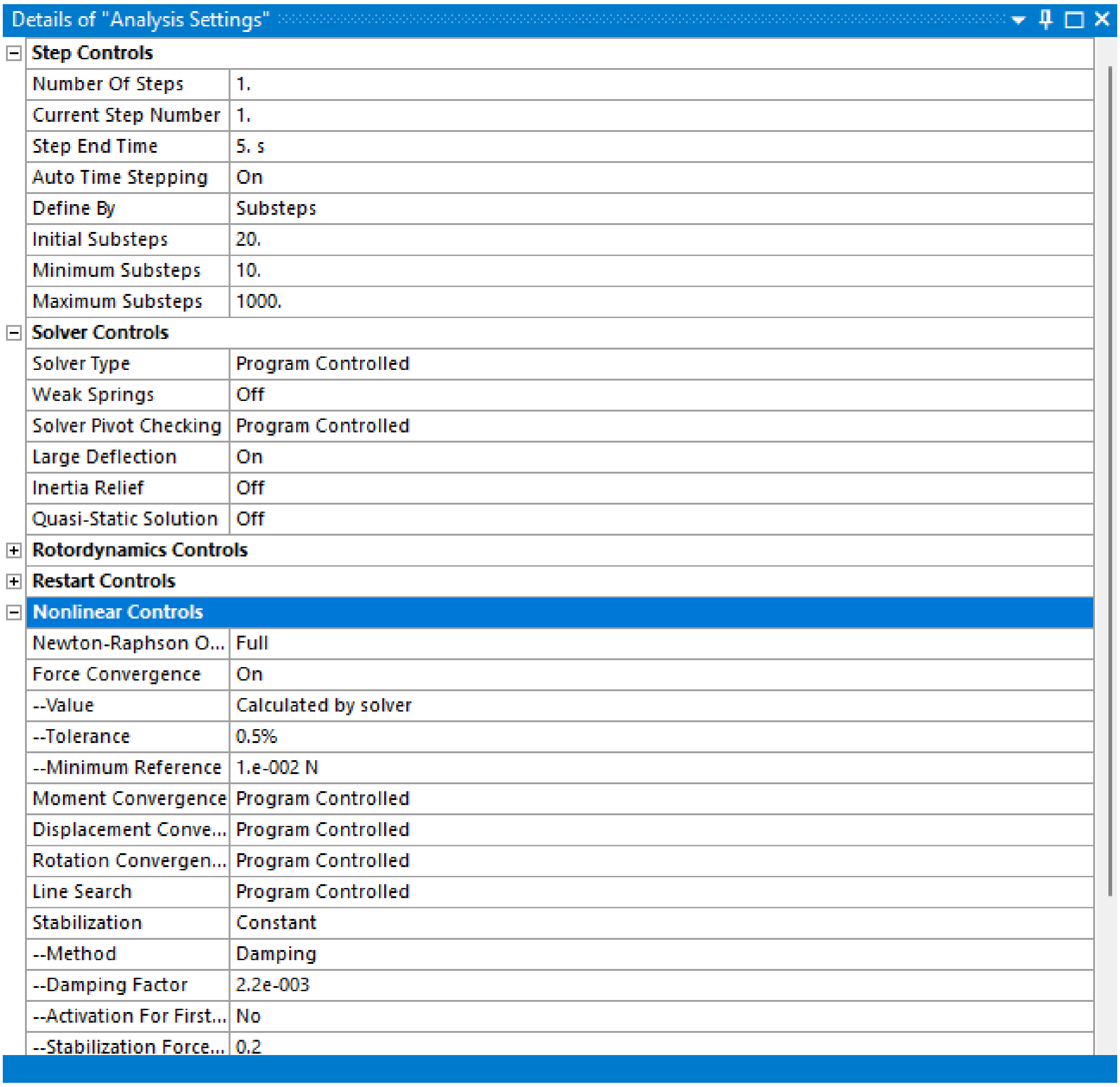

Details of "Analysis Settings"

Step Controls	
Number Of Steps	1.
Current Step Number	1.
Step End Time	5. s
Auto Time Stepping	On
Define By	Substeps
Initial Substeps	20.
Minimum Substeps	10.
Maximum Substeps	1000.
Solver Controls	
Solver Type	Program Controlled
Weak Springs	Off
Solver Pivot Checking	Program Controlled
Large Deflection	On
Inertia Relief	Off
Quasi-Static Solution	Off
Rotordynamics Controls	
Restart Controls	
Nonlinear Controls	
Newton-Raphson O...	Full
Force Convergence	On
--Value	Calculated by solver
--Tolerance	0.5%
--Minimum Reference	1.e-002 N
Moment Convergence	Program Controlled
Displacement Conve...	Program Controlled
Rotation Convergen...	Program Controlled
Line Search	Program Controlled
Stabilization	Constant
--Method	Damping
--Damping Factor	2.2e-003
--Activation For First...	No
--Stabilization Force...	0.2

Figure 103: Analysis setting used in ANSYS.

A stabilisation method of constant damping is used as another non-linear control. The constant damping stabilization method helps to mitigate these issues by introducing artificial damping into the system.

Constant damping introduces a damping force that is proportional to the velocity of the nodal points in the finite element model. This damping force does not represent any physical damping in the system but is a numerical technique to stabilize the solution process. The damping force is typically small but sufficient to damp out numerical instabilities. This value will be discussed later in this research.

The choice of the damping magnitude is crucial; too little damping might not stabilize the solution, while too much damping can overly suppress the physical response of the system, leading to an inaccurate solution.

The damping force helps to smooth out abrupt changes or oscillations in the response, providing a more stable path toward convergence. This is particularly beneficial in scenarios where the solution oscillates or diverges due to abrupt changes in stiffness, material behaviour, or contact conditions.

It is important to use constant damping cautiously. The results should be checked for sensitivity to the damping parameters, and users should ensure that the damping does not dominate the physical response of the system. Verification with physical tests is required and this is what allows the damping constant to be adequately calculated based on the materials used.

Details of "Analysis Settings"

Displacement Conve...	Program Controlled
Rotation Convergen...	Program Controlled
Line Search	Program Controlled
Stabilization	Constant
--Method	Damping
--Damping Factor	2.2e-003
--Activation For First...	No
--Stabilization Force...	0.2
Advanced	
Inverse Option	No
Contact Split (DMP)	On
-- Max Number of S...	Chosen by Solver
Output Controls	
Stress	Yes
Back Stress	Yes
Strain	Yes
Contact Data	Yes
Nonlinear Data	Yes
Nodal Forces	Yes
Volume and Energy	Yes
Euler Angles	Yes
General Miscellaneo...	No
Contact Miscellaneo...	No
Store Results At	All Time Points
Result File Compres...	Program Controlled
Analysis Data Management	
Visibility	
[A] Force (X)	Display
[B] Force (Y)	Display
[C] Force (Z)	Display
[D] Remote Displace...	Display
[E] Remote Displace...	Display

Figure 104: Analysis settings 2.

7.7 Solution Information

The force convergence was mentioned during simulations, often when multiple bisections are occurring there will be an unconverged result. It is important to track as simulations generally run for multiple days before convergence occur.

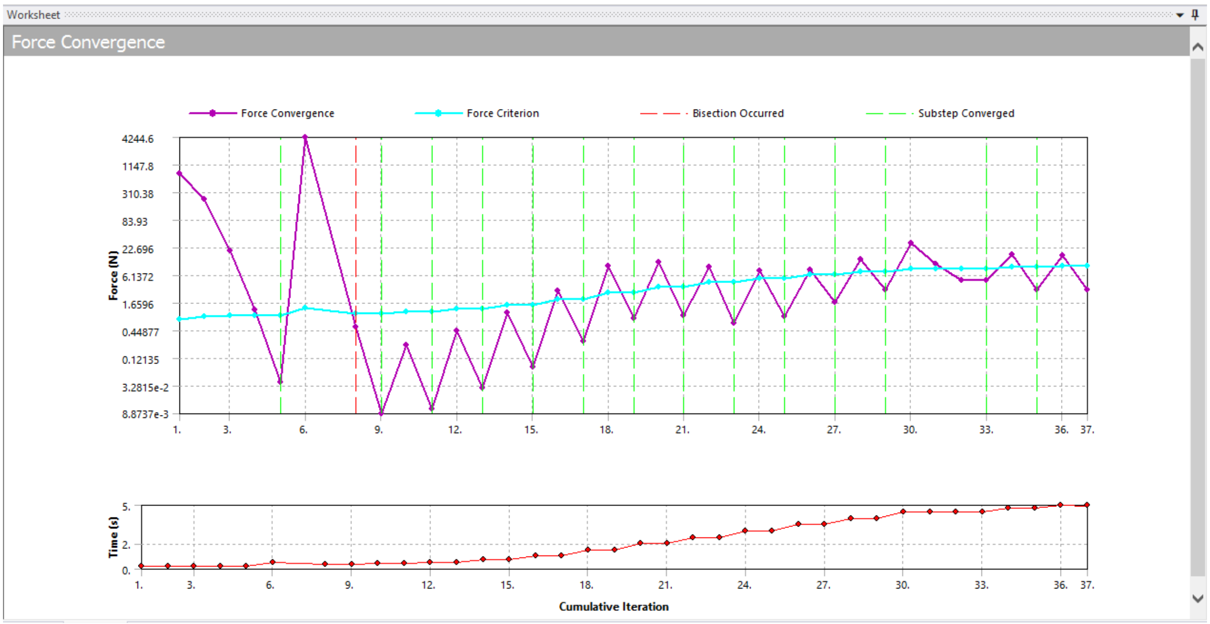

Figure 105: Force convergence of a non-linear simulation.

8. Results and Discussion

8.1 Deformation

Convergence of a result would be extremely difficult in there would be errors in element distortions. A recurrent challenge in simulations involving hyper-elastic materials is excessive element distortion. Due to the highly nonlinear nature of these simulations, localized regions within the model may experience extreme deformation, leading to non-physical configurations of certain mesh elements. For instance, in an ideal scenario, a hexahedron element should maintain an aspect ratio close to unity, with angles between its edges approximating 90 degrees. This geometric configuration facilitates the accurate mapping of nodal coordinates from the physical space to a cube in the natural coordinate space. However, when hyper-elastic materials are involved, excessive global or local deformation might occur, leading to a distortion of elements to such an extent that this mapping becomes increasingly inaccurate and eventually untenable, culminating in excessive distortion errors that prevent further solver progression. As seen in Figure 106 the distortion of elements caused an unconverged solution.

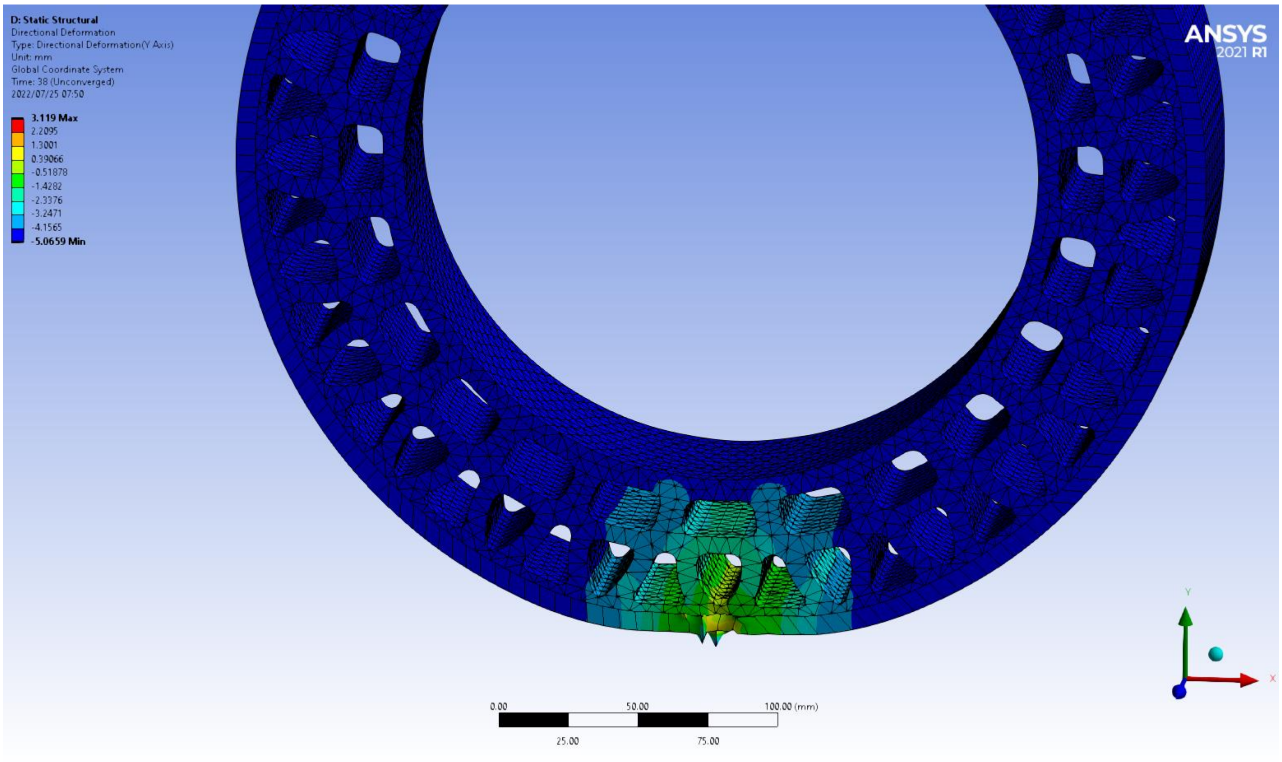

Figure 106: Unconverged deformation result with distorted elements.

At first the geometry was seen as too complex and simply too large with such a fine mesh. Concept 1 geometry was then used in simulations. However, the rim was also removed to reduce the mesh elements. The result is in Figure 107

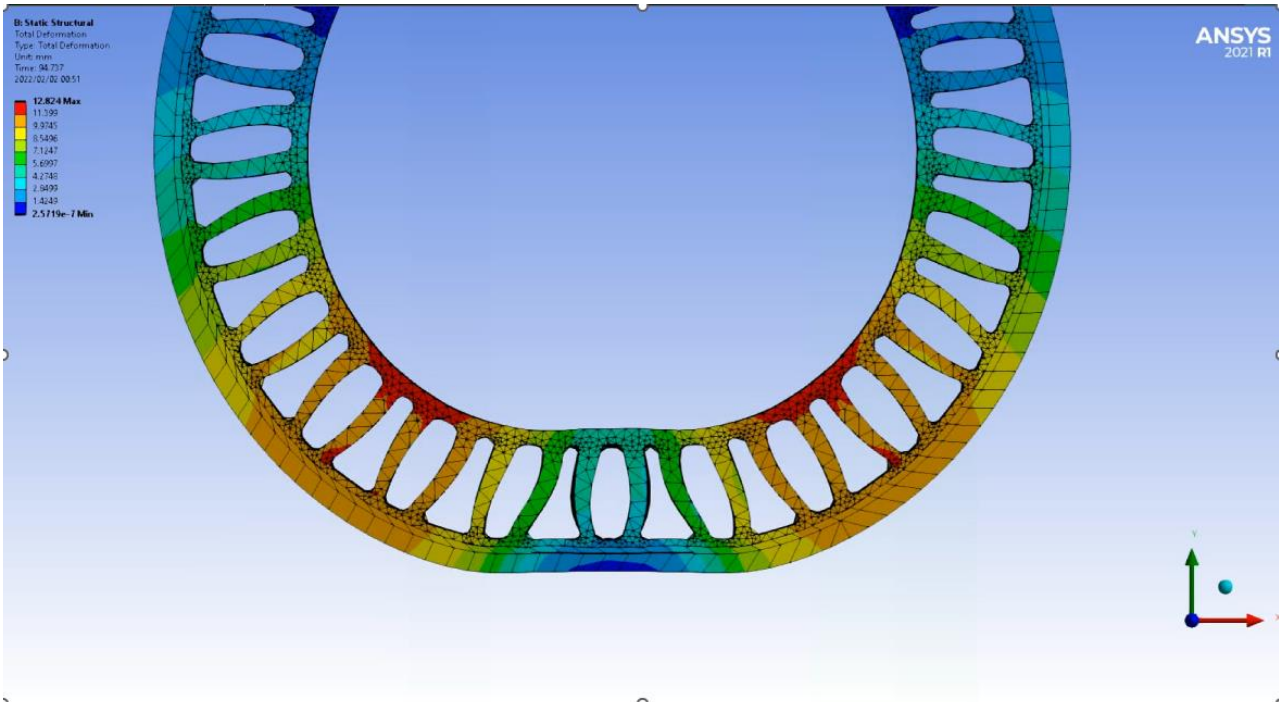

Figure 107: Concept 1 simulation.

Without the rim, the force and remote displacement would have to be inputted on the same face. This resulted in the scoping issue described previously. If the remote displacement was removed the circumference of the inner diameter would deform to an oval. This is not representative of the real-world scenario as the rim will restrain this deformation.

The rim was added back to the geometry however only the bottom section of the wheel was simulated as this was view as the critical region, with the aim of reducing the meshing elements. The results are seen in Figure 108 and Figure 109.

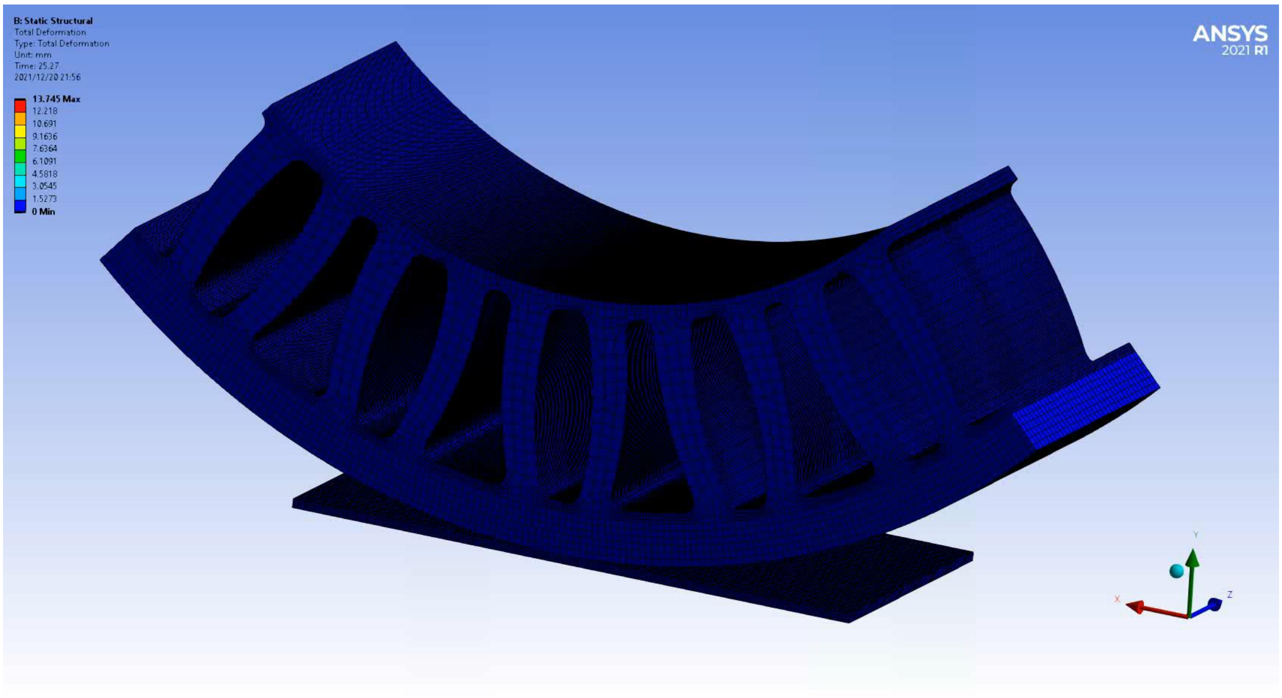

Figure 108: Sector simulation.

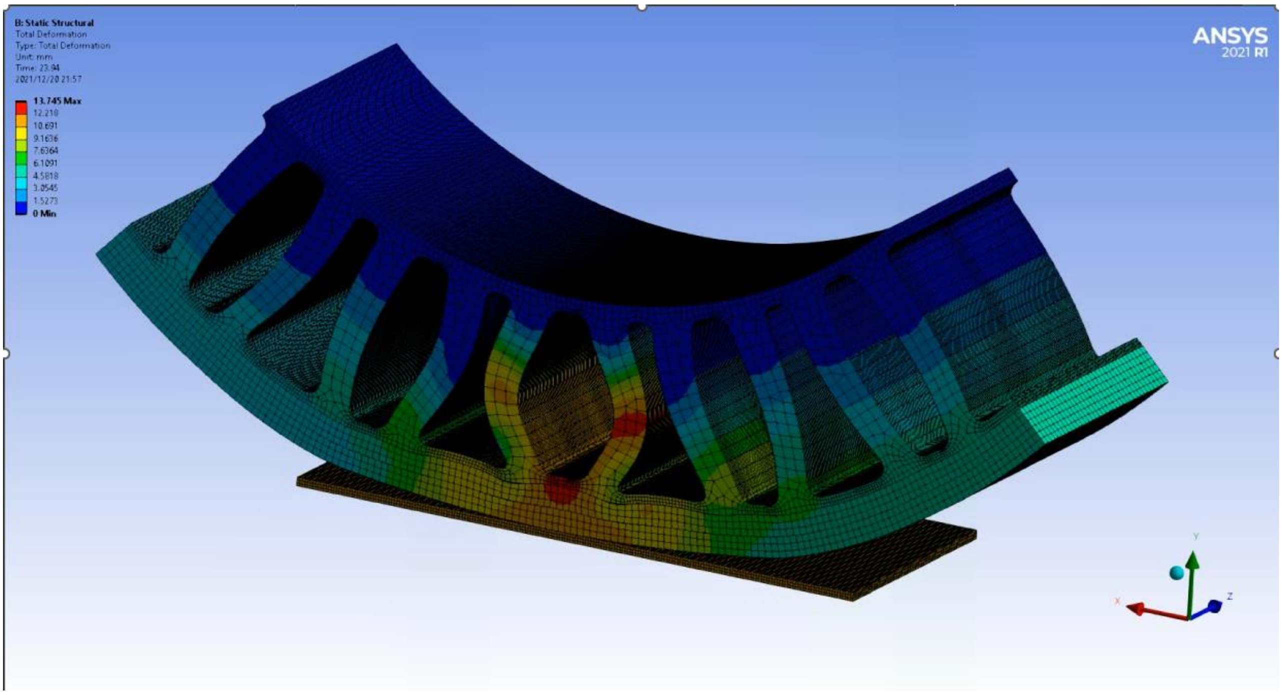

Figure 109: Sector simulation deformation.

This did not work as the wheel would flatten out as it was not constrained on the two ends by the rest of the wheel in tension. To correct this distortion, the following steps had to be implemented:

8.1.1 Mitigating Element Distortion:

To address element distortion errors, potential solutions can be categorized into two broad areas: mesh quality control and model setup refinement.

8.1.2 Mesh Quality Control

This involves using mesh elements that are less prone to distortion, selecting elements of appropriate shape, or implementing loads in smaller increments. In certain extreme cases, nonlinear mesh adaptivity may be employed, an advanced technique that enhances mesh quality through remeshing based on predefined quality criteria.

8.1.3 Model Setup Refinement

This entails validating the material definition for relevance to the specific case, ensuring the stability of the material model, and, in cases involving contact, confirming that all potential contact surfaces are accounted for. It might also necessitate adjusting contact settings or altering the design to redistribute localized high stresses and strains.

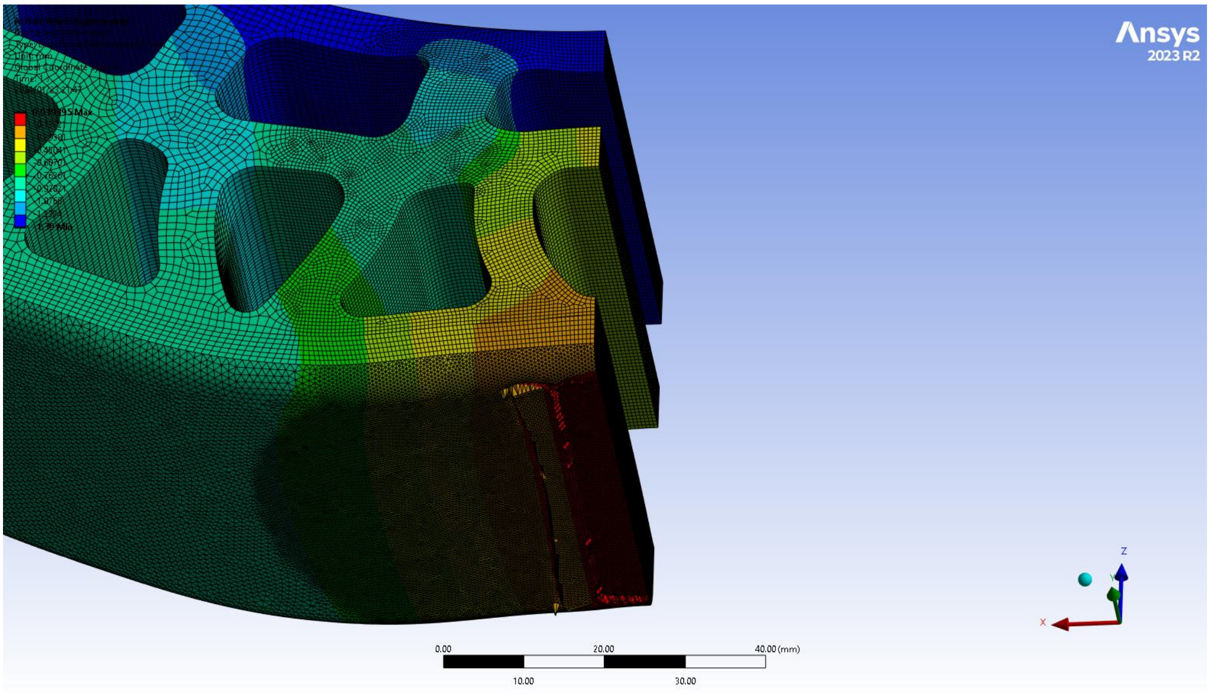

Figure 110: Mesh distortion in model.

In practice, diagnosing and resolving these issues in software such as ANSYS Mechanical involves understanding and interpreting error messages, utilizing features to identify and highlight excessively distorted elements, and implementing changes to the mesh settings and analysis parameters. For instance, the following as aided in achieving a converged result:

- Transitioning from higher order to linear elements, a linear mesh has improved convergence over various runs.
- Adjusting auto time-stepping parameters to a maximum of 1000 substeps and an initial substep of 10.
- Modifying the geometry to alleviate localized deformations are strategies that can be leveraged to advance the solution and mitigate excessive element distortion.

This has led to the final result in deformation with a total deformation of 4.61mm seen in Figure 111, taking into account the experimental result was a deformation of 4.19mm. There are no distorted elements and results closely match experimental data.

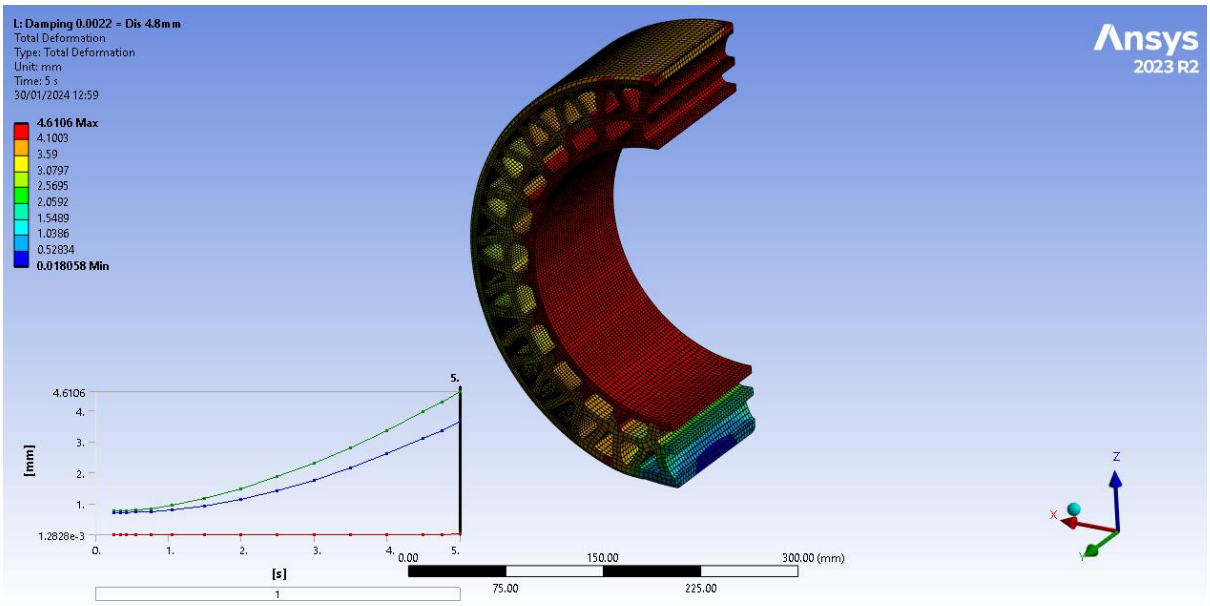

Figure 111: Final deformation result

A video of the deformation can be seen below or be the link that follows:
https://drive.google.com/file/d/18W3DJ3VGHx6lAxeMvDvEhw184l3IvcL8/view?usp=drive_link

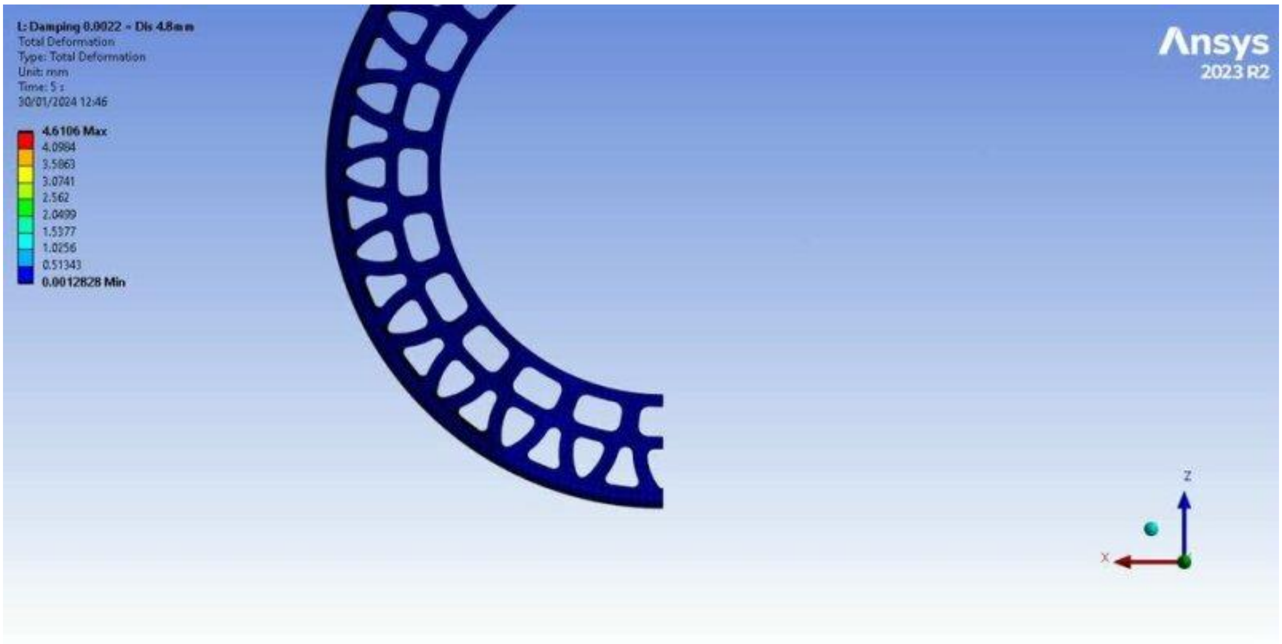

8.2 Directional Deformation

Directional deformation in ANSYS refers to a specific type of boundary condition where a displacement is applied along a specified direction on a part of the model. This feature is often used to simulate the effect of forces or to impose certain displacements within the simulation, this helps us understand how a structure or material will react to specific loads or movements. Directional deformation was assigned to the Z axis, to ensure the deformation in the Z plane is measured as in experimental testing a laser transducer was used to measure the Z plane deformation of the plate.

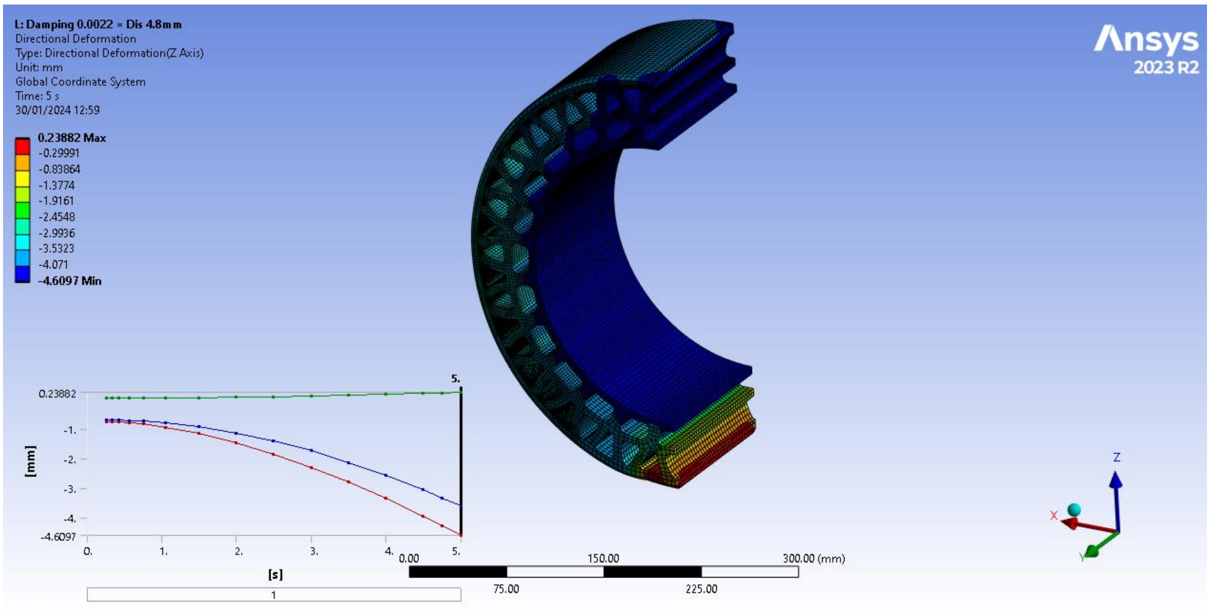

Figure 112: Direction deformation showing the result of the force.

To achieve this result, vigilant monitoring of the model's status and the prompt identification of potential complications, such as rigid body motion, during the solution phase is imperative. This vigilance is not merely procedural but a strategic approach to pre-emptively address issues, thereby conserving significant computational time and resources.

8.2.1 Addressing Stress Singularities and Refinement Depth in Adaptive Convergence:

In FEA, stress singularities may arise at re-entrant corners or vertices with boundary conditions, leading to unbounded stress escalation upon mesh refinement. It was essential to discern whether these singularities are located in critical areas of interest. If not, scoping tools can be used to isolate non-critical regions. For singularities in vital areas, introducing local features like fillets can alleviate the issue, offering a more accurate representation of the physical design. Unlike stress, deformation results invariably converge as singularities do not affect them.

During simulations element distortion would more than likely occur on the corner of the thread and the plate as seen in Figure 106. To gain convergence a fillet of the thread was added. Usually in simulations fillets are removed as it bears no consequence on the simulation result. However, in this non-linear simulation to prevent the abrupt change in deformation on the elements located in the corner of the geometry a fillet must be added.

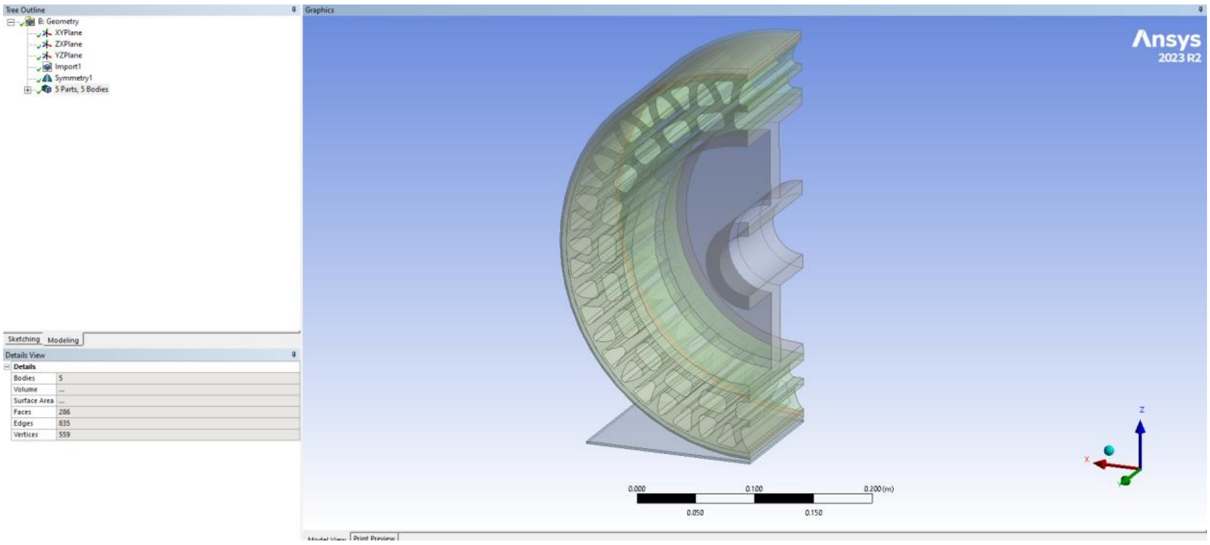

Figure 113: Fillets added to geometry and used throughout all simulations.

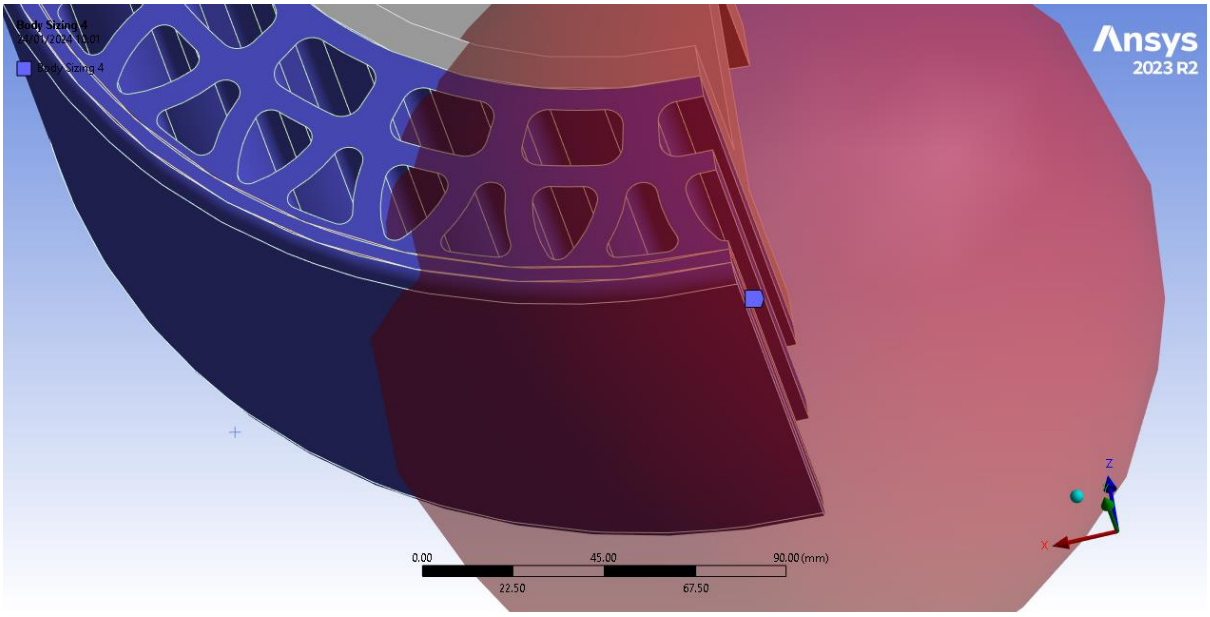

Figure 114: Radius of sphere of influence increased.

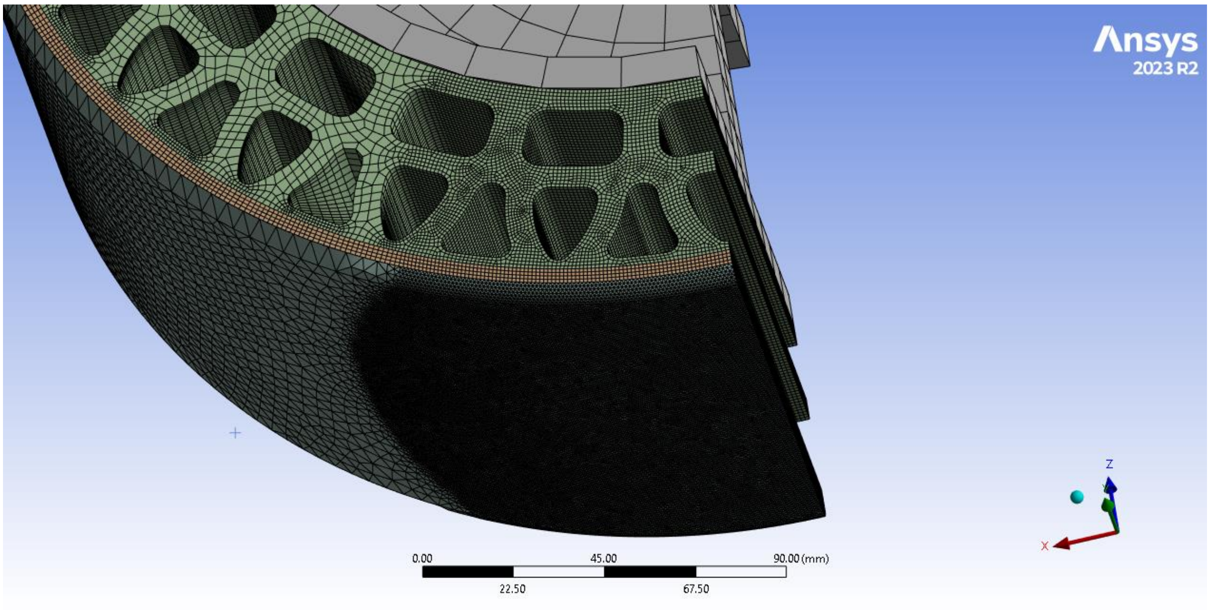

Figure 115: More refinement of mesh within the sphere of influence

8.2.2 Implementing Adaptive Convergence in Ansys:

Mesh refinement areas help achieve good numerical accuracy; a process fraught with potential errors. Modern tools like Ansys automate this procedure for FEA, significantly enhancing efficiency and accuracy. Mesh refinement like Figure 115 occurred by repeatedly solving the problem with progressively refined meshes.

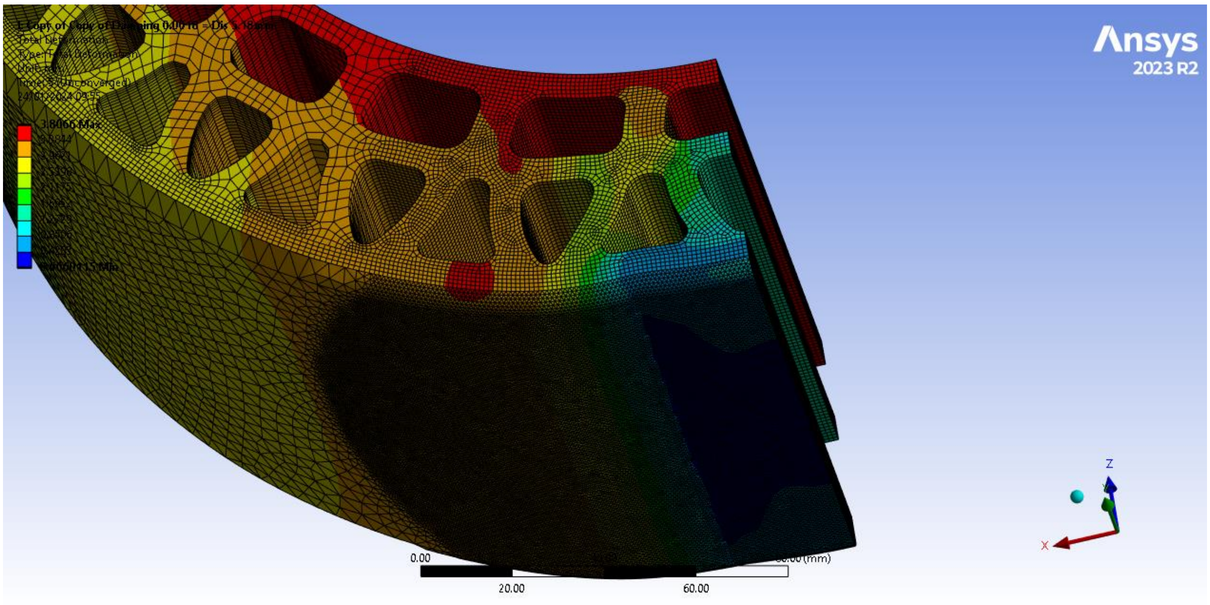

Figure 116: Mesh smoothness result after mesh refinement.

8.3 Strain

By looking at the strain result we have to go back to our material data to ensure that the strain calculated in the simulation is without the region on our material models. The strain from a fully converged result is a maximum of 0.18mm/mm. This can be seen in the video below with the link:
https://drive.google.com/file/d/1vDurIDMrlDYZ5_oXUs0T57rVA8GEyGVP/view?usp=drive_link

For the material models that was developed, it will be essential to stay within the limits of 0.5mm/mm strain as the shear strain data model peaks at this limit. Although this is quite a harsh limit considering the model is not under a predominantly shear loading, it provides confidence that the results are all within the bonds of the material model.

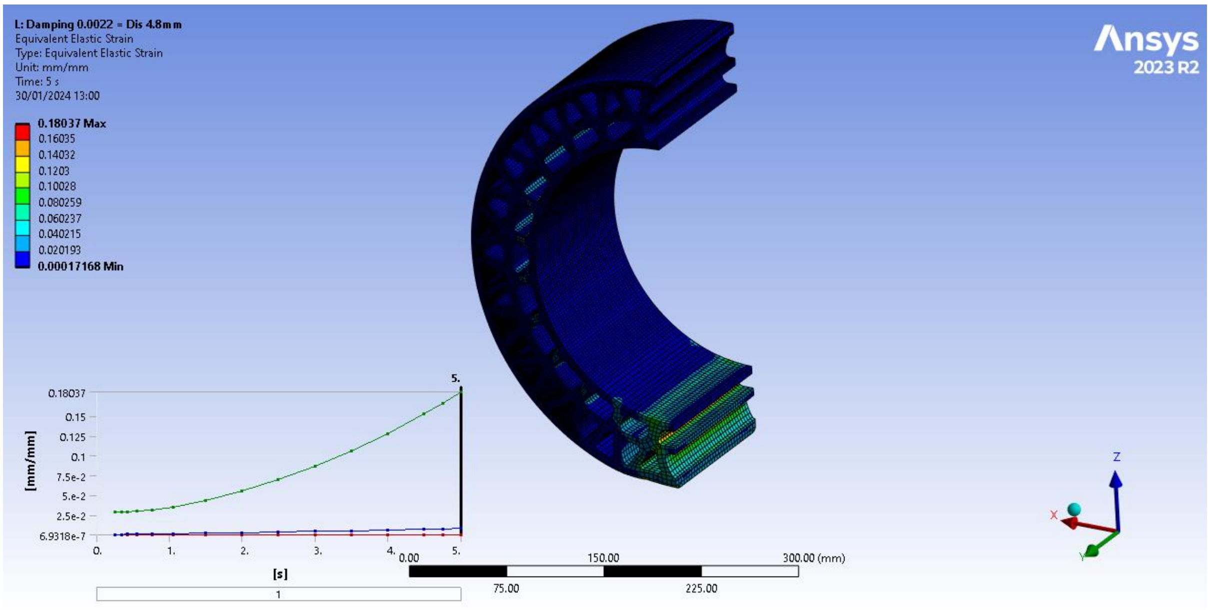

Figure 117: Strain result.

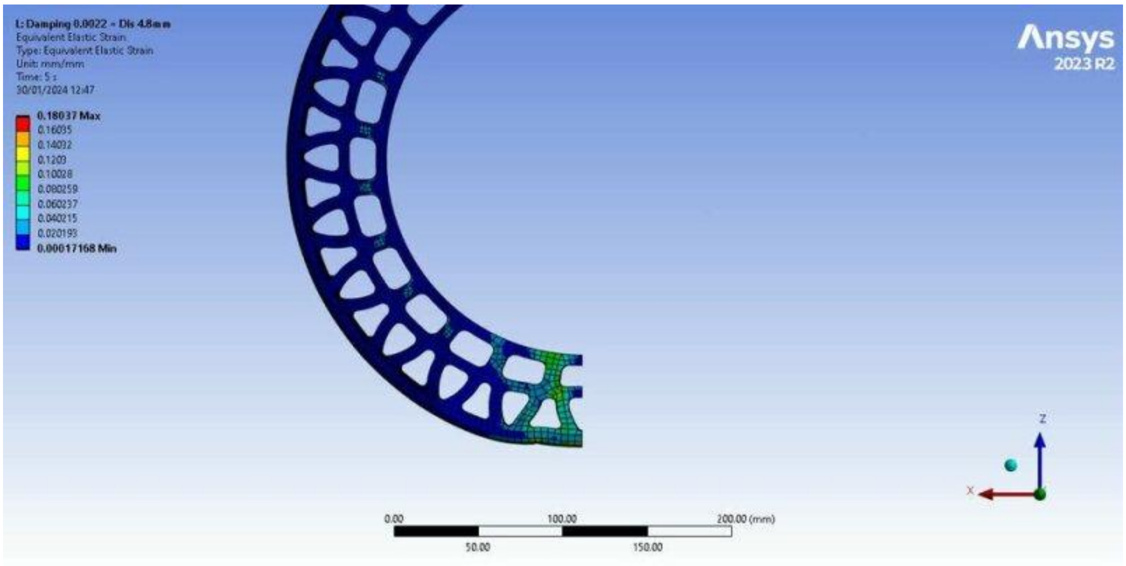

8.4 Stress

In non-linear simulations in ANSYS, the Von-Mises stress is crucial for evaluating materials under complex loading. By looking at the stress result, it allows the analysis to go back to the material data and analyse the stress state experienced. Taking into account the entire stress state of the material and not just individual stress components, providing a more comprehensive insight into the material's behaviour under real-world conditions.

The maximum stress is 3.9 MPa which is quite high in our material data for LF950A, however this maximum stress is in a small, localised region. The average stress distribution across the spokes in closer to 1.6MPa. Importantly, the stress distribution and how the structure design handles the load can be viewed. It is a similar picture when comparing experimental results in terms of the deformation characteristics. A video of the stress is seen with the link:
https://drive.google.com/file/d/1x_wVtwLbI9zkicfoV-Kyk8C099vrJ2XV/view?usp=drive_link

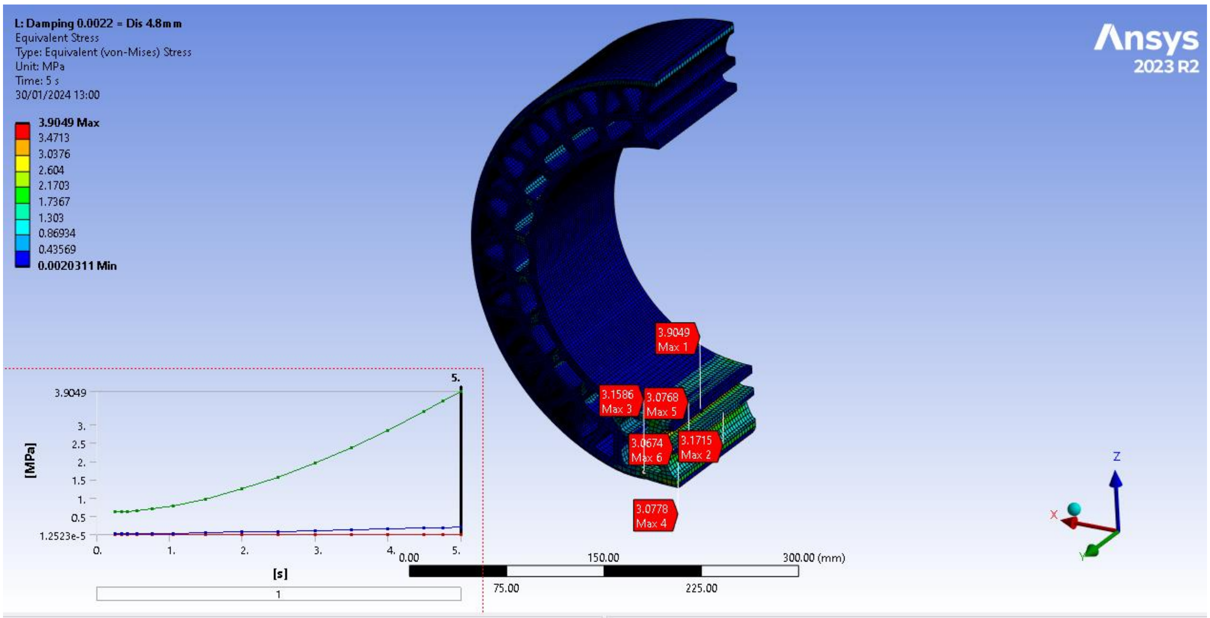

Figure 118: Final Stress result.

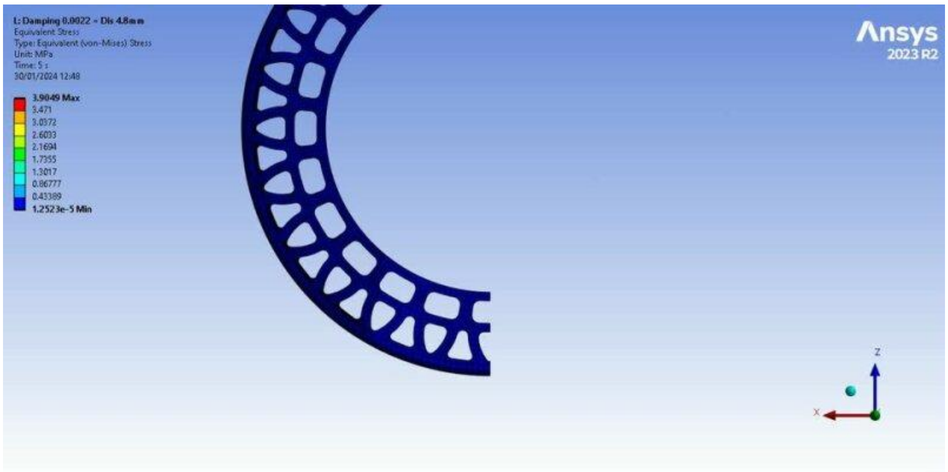

8.5 Shear Stress

Shear stress analysis is vital for understanding how materials behave under complex loading conditions that involve forces acting parallel to the material's surface. Although this is not the dominant factor in the simulation run, it helps in assessing the structural integrity, especially in materials and joints subjected to multi-axial stress states. Accurate modelling of shear stress is crucial for designing a viable structured wheel.

The maximum shear stress is 0.5 MPa which is very small but expected on the loading used on the wheel. It is a similar picture when comparing experimental results. A video of the stress is seen with the link:
https://drive.google.com/file/d/1WiHHdoO7Ugwgf6Odi6e0-0HRO8ULlImf/view?usp=drive_link

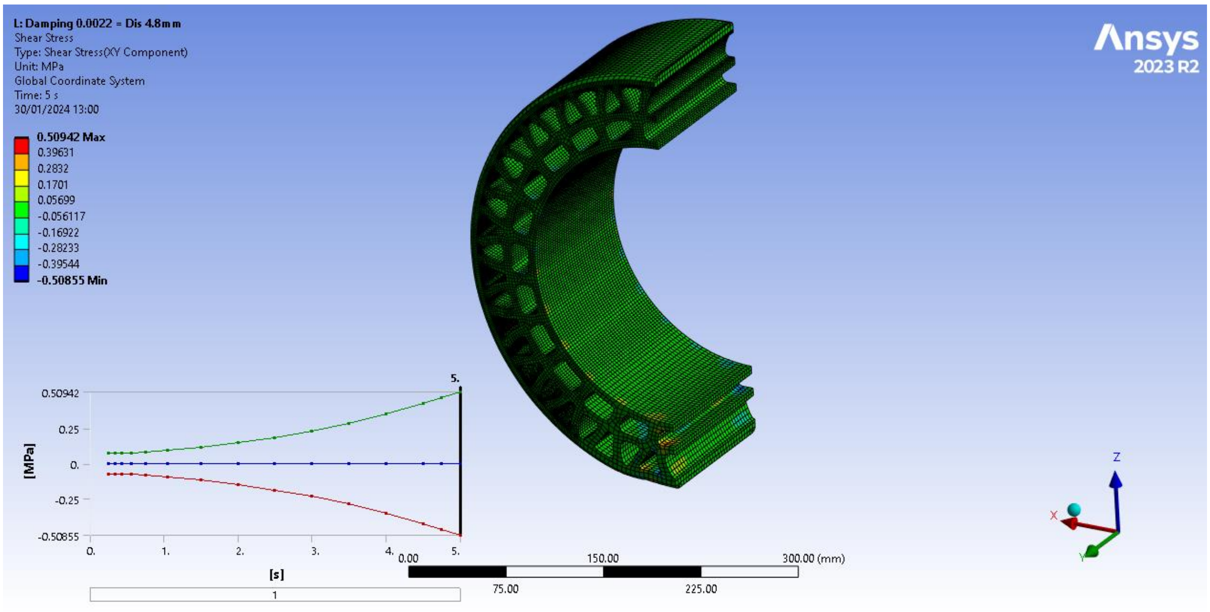

Figure 119: Shear stress

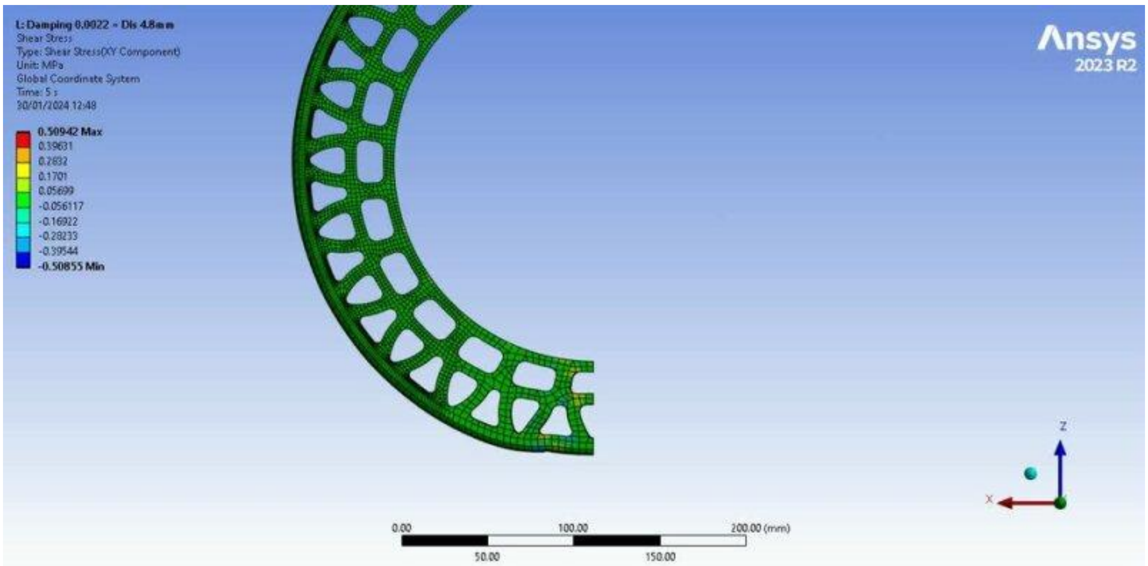

8.6 Contact Pressure

Contact pressure is a critical parameter for analysing the stress at interfaces between contacting bodies. It is essential for assessing the load distribution, potential wear, and failure at the contact regions. Accurate modelling of contact pressure helps in understanding how different parts interact under load, guiding design improvements and ensuring the structural integrity of the assembled components.

The maximum contact pressure is 7.63 MPa with a wide distribution which is expected due to the uniform structure design. A video of the stress is seen with the link:
https://drive.google.com/file/d/1klntLvXtDBsV4pODmw1hH7K2Aeur2TwG/view?usp=drive_link

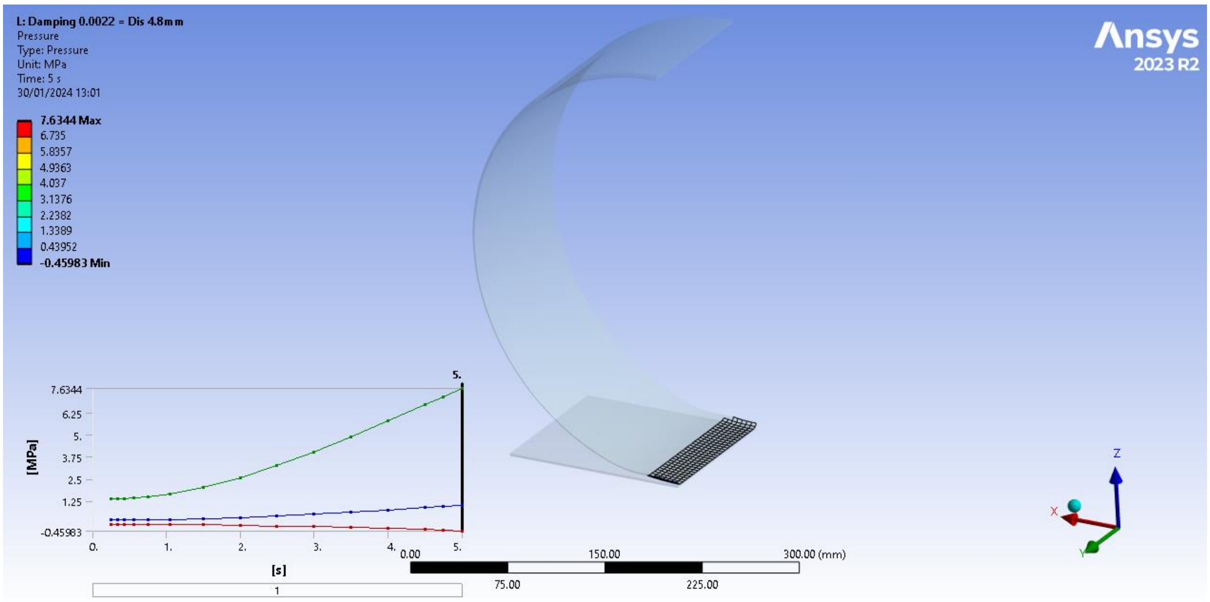

Figure 120: Contact Pressure

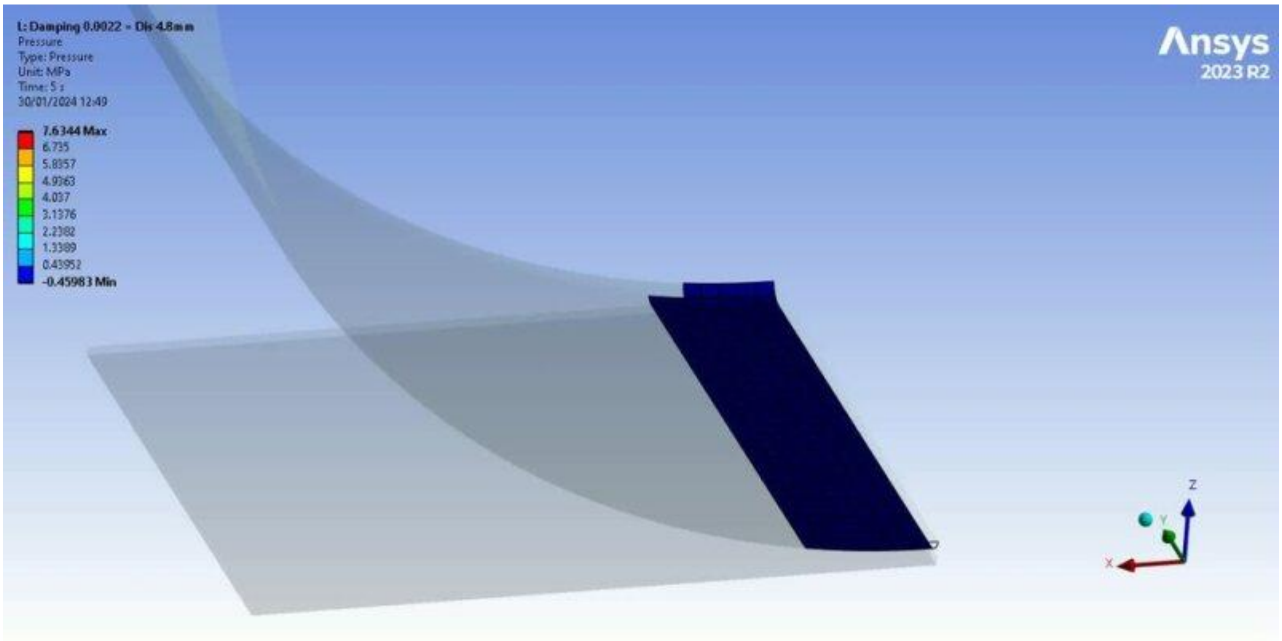

8.7 Modal Analysis

Modal analysis in a linear simulation in ANSYS is an advanced technique to understand the dynamic behaviour of structures. This involves assessing natural frequencies, mode shapes, and the damping characteristics of a structure when subjected to real-world, non-linear influences like large deformations, complex material properties, and advanced contact interactions, providing a comprehensive understanding of the structure's potential vibrations and dynamic stability under various loading conditions. To perform a modal analysis, the material model had to be linearised. This can be done in a software like MATLAB or MS Excel.

The modal analysis denotes that the critical natural frequencies were 10.22Hz and 4.63Hz. The deformation of 29.7mm when excited at a frequency of 10.22Hz is concerning and this can lead to some refinement on the design of the structured wheel.

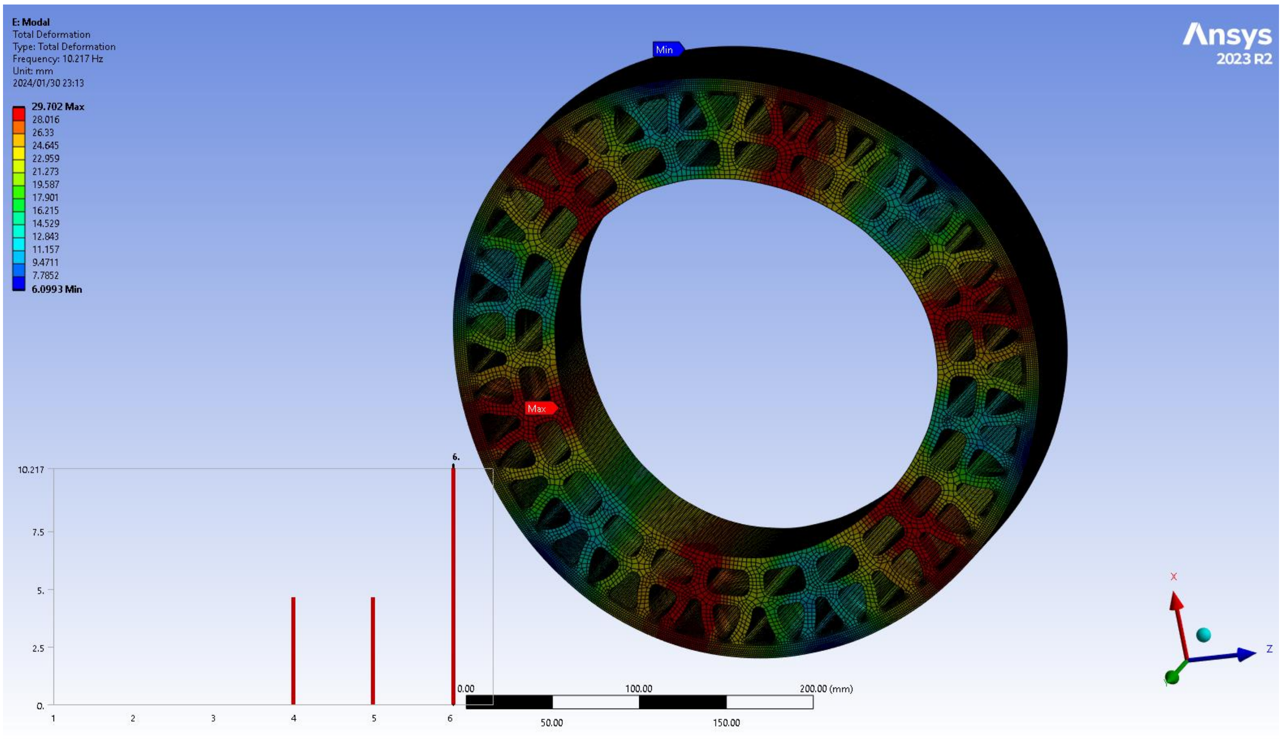

Figure 121: First modal frequency

https://drive.google.com/file/d/1FfUGSevGzNbdVXndmIJsGHm0lmlhcTeF/view?usp=sharing

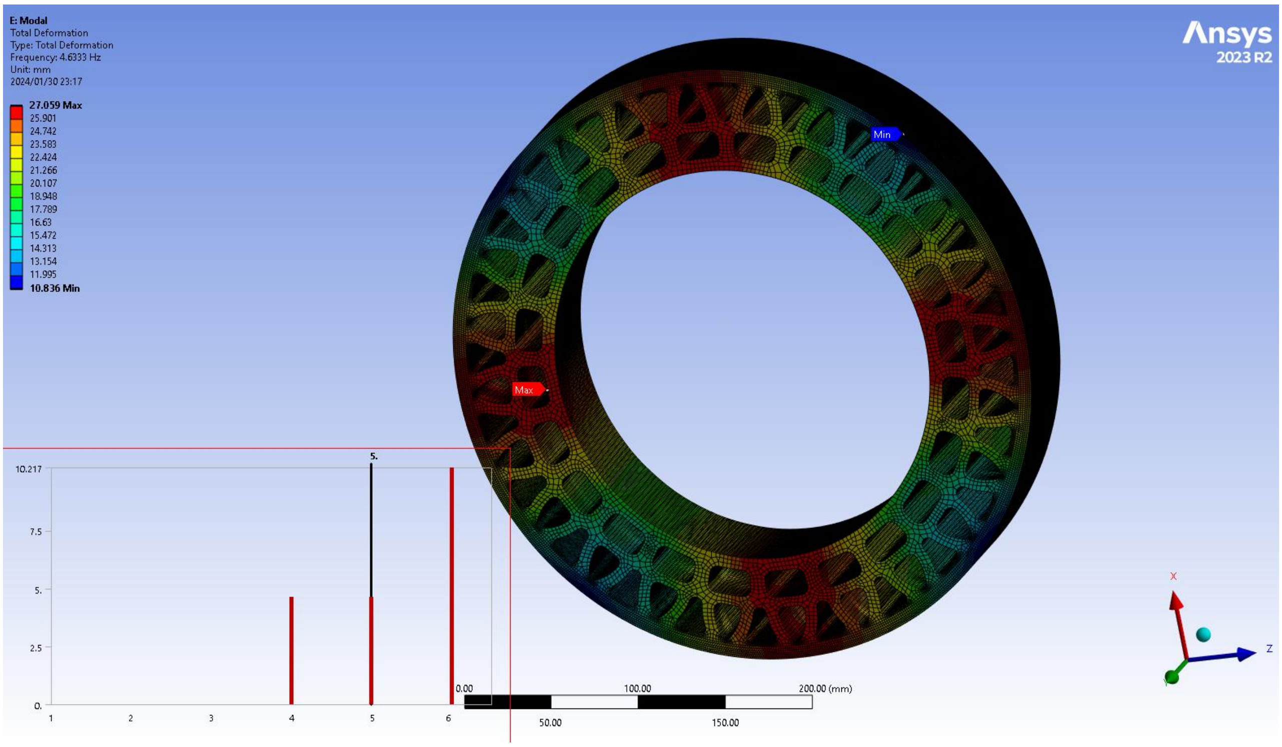

Figure 122: Second modal frequency

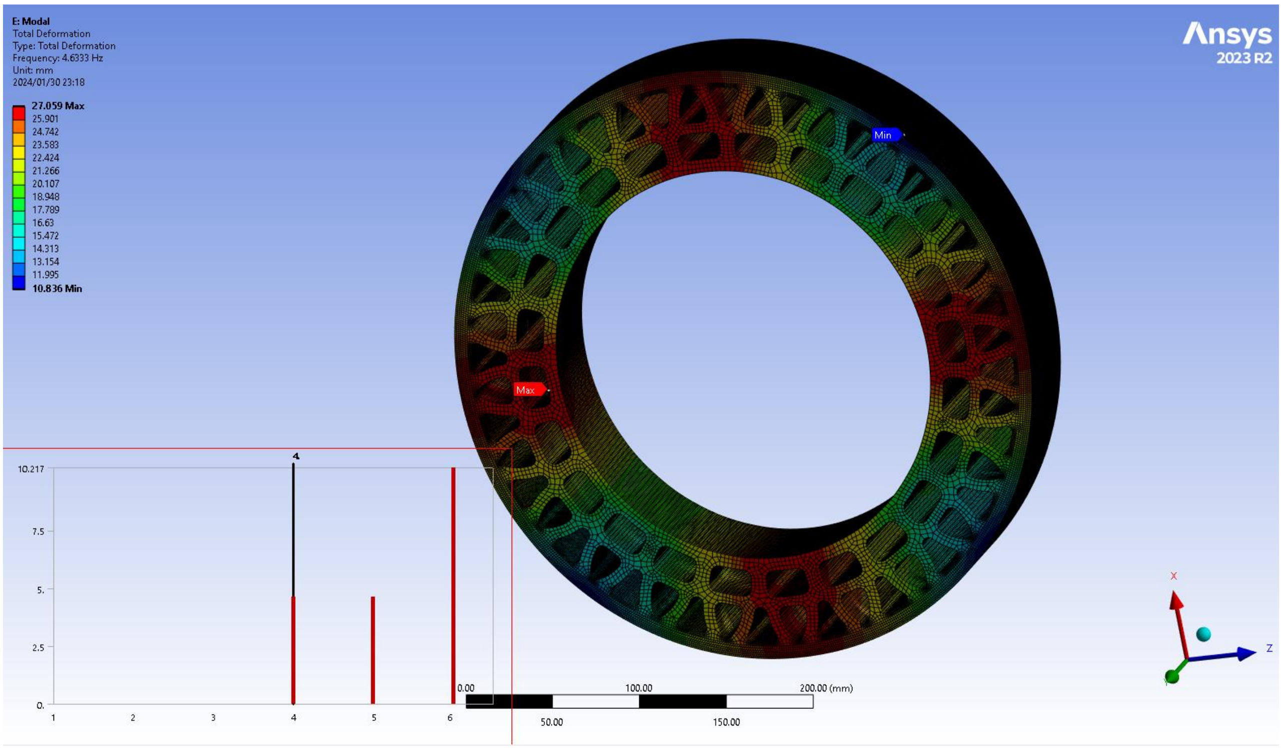

Figure 123: Third modal frequency

8.8 Experimentation vs FEA Results

This wheel design was testing at a client which performed a vibrational analysis on the wheel. The client wanted to assess the suitability of this wheel for an unmanned cleaning machine in Germany. When installing the wheel, a vibration monitor was attached to the axel of the wheel to measure vibrations over 5mmx5mm blocks. As seen in Figure 124 the structured wheel as some significant vibrations with the most notable occurring at 10.94Hz. This correlates with the FEA result in which the frequency of vibration with the maximum impact was seen at 10.22Hz.

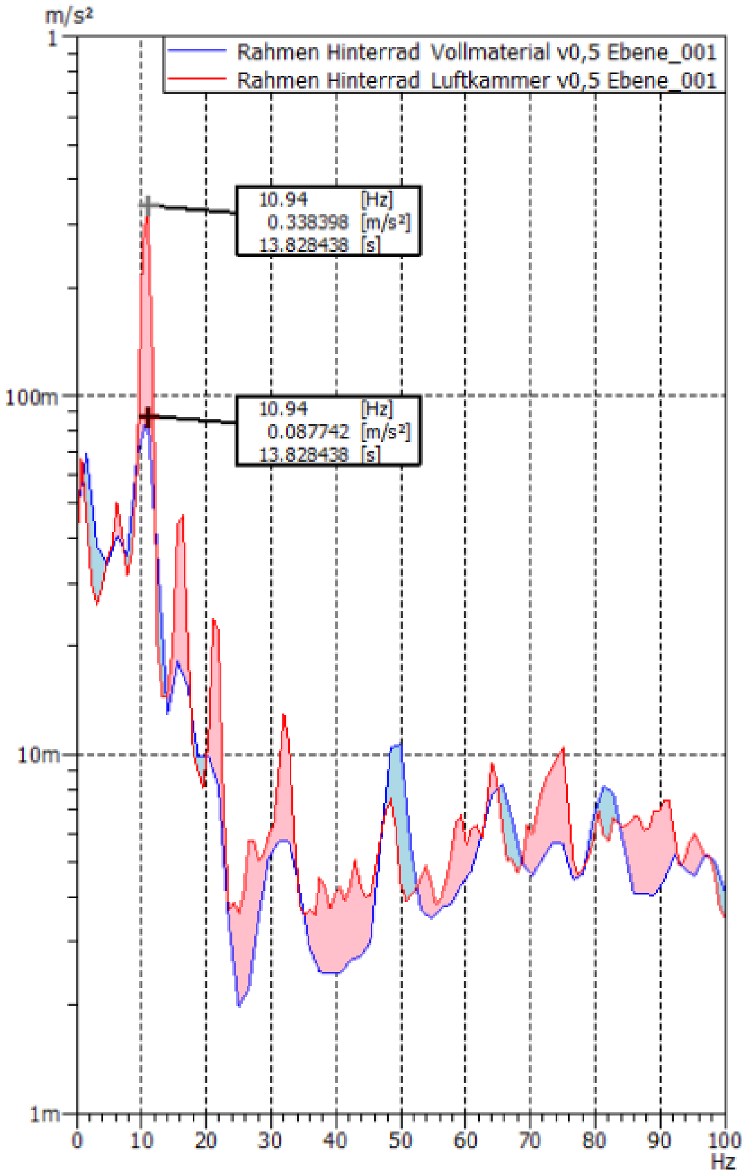

Figure 124: Vibration results from a prospective client.

When comparing the FEA deformation data with the experimental it can be seen that the damping factor in the non-linear analysis setting plays a vital role in the overall result. This damping factor is specific for our material selection as well as to control convergence as mentioned previously. Damping factors from 0.000001 to 0.1 was analyses but the relevant ones were plotted on the graph below.

The graphical representation in Figure 125 shows a comparative study between experimental data and FEA data concerning the deformation behaviour of a PU wheel under a ramped load to 10 000N. It is observed that the damping factor, a critical parameter in the non-linear analysis framework, exerts a significant influence on the simulation outcomes. This factor not only tailors the material-specific response but also governs the convergence behaviour within the computational model, as highlighted in prior discussions.

In the scope of this investigation, a comprehensive range of damping factors, extending from 0.000001 to 0.1, were subjected to analytical analysis. However, for clarity and relevance, only a selected subset of these factors has been depicted on the graph in Figure 125. These particular values were chosen based on their effectiveness in aligning the FEA results with the empirical data, thereby enhancing the reliability of the simulation in relation to the actual material behaviour.

The graph presents a correlation between the applied load (kN) and the resultant deformation (mm) of the wheel. It is noteworthy that as the damping factor decreases from 0.001 and below, there is a discernible deviation in the deformation curves from the experimental benchmark. This deviation underscores the damping factor's pivotal role in accurately capturing the response of the PU wheel.

The experimentally derived deformation data, represented by the red line in Figure 125, serves as a baseline for evaluating the accuracy of the FEA models. The FEA curves, each corresponding to a distinct damping factor, provide insight into the sensitivity of the material's response to variations in damping. It is apparent that a damping factor of ≥ 0.0025 is too large as this under accounts for the deformation at lower loads, 0kn to 7kN. By interpolating this result, it will also overpredict the deformation in loads >20kN.

Using a damping factor of 0.0022 provides an accurate correction between experimental and FEA results. This result is a parabolic result in FEA compared to a linear response in the experimental. At the time of writing this research work has been conducting to simplify the FEA simulation to analyse a path line for deformation to compare with experimental data. However, when linearising the FEA result mathematically, the result obtained is almost identical to the experimental results.

In summary, this analysis underscores the importance of carefully calibrating the damping factor within non-linear FEA settings to ensure congruence with experimental observations. Such calibration not only enhances the model's precision but also contributes to a deeper understanding of the material's behaviour under load, which is crucial for the informed design and analysis of PU-based components in mechanical systems.

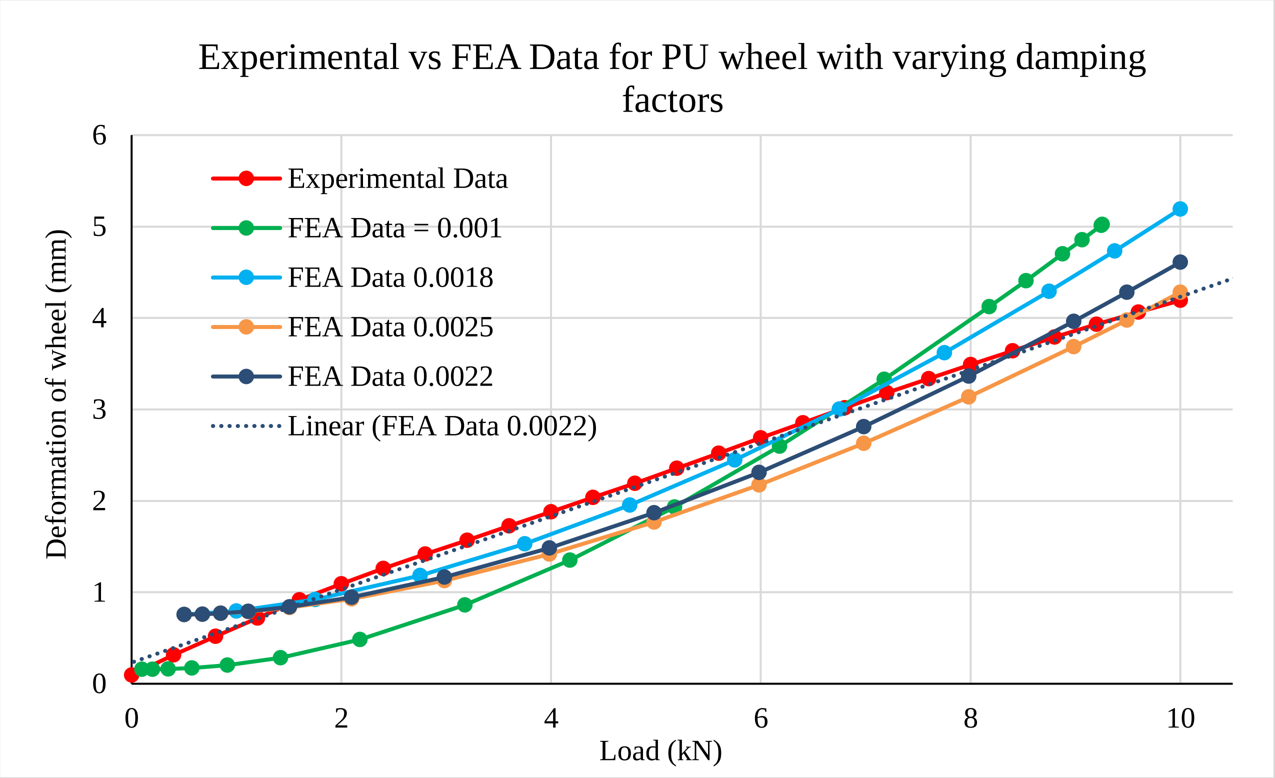

Figure 125: Experimental vs FEA Data for PU wheel with varying damping factors.

An error analysis quantifying the differences between the simulated and experimental data was conducted and the results are in Table 23. The use of statistical measures such as mean standard deviation help analyse the differences between data. The analytics are within a reasonable tolerance and can verify that the FEA Data can be trusted and used with good accuracy between 0kN and 10kN.

Table 23: statical analysis of data

Calculated statistical property	Experimental Data	FEA Data
Average deformation	2.261764	2.048211
Standard deviation on deformation	1.24041	1.412304
Standard error	0.243264	0.364655

8.8.1 Influence of Material Models:

Using different material models (e.g., neo-Hookean, Mooney-Rivlin, Ogden) has also changed results significantly. The 3 models selected in the research was the most stable and achieved the best results compared to experimental data. Others like the Ogden displayed too little deformation over characterising the stiffness of the PU.

8.8.2 Assumptions and Limitations:

The hyperelastic assumptions made in 3.6.1 Material Assumption as a hyperelastic elastomer is correct and is required for the hyperelastic model. This does impose that hysteresis effects are not taken into account. DMA testing, which is the dynamic testing of elastomers will have to be conducted for a better understanding of this hysteresis effects.

8.8.3 Practical Implications:

This research has led to a foundation for an approach to design and develop PU wheels based on accurate prediction of load bearing and model damping characteristics.

9. Conclusions

In this dissertation, understanding hyperelasticity, with a particular focus on the various characteristics like the deformation of polyurethane (PU) wheels was a key focus. The convergence of simulation results in the presence of element distortions presented a formidable challenge, primarily due to the highly nonlinear nature of hyperelastic materials. The findings show the critical role of damping factors in finite element analysis (FEA), demonstrating their significant impact on the simulation outcomes and convergence behaviour.

Through detailed adjustments in mesh quality control and model setup refinement, I successfully mitigated the issues associated with element distortion. This was achieved by employing mesh elements less susceptible to distortion, optimizing the geometric design to reduce localized high stresses and strains, and adjusting analysis parameters for improved convergence. The application of such strategies helped achieve a final deformation result that closely aligns with experimental data, underscoring the accuracy and reliability of the FEA model.

9.1 Answering the Critical Research Question:

1. In the characterisation of PU, there are no universally accepted set of experimental procedures specifically tailored for the assessment of elastomeric materials such as PU. Given the tendency of PU to exhibit hyperelastic behaviour, characterised by large strains with minimal load applied, a comprehensive analysis necessitates the generation of stress-strain profiles across the three primary axes or state planes. This endeavour requires the implementation of a suite of experimental and modelling methodologies, notably:
   - Uniaxial compression testing,
   - Uniaxial tensile testing,
   - Planar shear testing.

   While volumetric compression testing can be conducted, it is not a necessity to incorporate volumetric compression data within the curve-fitting phase, given the assumption of material incompressibility.

   Another pivotal aspect of these tests is the strain rate, which should be congruent with the anticipated application loads. The selected strain rate for evaluating PU behaviour under quasi-static conditions is notably slow, set at 0.02 s^{-1}. If impact assessments were required, for example the simulation of PU interactions with substantial obstacles, such as obstacles like rocks on a terrine, a higher strain rate of approximately 0.1 s^{-1} is used. This approach ensures that the material's response under various loading conditions is accurately represented, thereby facilitating a more robust understanding of its mechanical properties.

2. The analysis of experimental data to delineate the non-linear behaviour of materials with a minimal dataset is pivotal. Through this process, a response function is established to accurately reflect the material's behaviour under varying conditions. The crux of selecting an appropriate material model lies in its capacity to closely replicate experimental outcomes, presenting a significant challenge. The complexity of a material model does not inherently equate to its suitability, as considerations of curve fitting accuracy and computational efficiency during simulations are paramount. Enhancing the selection criteria for material models facilitates a more thorough evaluation, thereby enabling the identification of a model that provides a more precise representation of the material's characteristics.

In the determination of the C_{ij} constants, employing the absolute error criterion appears to be a judicious approach, given its consistency in yielding comparable results across different material models. Notably, the inclusion of an extensive array of C_{ij} constants does not significantly affect computational processing time, which tends to remain consistent across various models.

It is imperative to underline that findings from these analyses should not be generally extrapolated to all hyperelastic materials, as they are specific to the material under investigation. Only the methodology can be applied generally to all hyperelastic materials. In conclusion, after evaluating various conditions and ensuring model stability and analytical convergence, the Mooney-Rivlin models selected for describing Polyurethane (PU) include the Mooney-Rivlin 9 for LF950A material, Mooney-Rivlin 2 for LF750D material, and Mooney-Rivlin 5 for V6060 material.

These Mooney-Rivlin models demonstrate optimal alignment with experimental data, at strain levels up to 150% at ambient temperature and show a reasonable correlation at lower strains (up to 60%) with the curve fit and experimental data. This methodology facilitates the derivation of material coefficients, which are detailed in Table *20*, Table *21* and Table *22*.

3. A comparative analysis between FEA and experimental outcomes concerning the behaviour of PU under various load conditions is presented. The error analysis conducted to validate the FEA model revealed that the statistical deviation between the simulated and empirical data remained within acceptable bounds, showing the model's accuracy. Specifically, the FEA predictions indicated a maximum deformation of 4.61mm, compared with the experimental observations of 4.19mm for the maximum deformation. This comparison bolsters the credibility of the FEA model as an efficacious tool for predicting deformation behaviours across a load spectrum of 0kN to 10kN, with the calculated percentage error in maximum deformation standing at 9.06%.

Further analysis revealed an average deformation of 2.26mm during experimental testing, compared to 2.05mm in the simulation results, yielding a percentage error of 9.44%. Additionally, the standard deviation from experimental measurements was recorded at 1.24, while simulation outcomes presented a slightly higher standard deviation of 1.41, leading to standard errors of 0.24 and 0.36 for experimental and simulated deformations, respectively.

Moreover, modal analysis further showed the natural frequency and damping characteristics of the wheel design. The FEA predictions accurately reflected deformation behaviours at a critical frequency of 10.22Hz, with a measured deformation of 4.6mm, while experimental findings indicated a critical frequency of 10.94Hz. This concordance between FEA and empirical data, with a percentage difference in natural frequency of 6.58%, reaffirms the utility of the FEA model as a reliable predictive framework for analysing natural frequency behaviours, predicated on the developed material models.

The observed percentage differences are all under 10% between the experimental and simulated data afford a substantial degree of confidence in the simulation results, particularly in the context of designing non-pneumatic wheels and evaluating their load-bearing capabilities.

4. Optimising the design using FEA results. This can be do using the maximum load requirement and specifying the maximum deformation constraint. The spokes of the carcass can be made thinner to be within deformation limits while saving on the amount of PU used in the wheel making it lighter and cheaper.

The research underscored the importance of directional deformation, as it reflects the realistic response of the PU wheel to applied loads and movements. Stress singularity mitigation was another critical aspect of this research, ensuring the fidelity of our results despite the presence of re-entrant corners or vertices. The addition of fillets in the simulation accounted for abrupt changes in deformation, enhancing the structural integrity of the model.

The comparative analysis between FEA and experimental data revealed that a specific range of damping factors, particularly around 0.0022, provided the closest correlation to the experimental benchmark, highlighting the nuanced sensitivity of the material's response to damping variations. This insight is pivotal for the accurate prediction and design of PU-based components within mechanical systems.

The influence of material models was also investigated, revealing that among the various models explored, the Mooney-Rivlin, provided the most stable and accurate results in alignment with experimental data. The research acknowledged the limitations inherent in the hyperelastic assumptions, suggesting that dynamic mechanical analysis (DMA) testing could offer a more profound understanding of hysteresis effects in future studies.

In conclusion, this comprehensive analysis has laid a robust foundation for the design and development of PU wheels, predicated on a precise prediction of load-bearing capacities and damping characteristics. It has also provided a methodological framework for addressing and overcoming the complexities associated with simulating hyperelastic materials, which is critical for advancing the field of mechanical engineering and enhancing the design of resilient and reliable components in various industrial applications.

10. Optimisation and future work

Future research should extend to encompass a broader spectrum of load scenarios, such as the dynamics of a wheel in motion, thermal behaviour analysis of PU and the wheel's performance on uneven terrains. This expansion necessitates building upon the foundational FEA methodology established in this study.

Concurrently, it is imperative to undertake experimental validations for these diverse load cases, ensuring the verification and corroboration of the FEA simulations' outcomes. Larger loads of >50 000N will also be worked on to extrapolate the results in this research.

A mesh independence study can also be conducted to evaluate meshing, convergence and efficiency.

Furthermore, exploring a wider array of polyurethanes is recommended, aiming to meticulously balance the load-bearing capacity and damping properties, thereby enhancing the material's applicability in practical engineering solutions.

11. Project Budget

Currently there is not a definite project budget outlined for this project from UMP. Costs are approved as and when it is submitted.

Cost estimates are as follows which have been currently approved:

Description	**Cost**
ANSYS Mechanical premium license	R1 293,362.78
Material testing	R 300 000.00
Rig building	R 100 000.00
Experimental testing	R100 000.00
Mould manufacture	R 200 000.00
Running cost	R 50 000.00
Total	**R 2 043 362.78**

10. References

[1] - Admin (2022a) Polyurethane foam - structure, properties, & uses of C27H36N2O10, BYJUS. Available at: https://byjus.com/chemistry/polyurethane-foam (Accessed: 17 January 2024).

[2] - lanxess.com. (n.d.). ▷ Adiprene® | Urethane Prepolymers | LANXESS. [online] Available at: https://lanxess.com/en/Products-and-Brands/Brands/Adiprene [Accessed 10 Jan. 2023].

[3] - Ansys Granta: Materials information management. Available at: https://www.ansys.com/products/materials (Accessed: 17 January 2024).

[4] - MatDat.com (no date) Database of materials properties, Database of Materials Properties | MATDAT.com. Available at: https://www.matdat.com/DAT-Search.aspx (Accessed: 17 January 2024).

[5] - Stress–strain curve (2023) Wikipedia. Available at: https://en.wikipedia.org/wiki/Stress%E2%80%93strain_curve (Accessed: 17 January 2024).

[6] - M. Shahzad, A. Kamran, M.Z. Siddiqui, M. Farhan, "Mechanical characterization and FE modelling of a hyperelastic material",
2015; 18(5): 918-92

[7] - B. Suryatal, H. Phakatkar, K. Rajkumar, "Fatigue life estimation of an elastomeric pad by ε-N curve and FEA", Journal of surface
engineered materials and Advanced technology, 2015,5,85-92.

[8] - "What Is the Difference between a Hyperelastic Material and an Elastic Material in RecurDyn?" Support.functionbay.com, support.functionbay.com/en/faq/single/87/difference-hyperelastic-material-elastic-material-recurdyn.

[9] - Rhyne, T. B. and Cron, S. M., „„Development of a Non-Pneumatic Wheel,"" Tire Science and Technology, TSTCA, Vol. 34, No. 3, July – September 2006, pp. 150-169

[10] - M. Shahzad, A. Kamran, M.Z. Siddiqui, M. Farhan, "Mechanical characterization and FE modelling of a hyperelastic material", 2015; 18(5): 918-924.

[11]- Ferry, "Viscoelastic Properties of Polymers", Wiley, 1980.

[12] - Exploring hyperelastic material using Ansys Mechanical. Available at: https://www.ansys.com/resource-center/webinar/exploring-hyperelastic-material-using-ansys-mechanical (Accessed: 21 January 2024).

[13] - ASTM D412-16 (2016) Standard Test Methods for Vulcanized Rubber and Thermoplastic Elastomers-Tension. ASTM International, West Conshohocken, PA. https://doi.org/10.1520/D0412-16

[14] - Uniaxial tension testing (no date) Uniaxial Tension Testing | Veryst Engineering. Available at: https://www.veryst.com/services/testing/material-test-library/uniaxial-tension-testing (Accessed: January 13, 2023).

[15] - ISO 7743:2017 (2022) ISO. Available at: https://www.iso.org/standard/72784.html (Accessed: January 13, 2023).

[16] - Basu, A., Celestino, T. & Bortolucci, A. Evaluation of rock mechanical behaviors under uniaxial compression with reference to assessed weathering grades. Rock Mech Rock Eng 42, 73–93 (2009). https://doi.org/10.1007/s00603-008-0170-2

[17] - Judson T. Bauman, "Fatigue stress and strain of rubber components – guide for design engineers", Hanser publications, Munich, 2008

[18] - Inc., A.P. (no date) Axel Products Physical Testing Services. Available at: http://www.axelproducts.com/hyperelastic.html (Accessed: January 15, 2023).

[19] - Inc., A.P. (no date) Axel Products Physical Testing Services. Available at: http://www.axelproducts.com/hyperelastic.html (Accessed: January 15, 2023).

[20] - Srinivas, K., and Dharaiya, D., "Material And Rheological Characterization For Rapid Prototyping Of Elastomers Components", American Chemical Society, Rubber Division, 170th Technical Meeting, Cincinnati, 2006.

[21] - General aluminum alloy. Fatigue properties come from MIL-HDBK-5H, page 3-277.

[22] - Jin-Feng et al. (2008) and Lee and Su (1999)

[23] - Cavallo, C. (2020) All About 7075 aluminum (properties, strength and uses), Thomasnet® - Product Sourcing and Supplier Discovery Platform - Find North American Manufacturers, Suppliers and Industrial Companies. Available at: https://www.thomasnet.com/articles/metals-metal-products/all-about-7075-aluminum-properties-strength-and-uses/ (Accessed: 31 January 2024).

[24] - CILBOND® 49SF (no date) Hytrel® is a registered trademark of DuPont Vulkollan® is a registered trademark of Bayer Material Science, CILBOND® 49SF. Available at: https://www.rudolphbros.com/customer/docs/skudocs/cilbond-49sf-tds.pdf.

[25] - CILBOND® 49SF (no date) Hytrel® is a registered trademark of DuPont Vulkollan® is a registered trademark of Bayer Material Science, CILBOND® 49SF. Available at: https://www.rudolphbros.com/customer/docs/skudocs/cilbond-49sf-tds.pdf.

[26] - Lanxess (no date) Form No. TDS-241817-en Vol October 29, 2020. UL Prospector.

[27] - Friction and automobile tires. Available at: http://hyperphysics.phy-astr.gsu.edu/hbase/Mechanics/frictire.html#:~:text=Jones%20and%20Childers%20report%20coefficients,and%200.4%20for%20wet%20roads (Accessed: 29 November 2023).

[28] - Polyurethane's coefficient of friction: Gallagher (no date) Gallagher Custom Polyurethane Moulding. Available at: https://gallaghercorp.com/polyurethane-coefficient-of-friction/#:~:text=Polyurethane's%20Coefficient%20of%20Friction%20is,ranges%20from%200.2%20to%202.5 (Accessed: 29 November 2023).

[29] - Srinivas, K., and Dharaiya, D., "Material And Rheological Characterization For Rapid Prototyping Of Elastomers Components", American Chemical Society, Rubber Division, 170th Technical Meeting, Cincinnati, 2006.

[30] - Kuhn Tucker conditions - wu. Available at: https://statmath.wu.ac.at/courses/MEC_MM/download/handouts/MMEcon-handouts-16-Kuhn-Tucker_Conditions.pdf (Accessed: 31 January 2024).

Annexture A

Contents


```
% Saahil Bhartu
% 03/09/2021
% Data processing for material testing
```

Finding the names of all the excel files in the folder 'Loading' in the current working directory

```
  PTWnumber = '241';
  xls = '/*.xlsx';

%    format long g
%    format short

  FullString = strcat(PTWnumber,xls);
  Directory = dir(FullString);

  Names = {};
  for count0 = 1:size(Directory,1)
     Names{end+1,1} = Directory(count0).name;
  end



  % finding the curent working directory
     pwd;
     CurrentDir = pwd;
 % changing the working director to folder 'Loading' within the current one
     StandardDir = CurrentDir;
     FileName = strcat('\',PTWnumber);
     NewDir = strcat(StandardDir,FileName);
     %NewDir2 = strcat(StandardDir,FileName);
     cd(NewDir);
```

Reading the data files

```
  NoDoc = size(Names,1);
```

```
for z = 1:2
    for x = 1:3

        % odd number count
        if x ~= 1
            temp0 = rem(x,2);
            if temp0 == 0;
                y = x+1;
            elseif temp0 == 1;
                y = x+2;
            end
        else
            y = x;
        end

        % Setup the Import Options and import the data
        opts = spreadsheetImportOptions("NumVariables", 2);

        % Specify sheet
        StringNameNumber = strcat('Test # ',{' '},num2str(x));

        opts.Sheet = StringNameNumber{1,1};



        % Specify column names and types
        opts.VariableNames = ["Strain", "StressMPa"];
        opts.VariableTypes = ["double", "double"];

        % Import the data
        Temp = strcat(NewDir,'\',Names{z,1});
        DataSet = readtable(Temp, opts, "UseExcel", false);
        DataMatrix = table2array(DataSet(2:end,1:2));
        DataMatrixFinal(1:size(DataMatrix,1),(y):(y+1)) = DataMatrix(1:end,1:2);

        % Clear temporary variables
        % clear opts
    end
    if z == 1
        UC = DataMatrixFinal;
    elseif z == 2
        UT = DataMatrixFinal;
    end

end
```

```
% UT(UT(1:end,1:end) == 0) = NaN;
%  UTFinal = [];
%  UCFinal = [];

for g = 1:size(UT,1)
    if UT(g,1) == 0 && UT(g,2) == 0
        UT(g,1) = NaN;
        UT(g,2) = NaN;
    end
    if UT(g,3)== 0 && UT(g,4) == 0
        UT(g,3) = NaN;
        UT(g,4) = NaN;
    end

    if UT(g,5)== 0 && UT(g,6) == 0
        UT(g,5) = NaN;
        UT(g,6) = NaN;
    end

    % UTFinal(g,end+1) = mean(UT(g,1:2:end),'omitnan');
end



UTFinalStrain = mean(UT(1:end,1:2:end),2,'omitnan');
UTFinalStress = mean(UT(1:end,2:2:end),2,'omitnan');

UTFinalStress = UTFinalStress*1000000; % Changing from MPa to Pa

UTFinal = [UTFinalStrain UTFinalStress];

UTFinal = sortrows(UTFinal);


for h = 1:size(UC,1)
    if UC(h,1) == 0 && UC(h,2) == 0
        UC(h,1) = NaN;
        UC(h,2) = NaN;
    end
    if UC(h,3)== 0 && UC(h,4) == 0
        UC(h,3) = NaN;
        UC(h,4) = NaN;
    end
```

```
    if UC(h,5)== 0 && UC(h,6) == 0
        UC(h,5) = NaN;
        UC(h,6) = NaN;
    end
end

UCFinalStrain = mean(UC(1:end,1:2:end),2,'omitnan');
UCFinalStress = mean(UC(1:end,2:2:end),2,'omitnan');

UCFinalStress = UCFinalStress*1000000; % Changing from MPa to Pa

UCFinal = [UCFinalStrain UCFinalStress];

UCFinal = sortrows(UCFinal);
```

correction

UT

round(UTFinal(:,1),4);

```
op = length(UTFinal);

tgf = op - 2;



UTFinalPro = [];



for c = 1:tgf;
    if round(UTFinal((c+1),1),5) ~= round(UTFinal(c,1),5)
        UTFinalPro(end+1,:) = UTFinal(c,:);
    end
end


xlswrite(strcat(FileName, 'UT Data.xlsx'), UTFinalPro);
```

UC

```
% round(UCFinal(:,1),5);

ip = length(UCFinal);
tgif = ip - 2;
```

```
UCFinalPro = [];

for c = 1:tgif;
    if round(UCFinal((c+1),1),5) ~= round(UCFinal(c,1),5)
        UCFinalPro(end+1,:) = UCFinal(c,:);
    end
end


NameUC = strcat(FileName, 'UC Data.xlsx');

xlswrite(NameUC,UCFinalPro);
```

Published with MATLAB® R2023b